The Thesis Committee for Mayuri Murugesu

Certifies that this is the approved version of the following thesis:

Improved Upscaling Scheme for Steam Assisted Gravity Drainage (SAGD) and Semi-Analytical Modeling of the SAGD Rising Phase

APPROVED BY

SUPERVISING COMMITTEE:

Supervisor: _____

Sanjay Srinivasan

_____

Larry W. Lake

Improved Upscaling Scheme for Steam Assisted Gravity Drainage (SAGD) and Semi-Analytical Modeling of the SAGD Rising Phase

by

Mayuri Murugesu, B.S.Pet.Eng.

Thesis

Presented to the Faculty of the Graduate School of

The University of Texas at Austin

in Partial Fulfillment

of the Requirements

for the Degree of

Master of Science in Engineering

The University of Texas at Austin

May 2015

Dedication

To my Gurudev, Jagadguru Shri Kripaluji Maharaj.

To my Supreme Beloved Krishna and Radha Maiya to whom I owe everything to.

To my parents and siblings for their endless love and support.

Acknowledgements

Throughout my entire educational experience at UT Austin, I have been inspired, challenged, motivated, and supported by many people. It gives me immense pleasure to acknowledge a few of them to whom I owe my deepest gratitude.

First of all, I would like to thank my research advisor, Dr. Sanjay Srinivasan, for giving me the opportunity to work with him and for providing his invaluable guidance and support throughout my entire time at UT Austin. With the right mentorship, even the toughest challenge seems easy. He is such an advisor and I feel extremely grateful and blessed to have worked with him and been under his care. My profound thanks to Dr. Larry W. Lake for dedicating his time and efforts to serve as the second reader of my thesis and providing me with his valuable suggestions and feedbacks.

I would like to thank Hariharan Ramachandran and Azor Nwachukwu for their insightful discussions and support, which helped me tremendously in accomplishing some of my research objectives. To Jin and Frankie who provided me with timely administrative assistance and great advice on numerous occasions. My heartfelt thanks to the faculty at the Department of Petroleum and Geosystems Engineering at UT Austin from whom I have had the wonderful opportunity of learning from and satiating my thirst for knowledge. I would also like to thank ConocoPhillips for providing the funding for some of this work and Computer Modeling Group (CMG) for the provision of their simulation software, STARS^{TM}, that was used in this work.

Additional thanks goes to all my friends and colleagues who helped and supported me throughout my study at UT Austin and made my time here a pleasant one. In

particular, I would like to thank Sayantan Bhowmik, James Choi, Travis Hampton, Sang Hyon, Hoonyoung Jeong, Krupa Kannan, Dhananjay Kumar, Kwangjin Lee, Henry Li, Lianping Li, Prachi Mehta, Baehyun Min, Morteza Naraghi, Deji Olaluna, William Ozowe, Arindham Raina, Colin Schroeder, Harpreet Singh, and Haiyan Zhou.

Last but not the least, I would like to express my deepest gratitude to my parents. I cannot thank them enough for their support, patience, love and the sacrifices they have made so that I may be happy. I would like to thank my sister, Abitha Murugeshu Heimbuck, for the love that she showered in the form of valuable advice and encouragement during hard times, and my brother, Thanesh Murugesu, for always putting a smile on my face.

Abstract

Improved Upscaling Scheme for Steam Assisted Gravity Drainage (SAGD) and Semi-Analytical Modeling of the SAGD Rising Phase

Mayuri Murugesu, M.S.E.

The University of Texas at Austin, 2015

Supervisor: Sanjay Srinivasan

Steam assisted gravity drainage (SAGD) process commonly applied for heavy oil and bitumen recovery consists of two production phases: a steam rising phase and a spreading phase. Extensive research has been done on modeling the SAGD spreading phase, but fewer analytical/semi-analytical models exist for the unstable rising phase. This thesis presents a semi-analytical method, MS-SAGD, to model the SAGD rising phase. In addition, an improved upscaling technique that takes into account the unique flow geometry observed during SAGD is presented that enables more accurate predictions of oil recovery rates in heterogeneous reservoirs during both phases.

The MS-SAGD semi analytical method, based on the Myhill and Stegemeier frontal advance model for steam drive processes, tracks the growth of the steam chamber as a function of time. Two different oil production rate models are proposed and the comparison of results from flow and transport simulations is presented. Model 1 is similar to Butler's approach using the rising steam finger theory. Model 2 is obtained by modifying Butler's spreading phase model and applying it to the rising phase. Both models use the outputs of the MS-SAGD model to estimate the oil production rates during the SAGD rising phase.

The application of the MS-SAGD model is extended to heterogeneous reservoirs by treating the heated volume estimated by the original MS-SAGD model as an effective heated volume. In addition, the homogeneous permeability in the proposed oil production rate model is replaced with an upscaled effective permeability that is a function of time. The improved upscaling technique is based on a global approach that minimizes the differences between the fine scale and upscaled model pressure solutions. Sources and sinks by means of wells are used in the upscaling to simulate the convergent flow pattern observed during the SAGD process.

The proposed models outperform existing analytical/semi-analytical methods and are in good agreement with the results obtained from CMG-STARS^{TM} reservoir simulation. Both oil production rate models perform comparatively well, producing similar results in terms of cumulative oil production. However, Model 2 performs better than Model 1 in describing the overall behavior of the oil production observed in the reservoir simulation and is thus a better model for the SAGD rising phase.

Table of Contents

List of Tables

List of Figures

Chapter 1: Introduction

With declining light oil discoveries (oil with API gravity greater than 25° API), the vast reserves of heavy oil and bitumen are becoming increasingly important as a future energy source. Worldwide, 7,878 billion barrels of heavy oil and bitumen have been discovered, with more than 566.2 billion barrels in North America alone (Meyer et al., 2007). Both heavy oil and bitumen are too viscous to flow in their naturally occurring state. Heavy oil has API gravity between 10° API and 20° API inclusive and viscosity greater than 100 cP (Meyer et al., 2007). Bitumen has API gravity less than 10° API and viscosity commonly greater than 10,000 cP. Thermal processes that involve the injection of heat via steam into these unconventional reservoirs are widely applied to reduce the oil viscosity and produce it to the surface.

Steam assisted gravity drainage (SAGD) is an enhanced oil recovery (EOR) technique that has been successfully applied in the production of heavy oil and bitumen. Steam is injected through a horizontal injection well that is placed typically 5m – 10m above a horizontal production well (Dang et al., 2012). The injected steam rises to form a steam chamber that grows upwards and sideways as shown in Figure 1.1. Successful implementation of SAGD can result in recovery factors of 50% and higher (Sheng 2013). However, the process is very energy intensive and can be expensive. In order for it to be economical, the energy efficiency measured in terms of cumulative steam oil ratio (cSOR) is generally in the range of 2-4 tonnes/m^3 (Sheng 2013). This thus warrants a quick and accurate analysis of the SAGD process before major investments and implementation in the field. Full physics numerical simulation models can serve this

purpose and are beneficial in that they can be used to design field implementations of the SAGD process, but they can be time consuming and computationally expensive, especially for thermal processes that need to be resolved using fairly small grid sizes. In addition, the quality of numerical solutions can be affected by numerical issues such as dispersion, thereby motivating the need for simpler models that can capture the overall physics of the process at reduced computational cost and time.

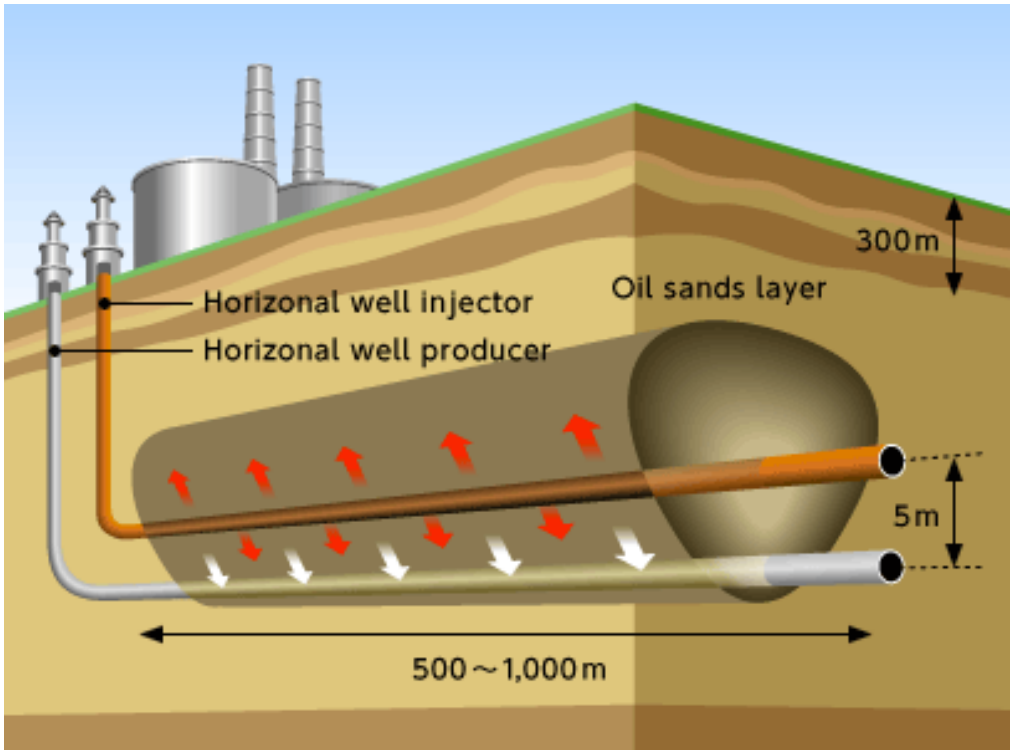

Figure 1.1: Steam Assisted Gravity Drainage Process (courtesy of JAPEX)

1.1 Research Objectives

Compared to full physics numerical simulation models, semi-analytical models developed by employing simplifying assumptions provide an attractive alternative to study the SAGD process while retaining a balance between computational time and accuracy of the results. In this work, we present the following models aimed at achieving this balance:

I. Semi-analytical models: Compared to full physics simulations models that could take more than a day to complete one simulation run, semi-analytical models give results within the span of a few seconds to few minutes. As such, it is highly desirable to have such models that can be applied at a field scale to assess the influence of operational and reservoir conditions on recovery. Steam assisted gravity drainage process consists primarily of the rising phase and the spreading phase. During the rising phase, the steam chamber grows rapidly in the vertical direction until it reaches the top of the formation. The spreading phase applies when the steam chamber has grown to the top of the formation and is expanding horizontally till it reaches the confines of the reservoir. Extensive research has been done on modeling the SAGD spreading phase but fewer models exist for the unstable rising phase. In this work, we present a semi-analytical model based on Myhill and Stegemeier frontal advance method to model the SAGD rising phase. The model is originally developed for application in isotropic, homogeneous formations and later extended for application in anisotropic/heterogeneous formations as well.

II. Coarser simulation models: A solution that would be attractive for studying the SAGD process in strongly heterogeneous heavy oil/bitumen formations is a coarsened/upscaled numerical model. The upscaled model would still retain the inherent heterogeneity observed in the field and capture the overall physics of the process, but would require less computational time and resources compared to a full physics fine scale simulation. This is attractive in situations where the heterogeneity may affect an operational decision to be made such as well placement. A large fraction of Athabasca oil sands deposits are ancient point bar systems that are characterized by bedded, sandstone-dominated strata with interbedded siltstone layers and mud channels that results in lateral and vertical lithological heterogeneity (Su et al., 2012). An example of such a system is illustrated in Figure 1.2. This motivates the need to evaluate SAGD performance in such fields using realistic models for reservoir heterogeneity. Upscaled models would serve this purpose very well. However, Kumar et al. (2013) noted that the current upscaling methods do not adequately represent the separate impact of shale correlation length and lens frequency on the growth of the steam chamber.

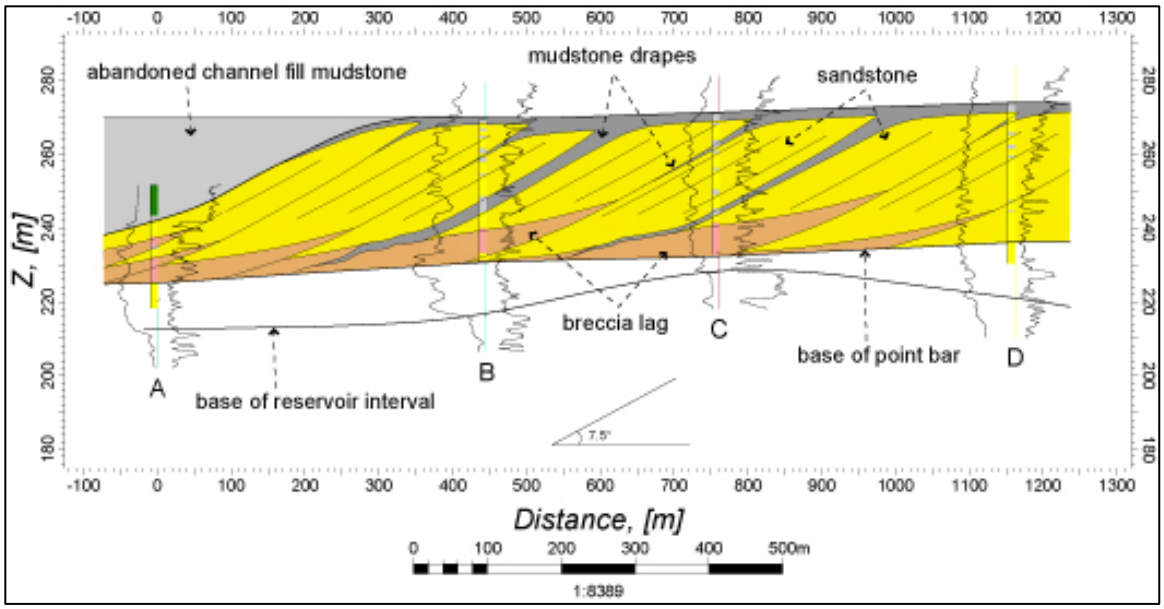

Figure 1.2: Cross Section of a Point Bar System (courtesy of CABS, University of Calgary)

As a result, models upscaled using conventional upscaling techniques predict the rise of the steam chamber and oil recovery incorrectly. In SAGD, the flow pattern is not uniform across the reservoir cross-section but convergent towards the production wells. This leads us to believe that the traditional upscaling methods that assume parallel flow between the injection and production face may not apply for SAGD processes. We present an upscaling technique that takes into account the unique flow geometry observed during SAGD.

1.2 Description of Chapters

Chapter 2 begins with an introduction to SAGD and goes further into a discussion of existing analytical/semi-analytical models and proxies for the SAGD process, focusing mainly on the SAGD rising phase. The impact of permeability anisotropy/heterogeneity

on SAGD performance present in literature is reviewed, and relevant background on conventional upscaling techniques is presented.

Chapter 3 presents an investigation of the application of conventional upscaling techniques to SAGD. Following this, an upscaling technique that takes into account the unique convergent flow geometry of the SAGD process is presented.

Chapter 4 presents a semi-analytical model based on the Myhill and Stegemeier frontal advance method to model the stream rising phase in SAGD. The semi-analytical model is originally developed for application in an isotropic and homogeneous formation.

Chapter 5 presents an extension of the modeling procedure in Chapter 4 to account for heterogeneity.

Chapter 6 summarizes the findings of this research and presents recommendations for future work.

Chapter 2: Background and Literature Review

This chapter presents relevant literature detailing the research on steam assisted gravity drainage (SAGD) and its field implementation. Special emphasis has been placed on reviewing analytical/semi-analytical models and proxies that have been developed to model the SAGD rising phase. The impact of permeability anisotropy/heterogeneity on SAGD performance discussed in the literature is reviewed, and the importance of incorporating shale barriers in SAGD models is highlighted. At the end, relevant background is discussed regarding conventional upscaling techniques, with primary focus on techniques used in upscaling absolute permeability.

2.1 Steam Assisted Gravity Drainage (SAGD)

Steam assisted gravity drainage (SAGD) is a thermal method for enhanced insitu recovery of heavy oil and bitumen. Steam is continuously injected through a horizontal injection well located 5-10 meters above a horizontal producer (Dang et al., 2012). The injected steam rises to form a steam chamber in the reservoir as shown in Figure 2.1. The steam pressure is usually maintained constant during this process (Butler, 1991). Injected steam flows within the sand in the chamber to the steam-bitumen interface and condenses, transferring heat to the colder oil sand. The heat reduces the viscosity of the oil near the chamber interface, and the heated oil and condensate drain by gravity to the production well below. As the liquids (oil and condensate) are removed, the space that is left in the pores is filled with steam. The steam chamber thus grows upwards and

sideways by continuously stripping off layers of heavy oil/bitumen at the edges of the steam chamber (Gotawala and Gates, 2008).

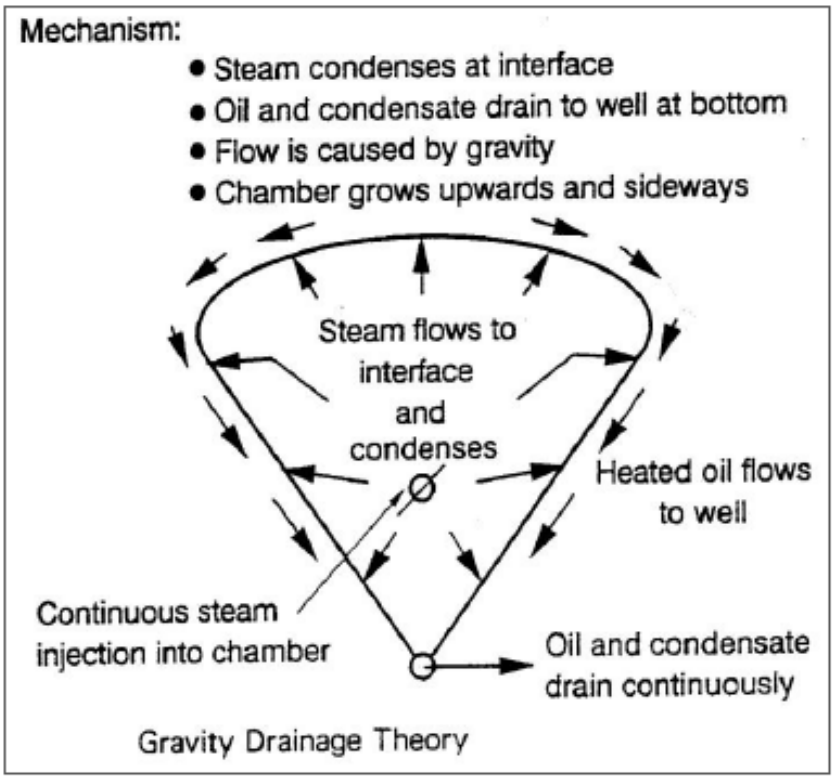

Figure 2.1: Conceptual Diagram of the SAGD Process (Butler, 1991)

The steam chamber growth typically occurs in three phases. First, the injected steam rises vertically from the injector – this is referred to as the rising phase. Once the rising steam intercepts the overburden or seal, it spreads laterally and expands horizontally. This is referred to as the spreading phase. The depletion phase is the last phase, where steam chamber collapses and production is reduced to an economical limit (Llaguno et al., 2002).

Although the rising phase precedes the spreading phase in the actual SAGD process, in the subsequent sections, we begin with a discussion of the SAGD spreading phase before moving on to the rising phase. This is because the commonly applied model for the rising phase, developed by Roger Butler, is based on his formulation of the spreading phase. This thus justifies a discussion of the spreading phase prior to the rising phase.

2.1.1 The Spreading Phase

The spreading phase also called the horizontal or lateral growth phase applies when the steam chamber has grown to the top of the formation and is expanding horizontally till it reaches the confines of the reservoir. Butler et al. (1981) first attempted to model the spreading phase of the SAGD process by assuming that the only transport mechanism was 1-D quasi-steady state heat conduction ahead of the steam chamber front, and by combining this with Darcy's law for the drainage of oil along the steam chamber wall, developed the expression for the oil rate given in Equation 2.1:

$$q_o = 2\sqrt{\frac{2\phi\Delta S_o k g \alpha H}{m v_{os}}} \qquad [2.1]$$

Where α is the thermal diffusivity, ϕ is the porosity, ν_{os} is the kinematic viscosity of oil at steam temperature, k is the permeability, H is the thickness of the reservoir, ΔS_o is the movable oil saturation, and m is a parameter that relates how the viscosity-temperature curve changes from reservoir to steam temperature and is obtained using Equation 2.2:

$$m = \left[\nu_S \int_{T_R}^{T_S} \left(\frac{1}{\nu} - \frac{1}{\nu_R} \right) \frac{dT}{T - T_R} \right]^{-1} \qquad [2.2]$$

Typical values for m vary between 3 and 5 for heavy oil and bitumen reservoirs (Butler, 1991).

Equation 2.1 indicates that the rate of drainage is a function of the drainage height and is independent of the shape of the interface or on its horizontal extension. Butler's model assumes that the reservoir is both homogeneous and isotropic. A homogeneous porous medium is one where the permeability in any direction does not vary with space and an isotropic porous medium is one where the permeability is the same in all directions (i.e. $k_x = k_y = k_z$, where x, y, and z are different coordinate directions). When the directional permeabilities of the porous medium are different, it is referred to as anisotropic. A heterogeneous medium is one where the permeability in any direction varies with space.

The drainage rate that would be obtained using Equation 2.1 overestimates the production because not all the head, h, is available as some of the head is required to move the oil horizontally to the well (Butler, 1991). Butler and Stephens (1981) corrected Equation 2.1, incorporating the concept of tangential drainage or "TANDRAIN", by replacing the 2 with 1.5 to account for the extra head needed to move bitumen accumulated at the base of the reservoir to the producer well. Their attempt was to account for both the horizontal flow to the producer well as well as the multiphase flow of oil and water towards the producer. Butler also obtained another equation that replaces the 2 in Equation 2.1 with 1.3 and this was called the Linear Drainage (LINDRAIN)

approximation (Butler, 1991). He assumed in the LINDRAIN approximation that the steam chamber-to-reservoir interface remains straight right up to the top of the reservoir and as the steam chamber grows in size, this straight interface becomes more inclined and longer (Butler, 1991).

Azom and Srinivasan (2011) modified Butler's equation for the spreading phase to account for permeability anisotropy by representing the permeability anisotropy as an ellipsoid and mapping the steam chamber geometry to the coordinate space of that ellipsoid. They replaced the permeability, k, in Equation 2.1 with an effective permeability, k_{eff}, that is a function of the directional permeabilities, k_v and k_h (Azom and Srinivasan, 2011). Reis (1992, 1993), Akin (2005), Nukhaev et al. (2006), Alali et al. (2009) and Azad et al. (2010) developed other models based on Butler's original model. The fundamental assumptions and formulations in all these models are similar to Butler's.

2.1.2 The Rising Phase

The rising phase follows the preheating of the formation (circulating steam in the injection and production wells). During this phase, the steam chamber grows very rapidly in the vertical direction and the process is thermally efficient as all of the latent heat released by the condensation of the steam is directed to heating the heavy oil/bitumen at the edges of the steam chamber (Chakrabarty et al., 2006).

Very few analytical/semi-analytical models and proxies are available for the SAGD rising phase as most of the studies on SAGD have focused on the more stable

horizontal spreading phase than the unstable rising phase. Butler (1991) first attempted to model the SAGD rising phase. Similar to the spreading phase, Butler assumed that the available head during the rising phase is less than the total height of the chamber, h, at any particular time. This is allowed for by replacing the "2" within the square root in Equation 2.1 with an unspecified factor, β. Furthermore, he assumed that the problem is two-dimensional and the shape of the steam chamber remains geometrically similar as it rises (Butler, 1991). Butler (1991) related the cumulative oil production during the rising stage to the mobile oil per unit area multiplied by the square of the chamber height according to Equation 2.3:

$$q_{cum} = \int_0^t q\, dt = \gamma \phi \Delta S_o h^2 \qquad [2.3]$$

Where γ is a shape factor reflecting the shape of the steam chamber.

Equation 2.3 indicates that the oil production is directly proportional to the shape factor, γ, the porosity, φ, the mobile oil saturation, ΔS_o, and the square of the height of the steam chamber, h. By differentiating Equation 2.3 with respect to time and equating it to Equation 2.1, he obtained the expression for the steam chamber height given by Equation 2.4:

$$h = \left(\frac{9}{4}\frac{\beta}{\gamma^2}\right)^{1/3} \left(\frac{kg\alpha}{m v_{oS} \phi \Delta S_o}\right)^{1/3} t^{2/3} \qquad [2.4]$$

Several experimental studies were conducted and by curve fitting the observed data to Equations 2.3 and 2.4, the value of γ and β were obtained and the following model given by Equation 2.5 was proposed for the oil flow rate as a function of time:

$$q = 3\left(\frac{kg\alpha}{m\nu_s}\right)^{2/3}(\varphi\Delta S_o)^{1/3}t^{1/3} \qquad [2.5]$$

In the derivation of Equation 2.5, Butler assumed that the shape of the steam chamber is approximately a sector of a circle at 64° as shown in Figure 2.2. The model does not predict the rate of rise of the steam chamber, and hence, the duration for the rising phase cannot be determined using Butler's (1991) model.

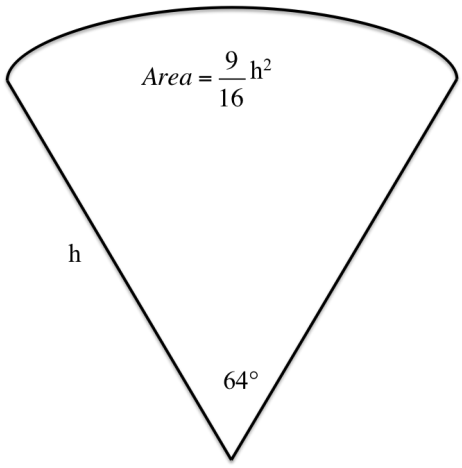

Figure 2.2: Approximate shape of rising chamber sector with shape factor, γ = 9/16 (Butler, 1991)

Another mechanism for steam rise proposed by Butler (1987) is the rise of interfering steam fingers. This model predicts the rate of rise of the steam chamber. In this approach, the frictional drag for the falling oil around a rising steam finger is balanced with the frictional drag within the finger and the driving force provided by gravity (Butler 1987). Butler assumes that the steam chamber rises at a constant rate and that the rate of rise of steam fingers is proportional to the absolute permeability of the reservoir and is a strong function of the steam temperature and oil viscosity (Butler,

1987). As a consequence of the assumption of the constant rate of rise, the theory predicts that small and large steam fingers will move upward at the same velocity given by Equation 2.6 (Butler, 1987).

$$V = \frac{kk_{ro}g}{(m+1)\nu_{os}\varphi\Delta S_o}\left\{\frac{(1-X_i)X_i}{(1-A)X_i^2+(A-B)X_i+B}\right\} \quad [2.6]$$

Where k_{ro} is the relative permeability for oil flow, X_i is the dimensionless steam finger-to-reservoir interface and is given by Equation 2.7, and A and B are constants (Butler, 1987).

$$X_i = \sqrt{\frac{B(1+2B)-B}{(1+B)}} \quad [2.7]$$

Murtaza and Dehghanpour (2012) indicated that there was a flaw in the derivation of Equation 2.6 by Butler and presented the following corrected model given by Equation 2.8 for the steam rise rate:

$$V = \frac{kk_{ro}g}{\nu_{os}\varphi\Delta S_o}\left\{\frac{(1-X_i)X_i}{-AX_i^2+(A-B+m+1)X_i+B}\right\} \quad [2.8]$$

Where X_i is given by Equation 2.9.

$$X' = \frac{\sqrt{B(m+1)}-B}{(m+1)-B} \quad [2.9]$$

The oil flow rate using this approach of rising steam fingers is given by Equation 2.10.

$$q_o = \phi\Delta S_o x V \quad [2.10]$$

The oil flow rate at the critical point of interference of two steam fingers is given by Equation 2.11.

$$q_{1o} = \phi\Delta S_o x_i V \quad [2.11]$$

Where x is the horizontal distance from the plane of symmetry of a rising finger and x_i is the half spacing between steam fingers.

Ito and Ipek (2005) studied the steam-fingering concept suggested by Butler (1987) by reviewing history matches of real field observation data. They concluded that steam fingers play an important role in the rise of steam chamber and that high-pressure operation is important for activating steam fingers. Murtaza and Dehghanpour (2012) extended Butler's analytical model (1987) for the rise of interfering steam fingers to account for three-phase flow. They concluded that in general, the analytical solutions underestimate the steam rise velocity compared to field values. Their proposed solution that includes flow coupling between oil and water predicts higher rise velocities compared to Butler's (1987), although they are still lower than measured field values (Murtaza and Dehghanpour, 2012).

Gotawala and Gates (2008) corrected Butler's derivation for the steam finger rise rate and showed that the length scale of the steam fingers range from pore-scale to tens of centimeters long, which is shorter than the conductive heat length scale. They indicated that the steam fingers are more like shallow undulations and do not appear to penetrate several meters into the oil sand as suggested by Butler (1987) and Ito and Ipek (2005) (Gotawala and Gates, 2008). Their simulation work shows that the steam chamber interface is stable with no growth of fingers, and the steam chamber largely moves like a piston (Gotawala and Gates, 2008).

Vanegas et al. (2008) proposed a proxy model based on Butler's semi-analytical solution of the process to predict the oil flow rate, cumulative oil production and

cumulative steam injection profiles during both the rising and spreading phases. Their proxy is based on the description of the hot interface advance through a 2-D section of a confined well pair, using conduction as a heat transference mechanism. The heterogeneity of the reservoir was explicitly incorporated in their proxy by averaging the reservoir properties along the discretized steam chamber-to-reservoir interface. Modifying factors are used to fit the proxy to flow simulation results to account for conformance and reservoir heterogeneity among other factors (Vanegas et al., 2008). Thus, the application of their proxy still requires full physics numerical simulations that have to be run a few times to calibrate the proxy for a particular heavy oil/bitumen field.

2.2 Effect of Permeability Anisotropy/Heterogeneity on SAGD Performance

Permeability anisotropy/heterogeneity can result from inter-bedded shale or presence of stochastically occurring streaks of shale distributed laterally through the porous media (Deutsch, 2010). It can also result from the presence of interbedded siltstones and mud channels that have permeability smaller than that of sandstone in the same formation (Su et al., 2012). For simplicity, we shall refer to all facies that have low permeability and acts as a barrier to steam and oil flow as shale in this work.

If the shale is of limited lateral extent, it can slow down the flow of oil draining to the production well and act as a reduced vertical permeability (Ipek et al., 2008). If the shale is continuous over a significant lateral extent, it can impede and re-route steam flow as well as oil flow. Although conductive heat transfer can continue through the shale, the

rerouting of steam can change the geometry of the steam chamber, leading to reduced thermal efficiency of the SAGD process (Ipek et al., 2008).

Kumar et al. (2013) performed numerical simulations for several cases of reservoir heterogeneity and found that naturally occurring low permeability barriers result in a steam chamber shape that is quite different from the one assumed in the literature for proxy model development, and severely limited the growth of the steam chamber. McLennan and Deutsch (2006) found that the flow performance during SAGD is heavily dependent and sensitive to the spatial distribution of permeability and the contrast between vertical and horizontal permeability.

Chen et al. (2007) studied the effects of reservoir heterogeneities on SAGD performance using a stochastic model for shale distribution. Numerical simulations were conducted with various realizations of shale distributions. Chen et al. (2007) observed that the effects of reservoir heterogeneity on steam rising and oil drainage are not the same throughout the extent of the reservoir formation because of the difference in the characteristics of the flows in different regions. They thus divided the SAGD flow region into the near well region (NWR) and the above well region (AWR). Their findings indicate that flow in NWR is very sensitive to the presence of shale that impairs vertical permeability. In the AWR, only long, continuous shale or a high fraction of shale adversely affected the SAGD performance in their study (Chen et al., 2007).

Le Ravalec et al. (2009) investigated the effects of heterogeneity on SAGD performance using numerical models. A set of reservoir models were randomly generated with 0 to 20% shale volume and it was shown that the influence of shale baffles depends

upon their locations relative to the well-pairs. It was concluded that the most detrimental location occurs when a shale baffle is located between the injector and producer (Le Ravalec et al., 2009). This is similar to the findings of Shin and Choe (2009).

Azom (2012) showed that the effect of anisotropy on SAGD is time dependent and that there exists a unique time corresponding to a given set of reservoir and fluid properties, after which the effect of permeability anisotropy ceases to impact the SAGD performance. They found that as the steam chamber spreads in an inverted triangular shape (during the spreading phase), the influence of the vertical permeability decreases while the influence of the horizontal permeability on bitumen rates increases with time (Azom and Srinivasan, 2011).

The above findings by various researchers clearly indicate the importance and need to capture the effect of permeability anisotropy/heterogeneity in SAGD models. Alali et al. (2009) used geometric averaging of the vertical and horizontal permeabilities of a reservoir to develop their semi-analytical model for the spreading phase, however they demonstrated the validity of their model only over a very small range of cases. The model developed by Azom and Srinivasan (2011) for application in anisotropic reservoirs is unable to directly account for the heterogeneity introduced by spatial distribution of shale and depends instead on the estimated value of the effective permeability, k_{eff}, and thus the directional permeabilities, k_v and k_h. This constraint applies not only to Azom and Srinivasan's (2011) model but also to all methods that tries to account for anisotropy/heterogeneity by means of an effective permeability, k_{eff}, thereby motivating

the development of a proper upscaling technique to obtain the effective permeability that accurately represents the heterogeneous media.

2.3 Upscaling Techniques

Upscaling involves the conversion of high-resolution geostatistical models to coarse scale models that are manageable for reservoir simulation, while retaining geological realism and effectively representing fluid transport in the reservoir (Salazar and Villa, 2007). In the simplest case, upscaling involves the computation of an effective permeability that adequately represents a heterogeneous media for incorporation into analytical or simulation models. The simplest form of upscaling is single-phase upscaling (Christie, 1996). For single-phase flow involving only one component, the only parameters to be upscaled are porosity and absolute permeability or transmissibility (Durlofsky, 2005). In this work, we will focus on the upscaling of absolute permeability. This involves the calculation of an effective permeability that results in the same total flux of a single-phase fluid through the coarse, homogeneous block as that obtained using the fine heterogeneous model (Christie, 1996), as illustrated in Figure 2.3.

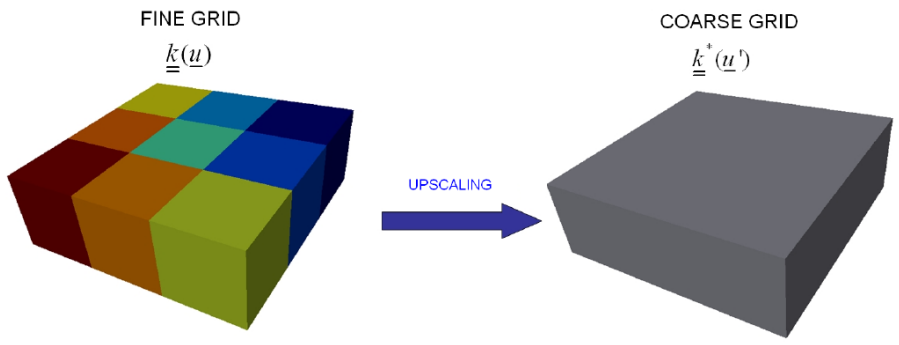

Figure 2.3: Upscaling of Permeability (Salazar and Villa, 2007)

The methods used in upscaling can be classified into analytical/static and numerical/dynamic approaches. Static averaging methods include power averaging procedures such as arithmetic, geometric, and harmonic averaging. These are the simplest techniques for computing grid block permeabilities (Durlofsky, 2005) as they do not require numerical solutions and are very efficient computationally. Arithmetic averaging provides an upper bound to the effective permeability and harmonic provides a lower bound. Arithmetic and harmonic averaging are used when reasonable assumptions can be made about the direction of flow with respect to the reservoir heterogeneity. For example, when flow is in the direction parallel to the major reservoir heterogeneity (for example reservoir bedding) arithmetic averaging is commonly applied (Salazar and Villa, 2007). Flow in the direction perpendicular to the major heterogeneity is referred to as series flow and in that case, it is best to perform upscaling using the harmonic mean of permeability values (Salazar and Villa, 2007). In cases where no particular assumption regarding flow direction can be made, geometric averaging is best applied (Salazar and Villa, 2007). A generalization of the three static averaging techniques discussed above is using the Power Law expression given in Equation 2.12 (Salazar and Villa, 2007).

$$k_\omega = \left(\frac{1}{n}\sum_{i=1}^{n} k_i^\omega\right)^{1/\omega} \qquad [2.12]$$

Where ω is the power averaging exponent and ranges between -1 and 1. For values of ω = 1, 0, -1, Equation 2.12 results in arithmetic, geometric, and harmonic averages respectively (Salazar and Villa, 2007). Other analytical techniques for permeability

upscaling include the renormalization approach (King, 1989) and the full tensor averaging technique (Kasap and Lake, 1990).

Dynamic methods involve the solution of Equation 2.14 for the pressure distribution using finite-difference methods (Salazar and Villa, 2007). Equation 2.14 is obtained by applying Darcy's law to the single-phase, incompressible flow conservation equation, neglecting gravity and capillary effects, given in Equation 2.13.

$$\nabla . \boldsymbol{u} = 0 \qquad [2.13]$$

$$\nabla . (\boldsymbol{k} \nabla p) = 0 \qquad [2.14]$$

Extensive reviews of existing flow based upscaling methods are given by Renard and de Marsily (1997), Farmer (2002), and Durlofsky (2005), among many others. Depending on the size of the region used for the calculation of the coarse scale quantities, these upscaling techniques can be characterized as local, extended local, global or quasi-global (Chen et al., 2003). In local approaches, the upscaled parameters are computed using fine scale regions corresponding only to the target coarse block under study, while fine scale information from nearby regions are also considered in the upscaling using extended local approaches (Chen et al., 2003). In both local and extended local approaches, boundary conditions are specified to estimate an effective permeability that yields the same flow rate as the fine grid calculation. Global methods utilize global fine scale flow simulations for the determination of coarse scale parameters whereas quasi-global approaches reduce the computational requirements of full global procedures by substituting some type of approximate global information in place of global fine scale results (Chen et al., 2003).

Kumar et al. (2013) used a flow based upscaling method (Durlofsky, 1991) to obtain effective directional permeabilities, k_v and k_h, for various realizations of shale distributions. This flow-based technique involves the solution of Equation 2.14 within the reservoir domain subject to periodic boundary conditions. A pressure gradient is imposed in the flow direction and a linear pressure profile on the two other opposite faces resulting in a non-symmetrical permeability tensor that takes into account the cross-flow term (Durlofsky, 1991). Kumar et al. (2013) observed that the upscaling could not adequately represent the separate impact of shale correlation length and lens frequency on the growth of the steam chamber. Kumar (2014) thus used a statistical upscaling scheme based on full 3D numerical simulation models. He developed a statistical response function that can be used to obtain the k_v/k_h ratio given the correlation length and the proportion of shale present.

Convectional upscaling techniques work quite efficiently for upscaling under uniform flow condition (illustrated in Figure 2.4a) i.e. when the fluid streamlines are roughly parallel from the inlet face to the outlet face, and where the local piezometric head or pressure values vary linearly. In SAGD, the flow pattern is no longer uniform but convergent towards the horizontal production well as shown in Figure 2.4b. This leads us to believe that for the SAGD process, these convectional upscaling approaches may not completely apply, motivating the need for an improved upscaling scheme. One such improved scheme is that presented by Kumar (2014), where he generated various correlations to obtain k_v/k_h ratio using the shale correlation length and frequency. In this

work, we propose a physics-based upscaling scheme to account for the convergent flow pattern observed in SAGD.

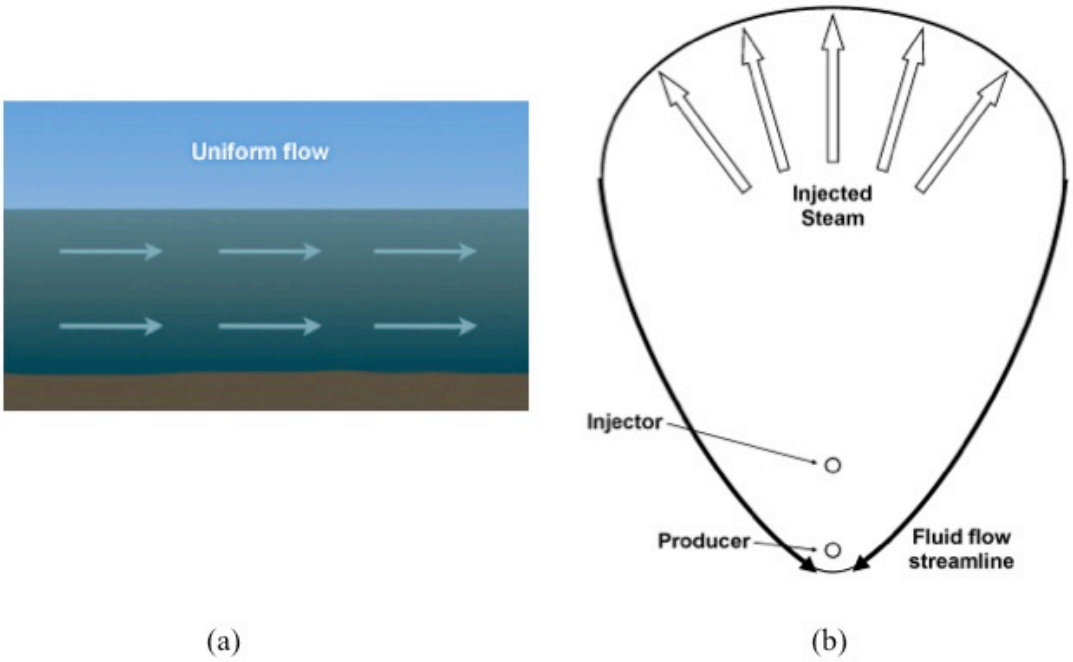

Figure 2.4: Flow Patterns (a) Uniform Flow Pattern (Courtesy of the COMET program) (b) Convergent Flow Pattern

2.4 Chapter Summary

In this chapter, we carefully reviewed the available analytical/semi-analytical methods to model the SAGD process and found that very few methods are available to quantitatively analyze and describe the SAGD rising phase. We also discussed the impact of permeability heterogeneity on SAGD through a detailed literature review. Relevant background on conventional upscaling techniques with primary focus on techniques used in upscaling absolute permeability was also presented. In the next chapter, we investigate conventional upscaling techniques applied to the SAGD process and discuss the

development of an improved upscaling method that takes into account the convergent flow pattern observed during the SAGD process.

Chapter 3: Improved Physics Based Upscaling Scheme for SAGD[1]

In the previous chapter, we reviewed the background literature investigating the impact of permeability heterogeneity on SAGD performance. These publications emphasized the need to account for heterogeneity in SAGD process modeling. Analytical/semi-analytical models for SAGD performance can be developed in terms of an effective permeability, similar to that in Azom and Srinivasan (2011) and the reservoir heterogeneity can be accounted for when computing the effective permeability. For such models in general, the heterogeneity observed in the field would need to be described by a single effective permeability value, k_{eff}, as illustrated in Figure 3.1a. As an extension, the effective permeability used in semi-analytical models could also be a function of time. This is further examined and demonstrated in Chapter 5. Another approach to incorporate heterogeneity in SAGD process modeling is to generate a coarse scale simulation model by upscaling the fine scale geostatistical model as illustrated in Figure 3.1b. Compared to the fine scale model, the coarse scale model will have smaller number of grid blocks and runs at reduced computational cost and time.

Both approaches mentioned above are dependent on a proper upscaling technique to compute the effective permeability corresponding to a heterogeneous permeability model. In the following sections, we first investigate the application of conventional upscaling techniques to SAGD by comparing the predictions corresponding to upscaled

[1] Dhananjay, K., Murugesu, M., and Srinivasan, S.: Modeling Effect of Permeability Heterogeneities on SAGD Performance Using Improved Upscaling Schemes. SPE Heavy Oil Conference, 10 – 12 June, Calgary, 2014.
Two different research works are presented in the above cited conference paper. Contribution by Dhananjay, K. to the work presented in this thesis is zero. Srinivasan S. is my research advisor and provided valuable input and guidance.

models to fine scale numerical simulation results. Findings from the investigation indicate the need for improved methods that minimize the difference between the results obtained from the upscaled and fine scale models. Hence, a physics-based upscaling method that takes into account the convergent flow geometry of the SAGD process is presented.

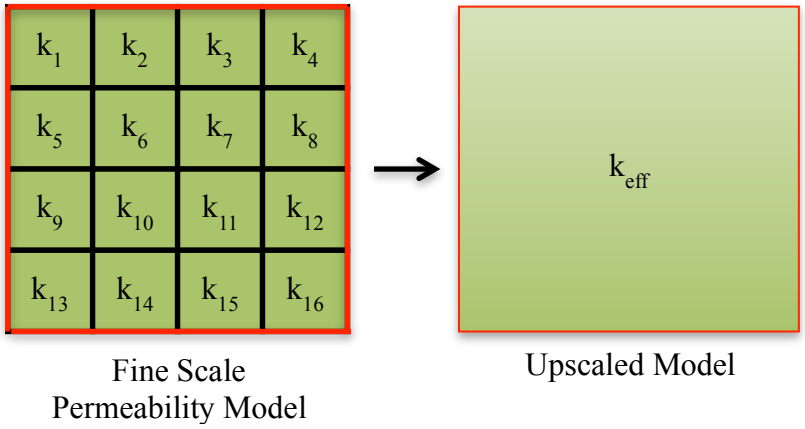

(a)

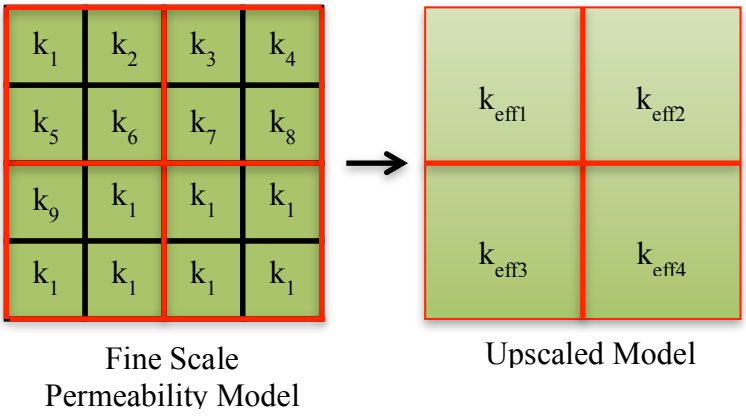

(b)

Figure 3.1: Upscaling Schemes: (a) Upscaling fine scale permeability model to generate a single effective permeability that can be used in semi-analytical models for predicting the performance of the SAGD process, (b) Upscaling fine scale permeability model to generate a coarse scale permeability model

3.1 Investigating Conventional Upscaling Techniques Applied to SAGD Process

To study the applicability of conventional upscaling methods to the SAGD process, two different upscaling techniques were selected: a static method and a dynamic method. Kumar (2014) modeled the impact of permeability anisotropy on SAGD using a statistical upscaling scheme. In his work, he found that compared to linear and harmonic averaging, geometric averaging produced the best initial match to the performance in a heterogeneous reservoir. Works by Matheron (1967), Bakr et al. (1978), and Dagan (1979, 1981) indicate that geometric averaging can be effective when permeabilities are log-normally distributed with low variance. Hence, geometric averaging, given by Equation 3.1, was selected for static averaging of heterogeneous permeabilities in this study.

$$k_{geo-eff} = \left(\prod_{i=1}^{n} k_i \right)^{1/n} \qquad [3.1]$$

The flow-based technique by Durlofsky (1991) that involves the solution of Equation 2.14 within the reservoir domain subject to periodic boundary conditions was selected as the dynamic upscaling method used in this study. In this upscaling technique, a pressure gradient is imposed in the flow direction and a linear pressure profile on the two other opposite faces, yielding symmetric, positive definite equivalent permeability tensors (Durlofsky 1991).

Both upscaling schemes illustrated in Figure 3.1 are investigated in the following sections. In Case I, a single effective anisotropic ratio is used to describe the

heterogeneity observed in the fine scale model illustrated in Figure 3.1a. In Case II, the permeability for each coarse scale block is obtained by upscaling a certain number of fine scale blocks according to the specified upscaling ratio (as illustrated in Figure 3.1b). For both cases, two dimensional (2D) stochastic shale models were generated at the fine scale using sequential indicator simulation (SISIM) in SGeMS, a geostatistical modeling software (Remy et al., 2009). The investigations were limited to a single SAGD well pair. A breakdown of the two cases and the respective models is given in Figure 3.2 below.

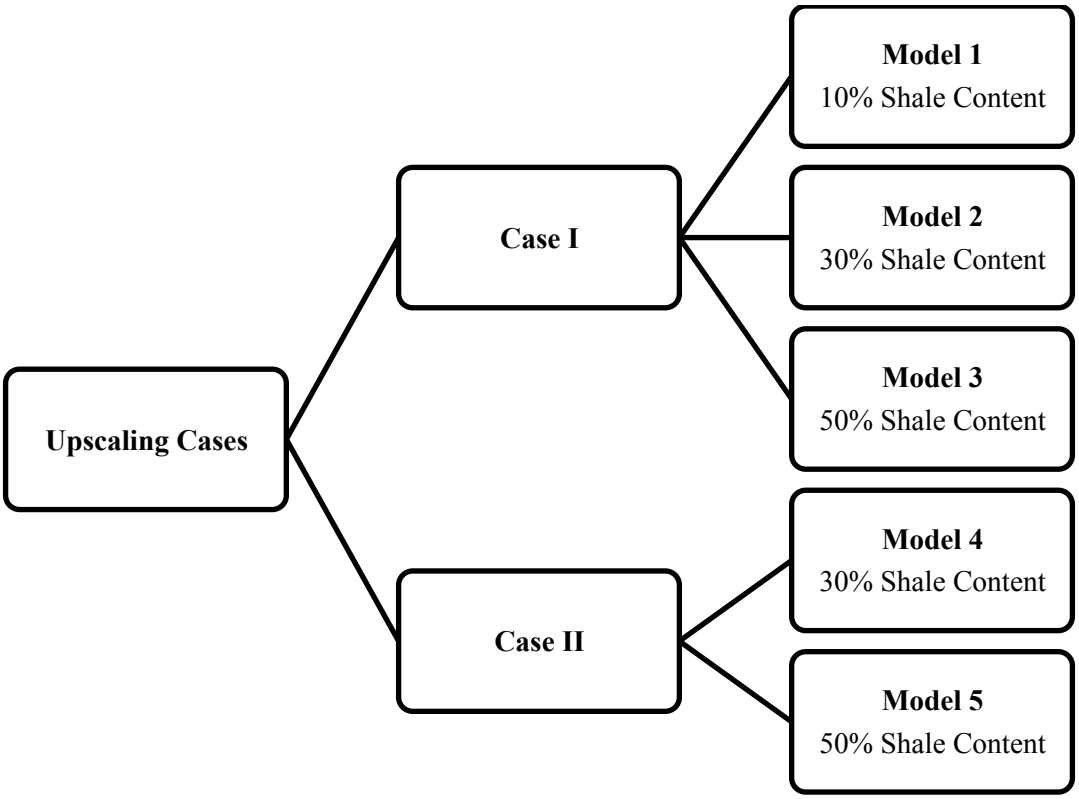

Figure 3.2: Summary of Upscaling Cases and Models Investigated

3.1.1 Case I: Effective Permeability for Application in Analytical/Semi-Analytical Models

Case I looks at upscaling the fine scale permeability model for application in analytical/semi-analytical models. Given the spatial distribution of shale lenses, an effective anisotropy ratio is computed using geometric averaging and the Durlofsky (1991) flow based upscaling technique described in the previous section. Three different stochastic shale models with shale frequencies of 10% (low), 30% (medium) and 50% (high) were generated in SGeMS as indicated in Figure 3.2. A maximum variogram range of 15m was assumed in the generation of these models. The stochastic shale distributions for the respective models are illustrated in Figures 3.3 – 3.5. For all three stochastic shale models, the directional permeabilities are equal i.e. $k_x = k_y = k_z$, and hence the k_v/k_h ratio at the fine scale is 1. Each model has 150 by 1 by 50 grid blocks with a grid size of 1m by 1m by 1m in the x, y and z directions, respectively.

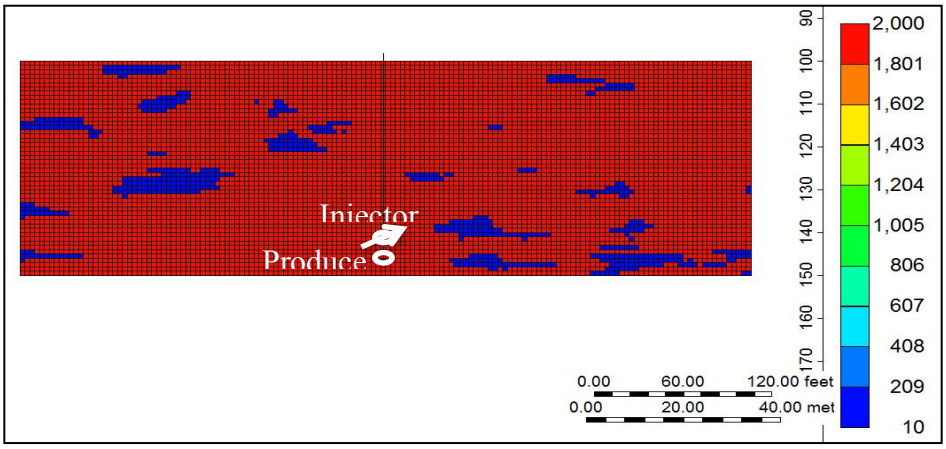

Figure 3.3: Permeability distribution for model 1 with 10% shale frequency

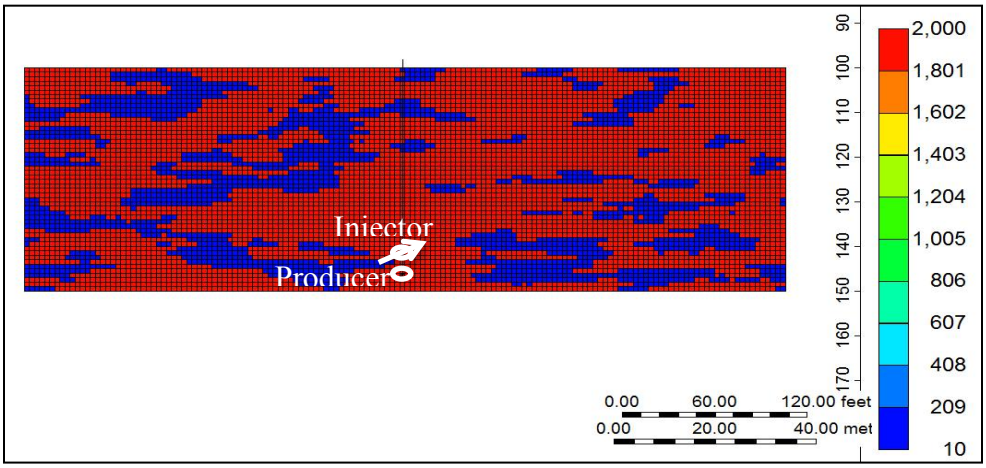

Figure 3.4: Permeability distribution for model 2 with 30% shale frequency

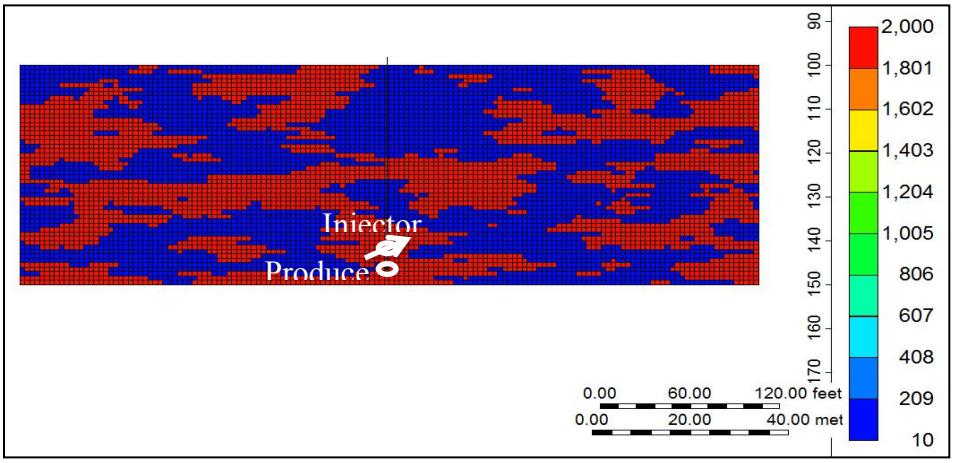

Figure 3.5: Permeability distribution for model 3 with 50% shale frequency

For each model, the effective directional permeabilities computed using both the static and the dynamic methods described above are given in Table 3.1. For the static method, geometric averaging was applied to obtain the effective horizontal permeability, k_h, and the effective vertical permeability, k_v. Since the fine scale model has a k_v/k_h ratio of 1, application of geometric averaging to obtain both effective permeabilities, k_v and k_h,

results in a k_v/k_h ratio of 1. For the Durlofsky flow based upscaling, the k_v/k_h ratio decreases from 0.68 to 0.26 as the shale frequency increases from 10% to 50%.

Table 3.1: Effective Directional Permeabilities for Case I Models Calculated Using Conventional Upscaling Techniques

Model	Durlofsky Flow Based Upscaling			Geometric Averaging	
	k_h (mD)	k_v (mD)	k_v/k_h	$k_h = k_v$ (md)	k_v/k_h
Model 1	1717	1168	0.68	1294	1
Model 2	817	352	0.43	468	1
Model 3	187	48	0.26	120	1

CMG's thermal simulator, STARS^{TM}, was used to run the numerical simulations using the fine scale and the upscaled models. Reservoir simulation grid dimensions and input parameters for the upscaled models are the same as the fine scale models except for the permeabilities. The relevant input parameters for the reservoir simulations are given in Table 3.2. The plot of viscosity change with temperature is given in Figure A.1 in the Appendix. All injection wells were set on maximum injection pressure constraint of 2400 kPa to compare the rates between the models. Each SAGD well pair was preheated for 6 months.

Table 3.2: CMG-STARS™ Input Parameters for Case I

Description	Value	Units
Reservoir thickness	50	m
Porosity	30	%
Thermal conductivity of reservoir rock	89856	J/(m-day-°C)
Volumetric heat capacity of reservoir	2.35E6	J/(m^3-°C)
Initial reservoir temperature	10	°C
Maximum injection BHP	2400	kPa
Steam injection quality	0.8	-
Minimum steam trap	10	°C
Minimum production well BHP	1500	kPa

Figures 3.6 and 3.7 present a comparison of the cumulative oil production and cumulative steam injection, respectively, between the fine scale model and the upscaled models for Model 1. Similar comparison plots for Models 2 and 3 are given in Figures 3.8 – 3.11. Comparison of the monthly oil production rates and monthly steam injection rates between the fine scale and upscaled models for Models 1 – 3 are presented in Figures A2 – A7 in the Appendix. The following observations can be made from the comparison plots:

- As already established from the literature review, the cumulative oil production and cumulative steam injection reduces as the frequency of shale increases.

- The results obtained from the geometric averaging are very close to those obtained from Durlofsky flow based upscaling technique for Models 1 and 2. A small discrepancy is observed between the results from the two upscaling techniques for Model 3.
- Both upscaling techniques result in lower steam injection rates and lower oil production rates compared to the base model (fine scale model).
- The difference between the fine scale and upscaled model solutions widen as the frequency of shale increases.
- The errors (given by Equation 3.2) in estimating the cumulative oil production using geometric averaging and Durlofsky flow based technique for Model 1 are about 27% and 25% respectively. For Model 2, the error in estimating the cumulative oil production using both techniques is about 61%. The errors in estimating the cumulative oil production using geometric averaging and Durlofsky flow based technique for Model 3 are about 70% and 80% respectively.

It can thus be concluded that application of these upscaled effective permeabilities computed using conventional methods would result in pessimistic results.

$$Error\ (\%) = \frac{\left|Q_{conventional\ technique} - Q_{Base\ case}\right|}{Q_{Base\ case}} * 100 \qquad [3.2]$$

Where Q in Equation 3.2 is the cumulative oil production.

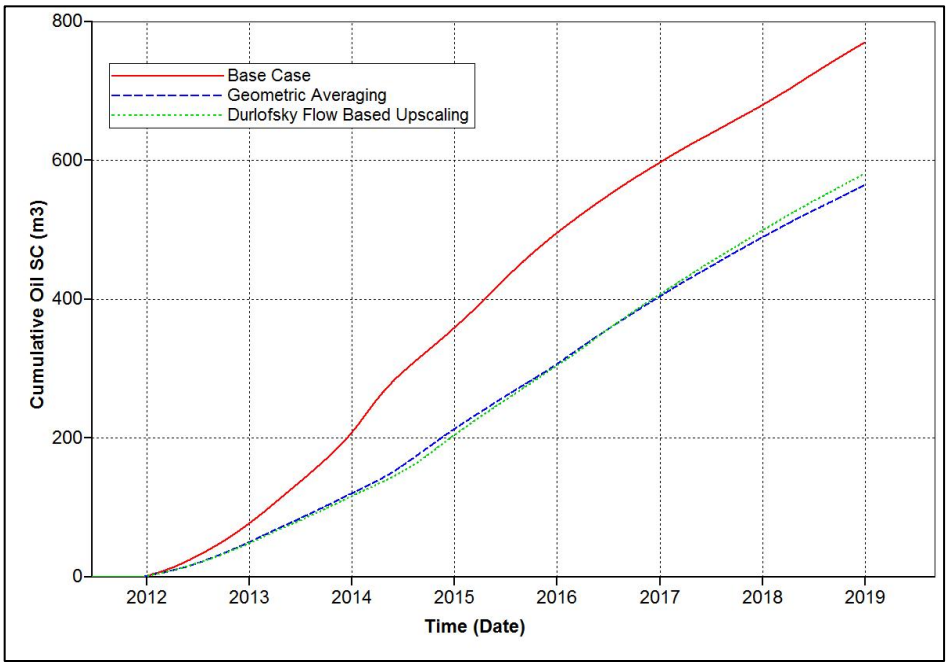

Figure 3.6: Model 1 (10% shale frequency) – Comparison of cumulative oil produced between fine scale model and models upscaled using conventional upscaling techniques.

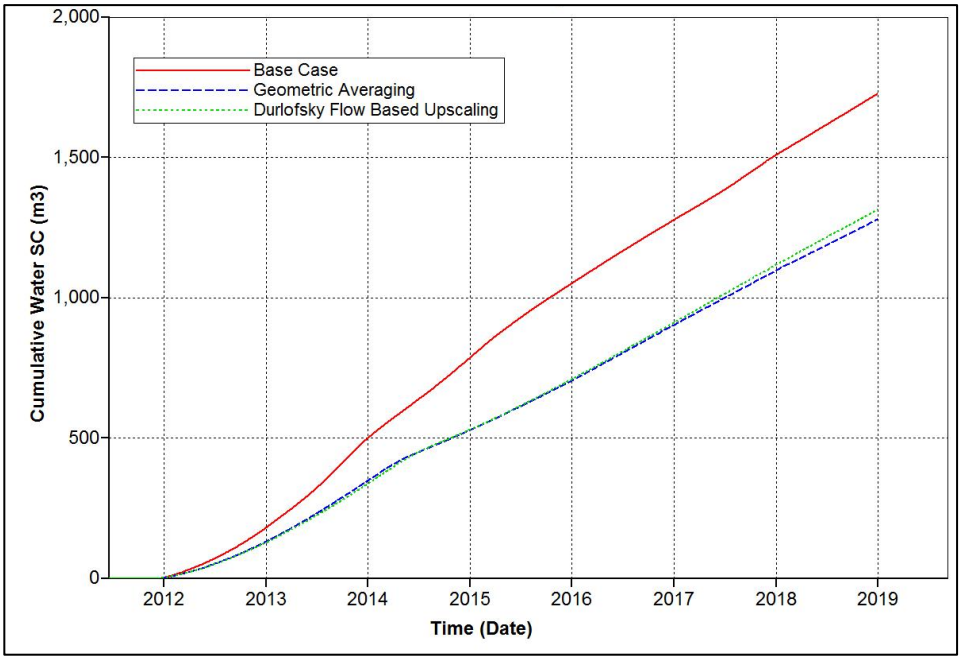

Figure 3.7: Model 1 (10% shale frequency) – Comparison of cumulative steam injected between fine scale model and models upscaled using conventional upscaling techniques.

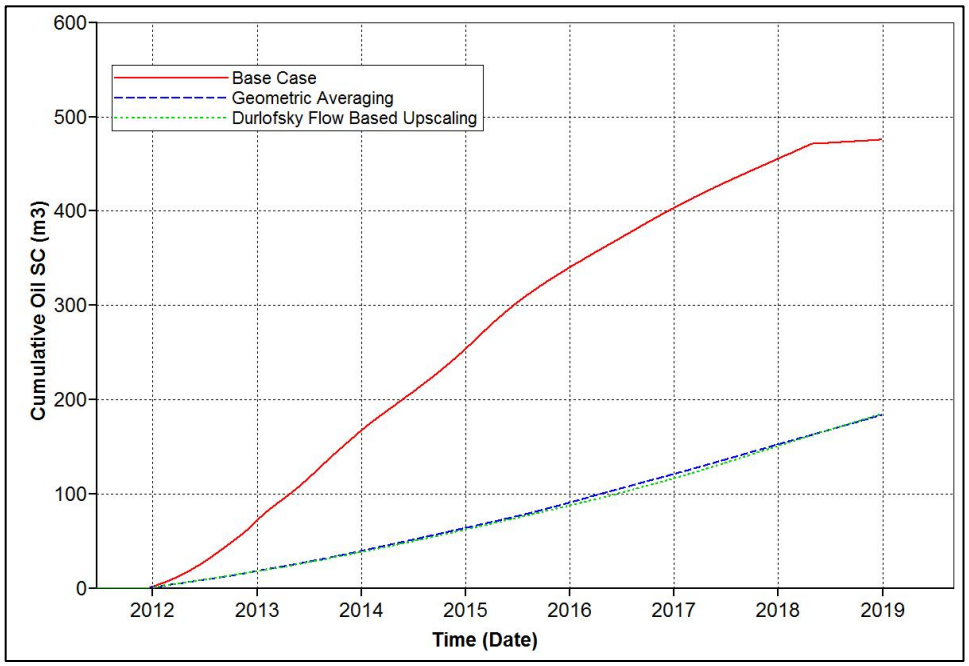

Figure 3.8: Model 2 (30% shale frequency) - Comparison of cumulative oil produced between fine scale model and models upscaled using conventional upscaling techniques.

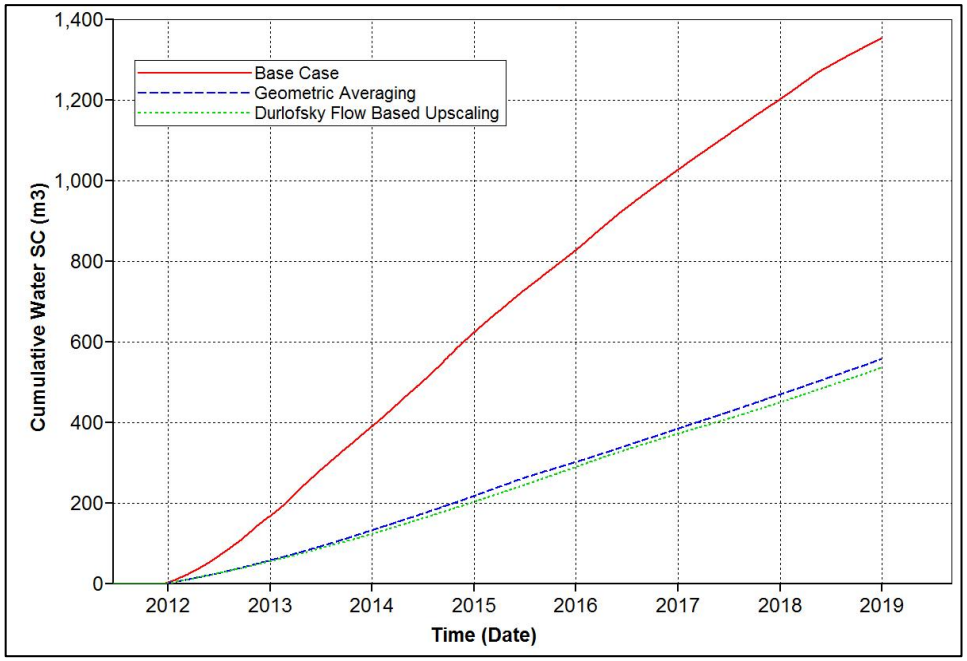

Figure 3.9: Model 2 (30% shale frequency) - Comparison of cumulative steam injected between fine scale model and models upscaled using conventional upscaling techniques.

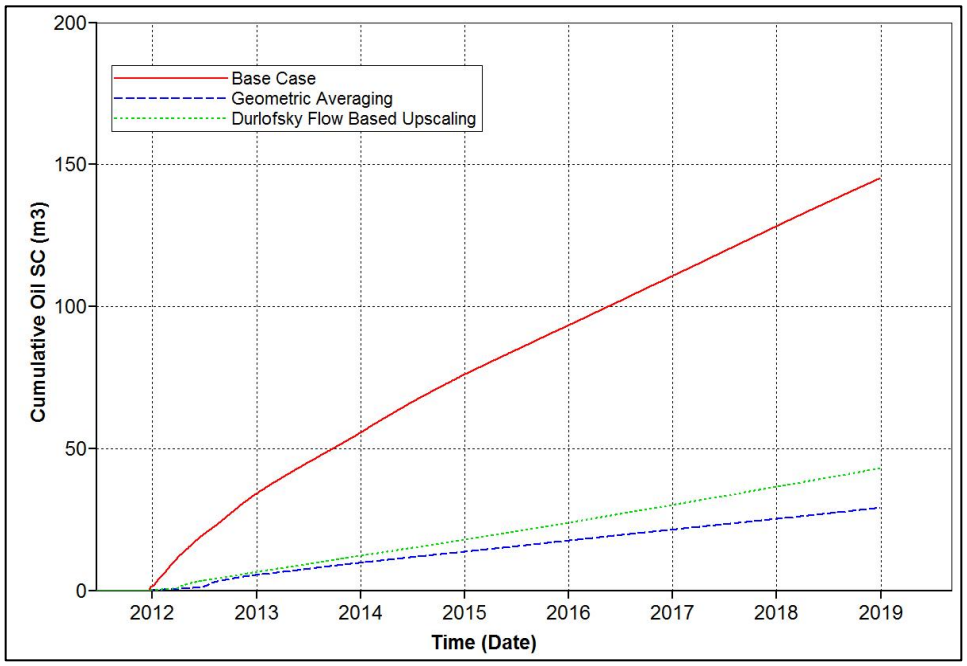

Figure 3.10: Model 3 (50% shale frequency) - Comparison of cumulative oil produced between fine scale model and models upscaled using conventional upscaling techniques.

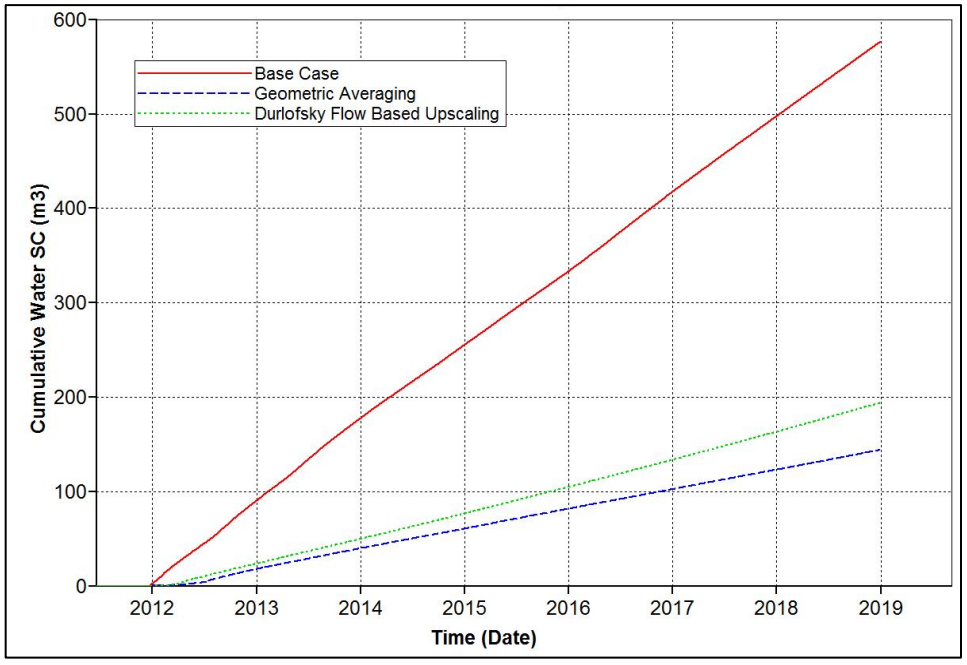

Figure 3.11: Model 3 (50% shale frequency) - Comparison of cumulative steam injected between fine scale model and models upscaled using conventional upscaling techniques.

3.1.2 Case II: Coarse Scale Permeability Model for Numerical Simulations

In Case II, given the spatial distribution of shale lenses at fine scale, upscaling is applied to generate a coarse scale permeability model as illustrated in Figure 3.1b. Results from Case I show that the upscaled values from geometric averaging are similar to those obtained using Durlofsky flow based upscaling technique. Hence, only the flow based upscaling technique was applied for Case II. Two-dimensional (2D) stochastic shale models containing 90 by 1 by 50 grid blocks with grid size of 1m by 20m by 1m in the x, y, and z directions, respectively, were generated using the sequential indicator simulation program (SISIM) in SGeMS (Remy et al., 2009). Two different shale frequencies were modeled: Model 4 with 30% shale content and Model 5 with 50% shale content. The correlation length of the discontinuous shale for the models is the same and is equal to 25m. For both models, the directional permeabilities are equal i.e. $k_x = k_y = k_z$, and hence the k_v/k_h ratio is 1.

An upscaling ratio of 4 is applied to generate the coarse scale models with 45 by 1 by 25 grid blocks at 2m by 20m by 2m in the x, y, and z directions, respectively. The upscaling ratio is defined as the ratio of the number of fine grid blocks to the number of coarse scale grid blocks. Thermal simulations are sensitive to the spatial discretization employed (Carlson 2006) and generally require much finer grid resolution compared to conventional light oil reservoir simulations. Hence, an upscaling ratio of 4 was selected to keep the grid sizes small enough to minimize numerical errors and also grid orientation effect.

CMG's thermal simulator, STARS^{TM}, was used to run the numerical simulations using the fine scale and upscaled models. Reservoir simulation input parameters for the upscaled models are the same as the base case/fine scale model except for the permeability model. The relevant input parameter for the reservoir simulations are given in Table 3.3. All injection wells were set to a maximum injection pressure constraint of 2400 kPa. For all models, the wells were preheated for 4 months. Figures 3.12 - 3.15 present a comparison of the cumulative oil production and cumulative steam injection between the fine scale model and the upscaled model for Models 4 and 5. Comparison of the monthly oil production rates and monthly steam injection rates between the fine scale and upscaled model for Models 4 and 5 are presented in Figures A8 – A11 in the Appendix.

Table 3.3: CMG-STARS^{TM} Input Parameters for Case II

Description	Value	Units
Reservoir thickness	50	m
Porosity	30	%
Thermal conductivity of reservoir rock	89856	J/(m-day-^{o}C)
Volumetric heat capacity of reservoir	2.35E6	J/(m^{3}-^{o}C)
Initial reservoir temperature	10	°C
Maximum injection BHP	2400	kPa
Steam injection quality	0.9	-
Minimum production well BHP	1500	kPa

Similar to Case I, the conventional upscaling technique results in lower oil production and cumulative steam injection compared to the fine scale model. It can also be observed that using a coarser permeability model instead of a single effective permeability to capture the entire fine scale model heterogeneity results in better matches with the base case. However, unlike Case I, we do not see a correlation between the shale frequency and the error associated with the upscaling. The errors in estimating the cumulative oil production for Models 4 and 5 are about 44% and 31% respectively. Thus, the upscaled model solution for Model 5 with 50% shale frequency has less error associated with it compared to the upscaled model solution for Model 4 with 30% shale frequency.

Although the errors associated with the conventional upscaling techniques are less for Case II compared to Case I, they are still rather high in the 30% range, further corroborating the findings of Kumar et al. (2013) that conventional upscaling techniques do not adequately reproduce the results observed in fine scale models. These results lead us to believe that a better upscaling scheme is needed for SAGD processes that takes into account the flow geometry and reduces the discrepancy between the fine scale and coarse scale model solutions. Since the heated oil and condensed water flow along the edges of the steam chamber to the production well because of the influence of gravity in the SAGD process, the flow pattern is convergent to the well as opposed to uniformly spaced streamlines had the entire bottom edge of the reservoir been subject to the boundary condition. In the next section, we take this flow pattern into account and propose an improved physics based upscaling technique for SAGD processes.

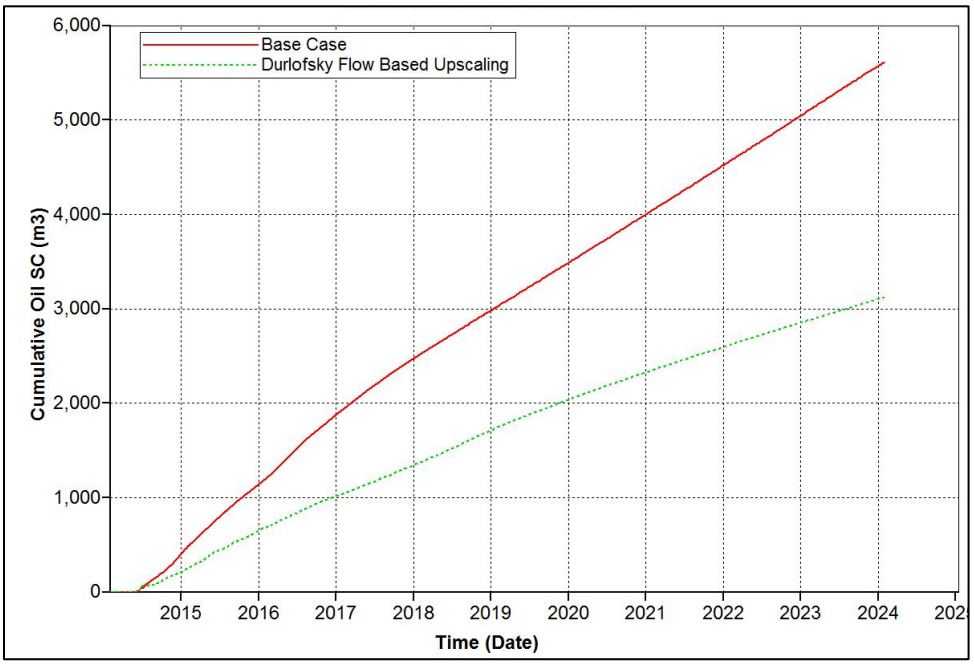

Figure 3.12: Model 4 (30% shale frequency) - Comparison of cumulative oil production between fine scale model and model upscaled using flow-based upscaling.

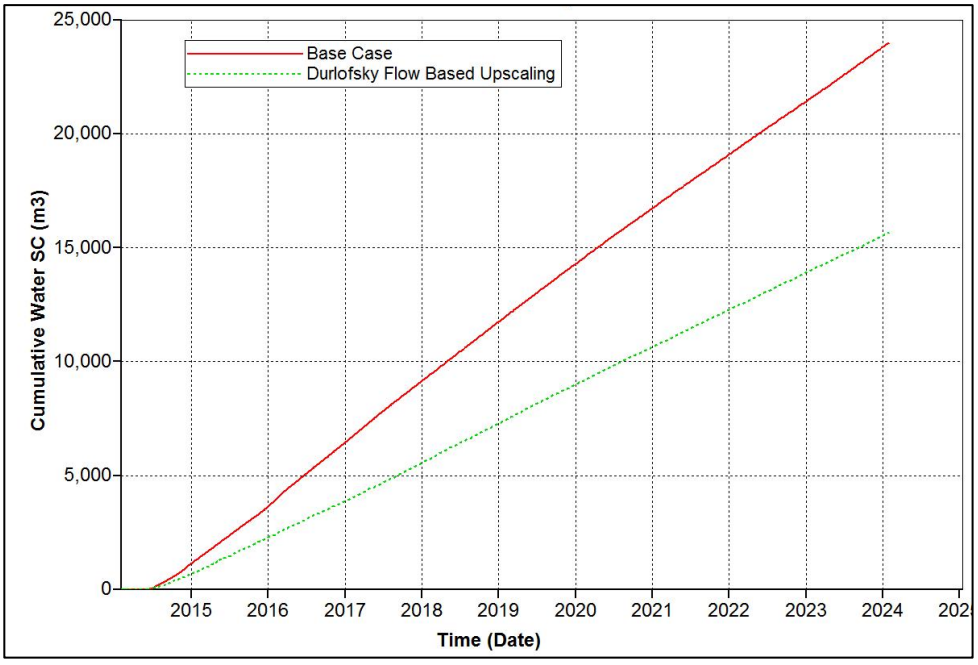

Figure 3.13: Model 4 (30% shale frequency) - Comparison of cumulative steam injected between fine scale model and model upscaled using flow-based upscaling.

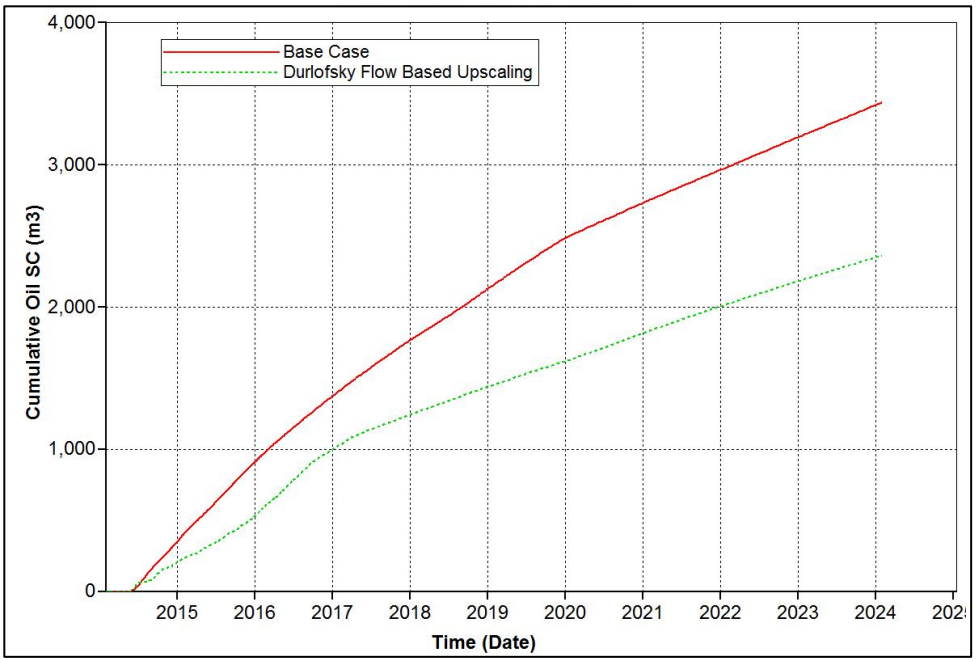

Figure 3.14: Model 5 (50% shale frequency) - Comparison of cumulative oil production between fine scale model and model upscaled using flow-based upscaling.

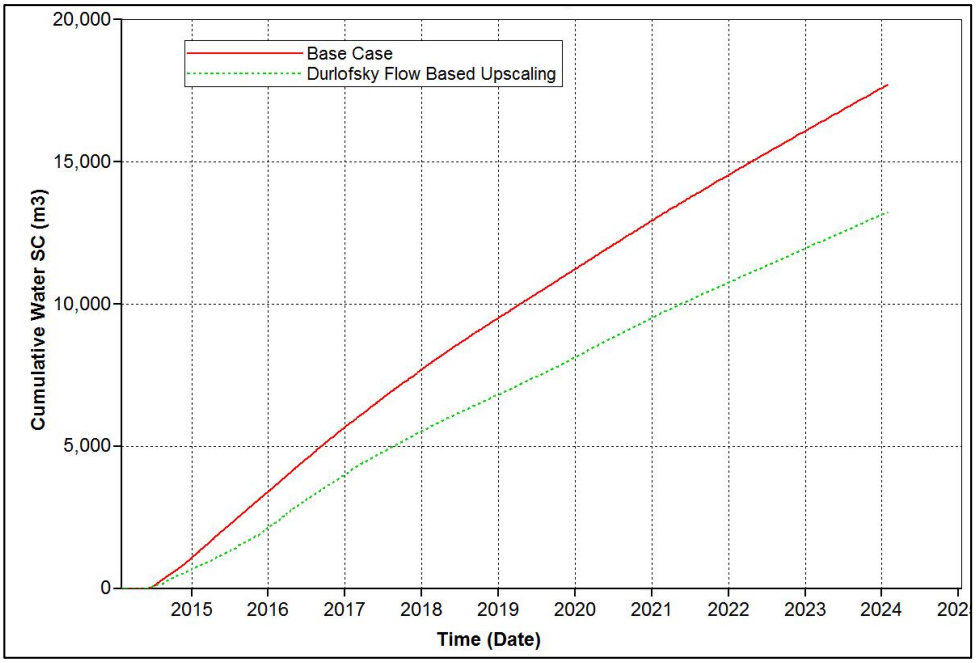

Figure 3.15: Model 5 (50% shale frequency) - Comparison of cumulative steam injection between fine scale model and model upscaled using flow-based upscaling.

3.2 Physics-Based Upscaling Technique

Flow-based methods of upscaling involve the solution of the pressure equation (Equation 2.14) within the reservoir domain. The fine scale flows are obtained either from the global solutions of the flow equation in the whole reservoir, or the local solutions in each grid block, referred to as global and local upscaling, respectively (Wu et al., 2002). Although local upscaling methods require much less computing power, they can be strongly affected by the boundary conditions such as no flow, periodic boundary condition (Durlofsky, 1991), or linear pressure boundary conditions (King et al., 1998, King and Mansfield, 1999), which may be appropriate far from the global boundaries of the reservoir (Holden and Nielsen, 2000). In this work, we formulate the proposed physics-based upscaling technique as a minimization problem based on the global upscaling method. The upscaled permeability is defined as the permeability that minimizes the pressure difference between the fine scale and coarse scale solutions corresponding to the global boundary conditions encountered during the SAGD process.

In the proposed physics-based upscaling technique, it is necessary to compute the fine scale pressure to solve the associated minimization problem. Solution for the fine scale pressures leads to a large linear system of equations where the number of unknowns is the number of fine scale blocks. In local upscaling techniques, a fine scale problem is solved for each coarse block. According to Holden and Nielsen (2000), the computing time needed for solving one fine scale pressure equation, defined on the entire reservoir, is comparable to the time needed by local upscaling methods for solving all the fine scale problems for all the coarse blocks. Hence, the proposed upscaling technique based on

minimizing the error between the fine scale and coarse scale solutions over the entire reservoir is not significantly more computationally expensive than local methods. In addition, the proposed upscaling technique is based on the solution of the single-phase pressure equation over the entire domain to compute the effective value of permeability that will yield the same solution on the coarser scale. The solution of this single-phase pressure equation is relatively cheap.

3.2.1 Model Setup for SAGD Flow Problem

In the SAGD process, the heated oil and condensed water flow along the edges of the steam chamber to the production well because of the influence of gravity. To simulate this convergent flow process in our upscaling, a sink term is specified at the bottom center of the model and a constant pressure is imposed at the top boundary of the model by use of source terms as shown in Figure 3.16. This setup of the model simulates the streamlines converging to the production well that is observed in SAGD processes.

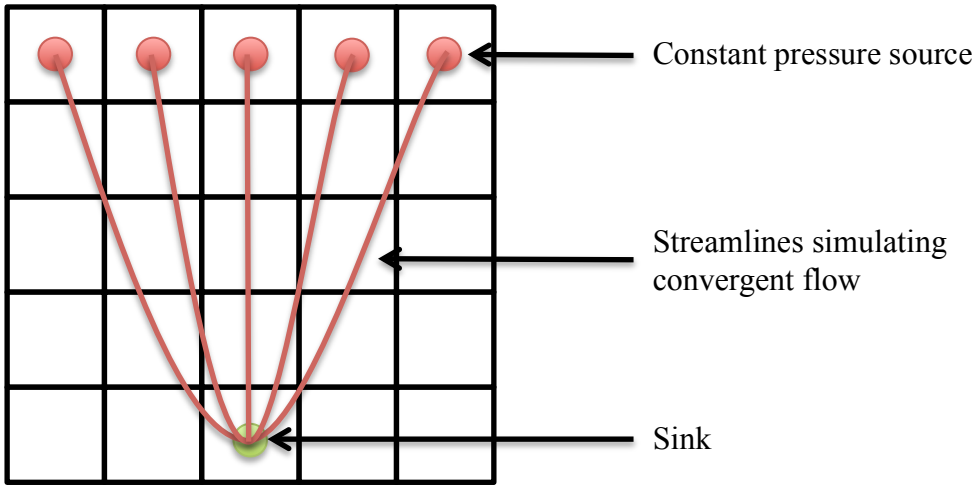

Figure 3.16: Simulation of convergent flow towards a point sink

Equation 3.3 gives the single-phase flow equation, ignoring capillary pressure, based on a finite difference scheme.

$$
\begin{aligned}
& c_{t_{ij}} V_{p_{ij}} \left(\mathrm{P}_{ij}^{n+1} - \mathrm{P}_{ij}^{n}\right) \\
& \quad = \Delta t \left[(T_x)_{i+\frac{1}{2},j} \left(\mathrm{P}_{i+1,j} - \mathrm{P}_{ij}\right)^{n+1} - (T_x)_{i-\frac{1}{2},j} \left(\mathrm{P}_{ij} - \mathrm{P}_{i-1,j}\right)^{n+1} \right] \\
& \quad + \Delta t \left[\left(T_y\right)_{i,j+\frac{1}{2}} \left(\mathrm{P}_{i,j+1} - \mathrm{P}_{ij}\right)^{n+1} - \left(T_y\right)_{i,j-\frac{1}{2}} \left(\mathrm{P}_{ij} - \mathrm{P}_{i,j-1}\right)^{n+1} \right] \\
& \quad + \Delta t \mathrm{Q}_{ij}^{n+1}
\end{aligned}
\qquad [3.3]
$$

Where ij is the location of the grid block, P is the pressure, T is the transmissibility, and Q is the rate for the source or sink term, and T is the transmissibility given by Equation 3.4 for the i+1/2, j interface. Similar calculations are done to obtain the transmissibilities for the other interfaces.

$$
(T_x)_{i+1/2,j} = 2\left(\frac{1}{\left({k_x h \Delta y}/{\mu \Delta x}\right)_{ij}} + \frac{1}{\left({k_x h \Delta y}/{\mu \Delta x}\right)_{i+1,j}}\right)^{-1} \qquad [3.4]
$$

Q is related to the specified source/sink pressure using Equation 3.5.

$$
Q_s = J_s (P_{wf,s} - P_{ij}) \qquad [3.5]
$$

Where "s" represents the source/sink term, J is the productivity index, P_{wf} is the specified pressure for the source/sink term, and P_{ij} is the grid block pressure.

3.2.2 Upscaling Algorithm

Upscaling begins with the definition of relevant inputs namely the grid specifications, the fine scale permeability field, k_F, initial guess(es) for the upscaled

model permeability, k_C, and the boundary conditions i.e. the definition of source and sink terms. Equation 3.3 is solved to obtain the fine scale pressures, P_F. Static averaging methods such as linear averaging (given by Equation 3.6), geometric averaging (given by Equation 3.1), and harmonic averaging (given by Equation 3.7) are used to obtain the initial guess(es) for the horizontal permeability, k_{hC}, and the vertical permeability, k_{vC}, of the upscaled model.

$$k_{ari-eff} = \frac{1}{n}\sum_{i=1}^{n} k_i \qquad [3.6]$$

$$k_{har-eff} = \frac{1}{\frac{1}{n}\sum_{i=1}^{n}\frac{1}{k_i}} \qquad [3.7]$$

We define an objective function (P_{OBJ}), given in Equation 3.8, as the sum of the square of the differences between the fine scale model and upscaled model pressure solutions.

$$P_{OBJ} = \sum (P_F - P_C)^2 \qquad [3.8]$$

Where P_F is the fine scale model pressure solution and P_C is the upscaled model pressure solution. Equation 3.8 is applicable to cases where the fine scale and upscaled models have the same number of grids, such as in Case I. In Case I, we obtain a single effective permeability while keeping the number of grids and grid sizes the same as the fine scale model. In upscaling cases that involve generating a coarse-scale permeability model (similar to Figure 3.1b), it is not possible to reconstruct the fine scale pressure at the center of the coarse scale grid block. Hence, for each coarse grid block *ij*, the

corresponding fine scale pressures, P_F^{ij}, are arithmetically averaged to obtain the coarse grid block pressure, P_{FC}^{ij}. Subsequently, P_{FC} is used in place of P_F in Equation 3.8 as shown in Equation 3.9.

$$P_{OBJ} = \sum (P_{FC} - P_C)^2 \qquad [3.9]$$

The vertical permeability of the upscaled model, k_{vC}, is iterated until the objective function is minimized below the specified tolerance. The horizontal permeability, k_{hc}, of the upscaled model is kept constant (equal to the initial estimate) during the iteration process. The summary of the upscaling algorithm is given in Figure 3.17.

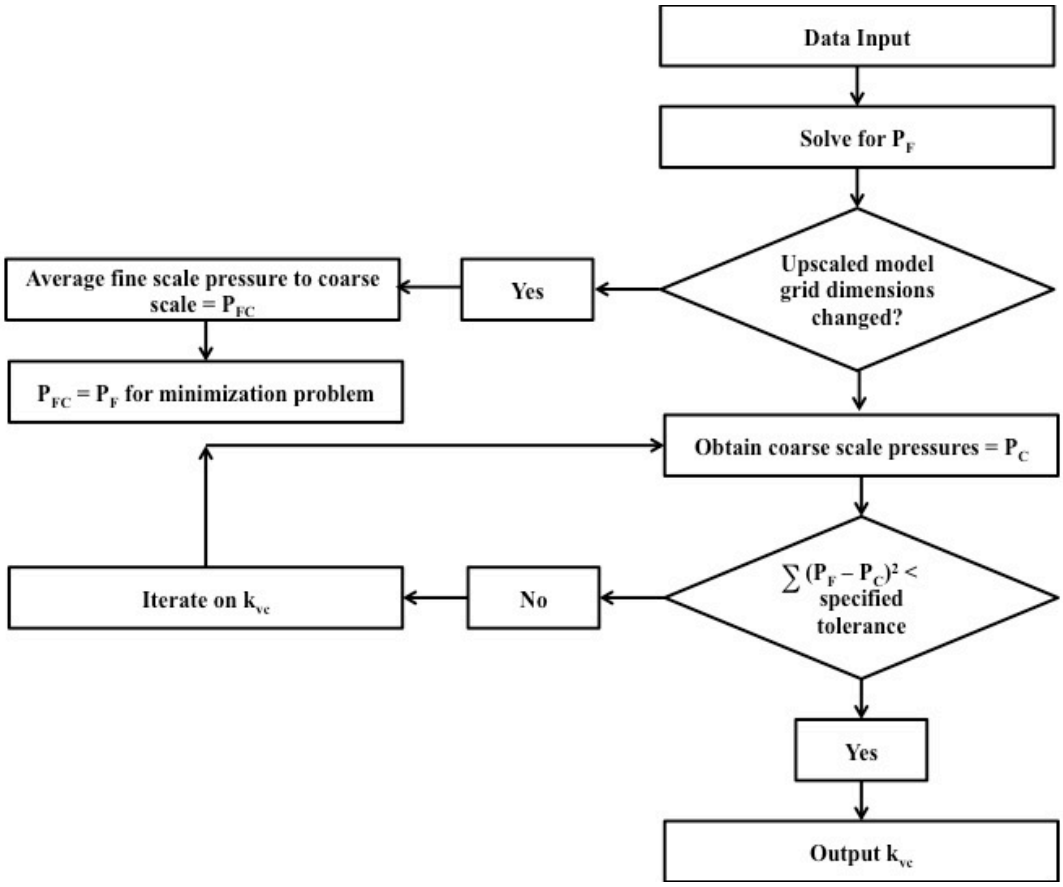

Figure 3.17: Flow Chart of Upscaling Algorithm

3.2.3 Demonstration Examples

The physics based upscaling technique is applied to Cases I and II from Section 3.1. The horizontal permeabilities for the upscaled Case I and II models were obtained by arithmetic averaging and geometric averaging, respectively. The initial guesses of the vertical permeability for the upscaled Case I and II models were obtained by harmonic averaging and geometric averaging, respectively. The effective directional permeabilities calculated using the physics-based upscaling for Case I models are given in Table 3.4. Similar to the traditional flow-based upscaling results, the k_v/k_h ratio decreases with an increase in the shale frequency from 0.83 to 0.11. The k_v/k_h ratios obtained for Models 1 and 2 using the physics-based upscaling is higher compared to that obtained using the traditional flow-based upscaling technique. The k_v/k_h ratio obtained for Model 3 using the traditional flow-based upscaling is higher compared to that obtained using the physics based upscaling technique.

Table 3.4: Effective Directional Permeabilities for Case I Models Calculated Using Physics Based Upscaling

Model	**Physics Based Upscaling**		
	k_h (mD)	k_v (mD)	k_v/k_h
Model 1	1840	1530	0.83
Model 2	1455	1011	0.69
Model 3	940	103	0.11

Comparisons of the cumulative oil production and cumulative steam injection between the base model (fine scale model) and upscaled models for Case I are presented

in Figures 3.18 – 3.23. The errors between the base models and upscaled models (shown in Table 3.5) for Models 1 and 2 have been successfully reduced from over 25% to less than 10%. The error for Model 3 has been reduced from over 70% to 51%. Although we have successfully reduced the error associated with the upscaled results for Model 3, it is still rather high, indicating that for highly heterogeneous formations (over 30% shale frequency), a coarse scale simulation model would be a better method of study compared to analytical/semi-analytical methods.

Table 3.5: Error in Upscaling for Cases I and II

Upscaling Technique	**Case I**			**Case II**	
Model	**Model 1**	**Model 2**	**Model 3**	**Model 4**	**Model 5**
Geometric Averaging	27%	61%	70%	-	-
Traditional Flow-Based	25%	61%	80%	44%	31%
Physics Based	7%	8%	51%	4%	10%

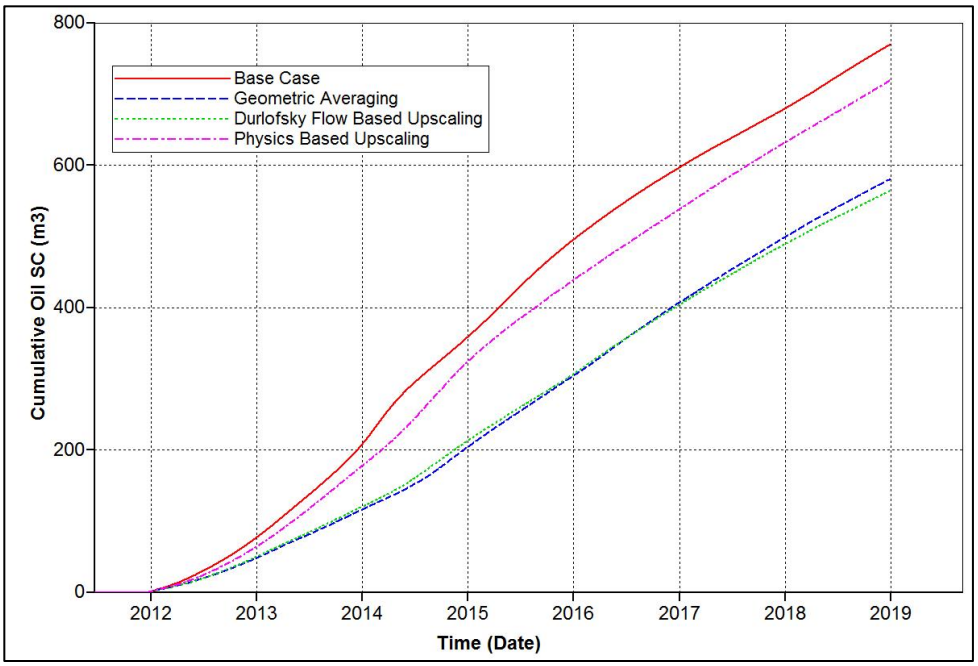

Figure 3.18: Model 1 (10% shale frequency) – Comparison of cumulative oil production between fine scale model and models upscaled using conventional techniques and physics-based upscaling.

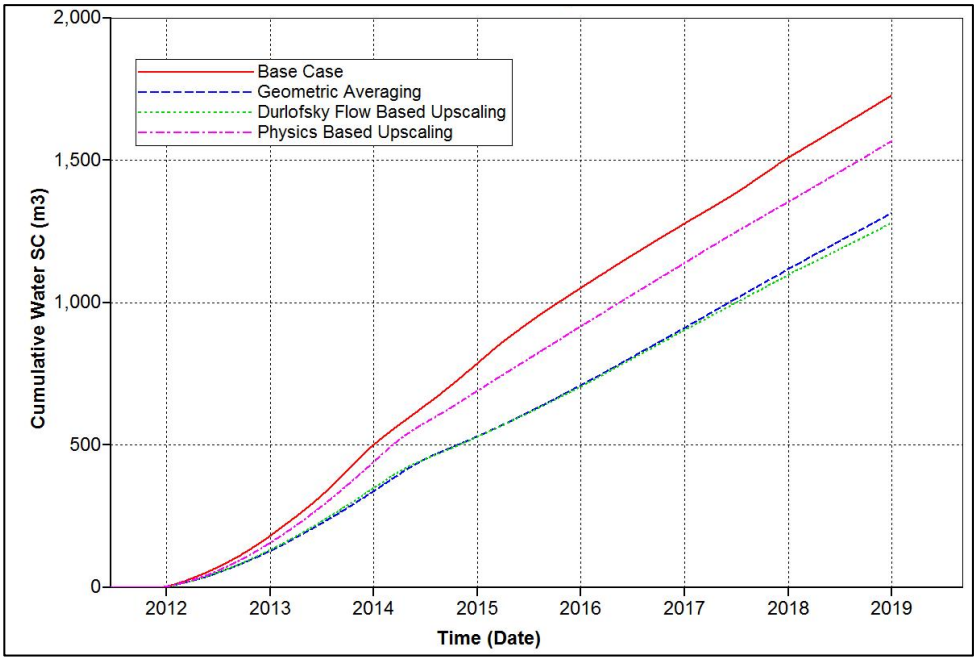

Figure 3.19: Model 1 (10% shale frequency) – Comparison of cumulative steam injection between fine scale model and models upscaled using conventional techniques and physics-based upscaling.

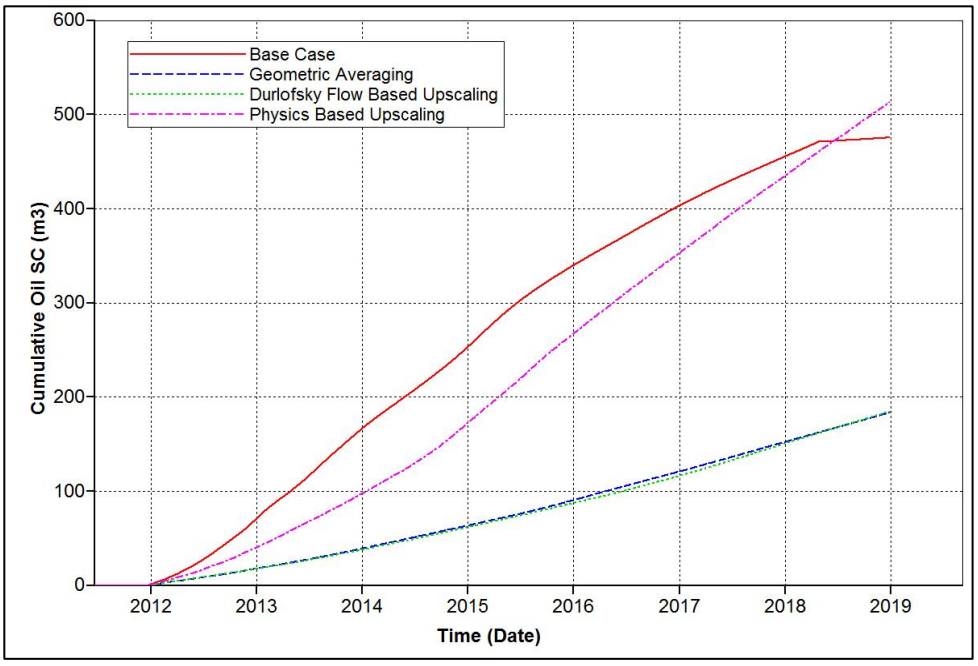

Figure 3.20: Model 2 (30% shale frequency) – Comparison of cumulative oil production between fine scale model and models upscaled using conventional techniques and physics-based upscaling.

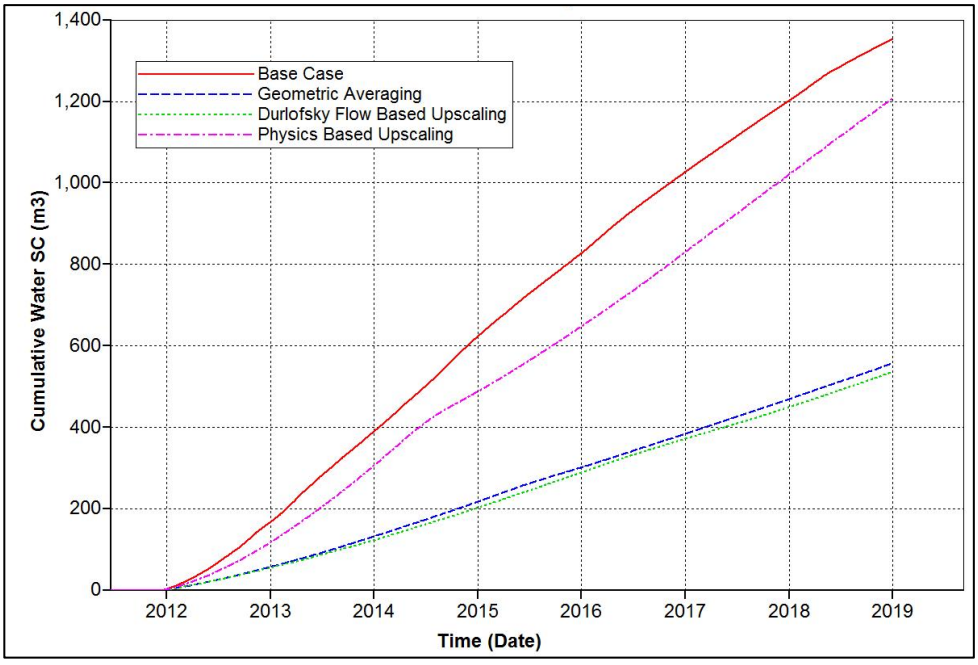

Figure 3.21: Model 2 (30% shale frequency) – Comparison of cumulative steam injection between fine scale model and models upscaled using conventional techniques and physics based upscaling.

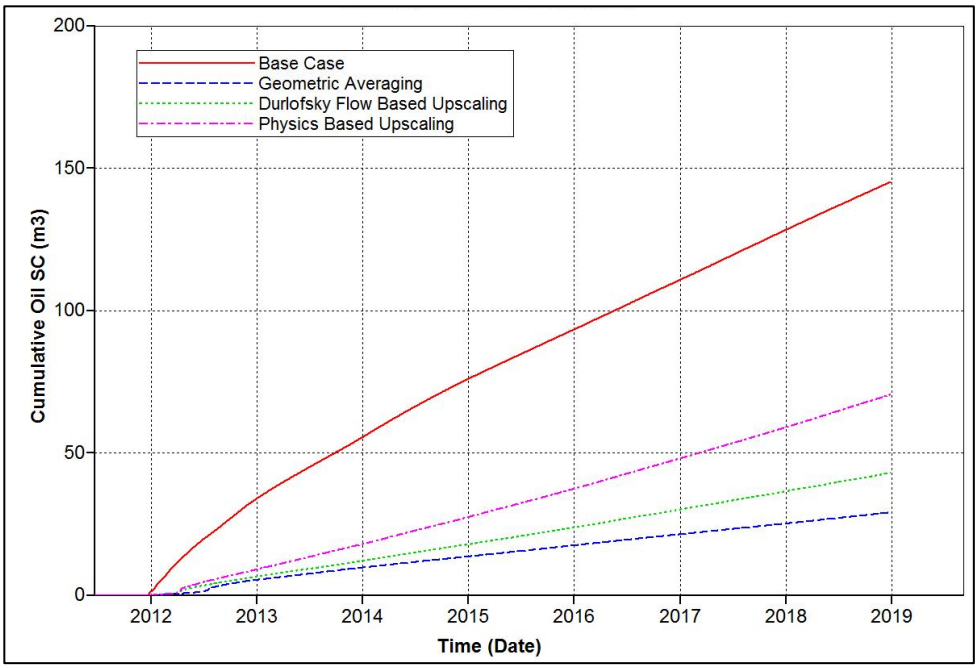

Figure 3.22: Model 3 (50% shale frequency) – Comparison of cumulative oil production between fine scale model and models upscaled using conventional techniques and physics-based upscaling.

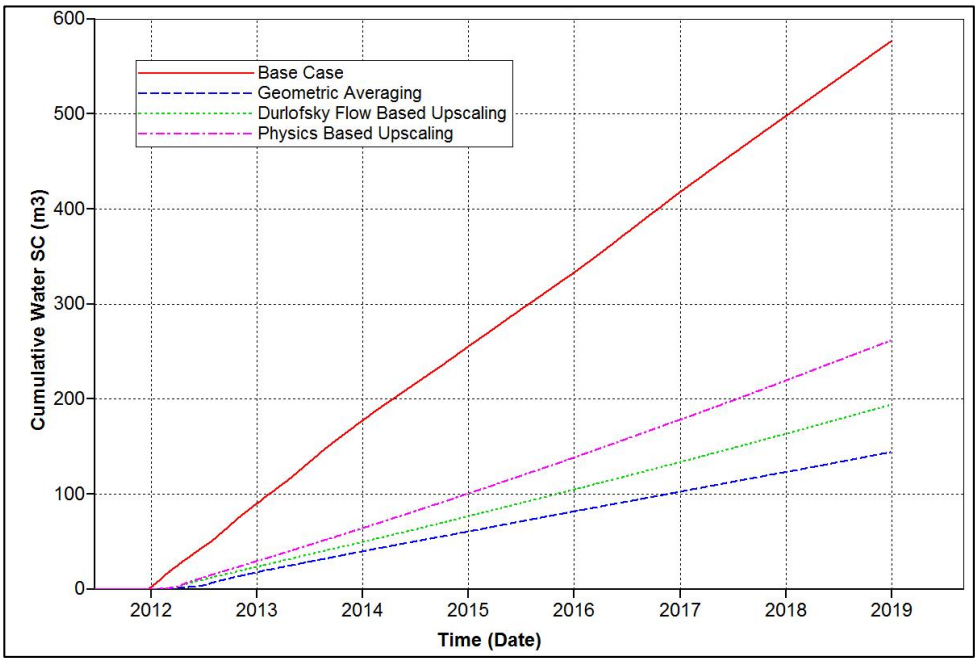

Figure 3.23: Model 3 (50% shale frequency) – Comparison of cumulative steam injection between fine scale model and models upscaled using conventional techniques and physics-based upscaling.

Comparisons of the cumulative oil production and cumulative steam injection between the base model (fine scale model) and upscaled models for Case II are presented in Figures 3.24 – 3.27. Similar to the findings of Section 3.1, the errors are less when using a coarser permeability model as opposed to a single effective permeability. The errors between the base models and upscaled models have been successfully reduced from over 30% to 10% and lower as shown in Table 3.5.

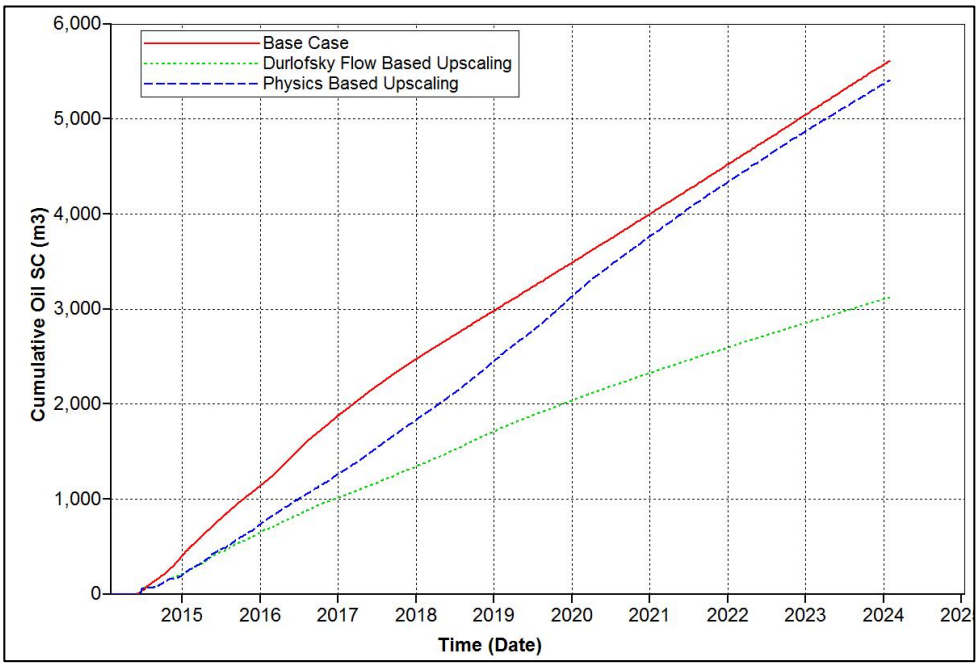

Figure 3.24: Model 4 (30% shale frequency) - Comparison of cumulative oil produced in fine scale model and models upscaled using traditional flow-based upscaling and physics-based upscaling.

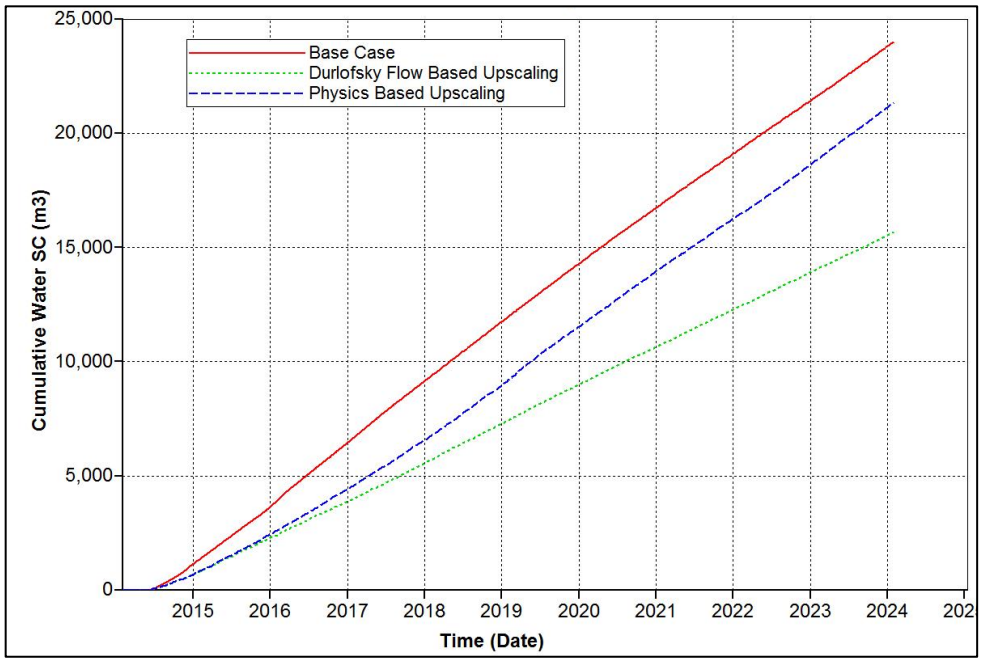

Figure 3.25: Model 4 (30% shale frequency) - Comparison of cumulative steam injected in fine scale model and models upscaled using traditional flow-based upscaling and physics based upscaling.

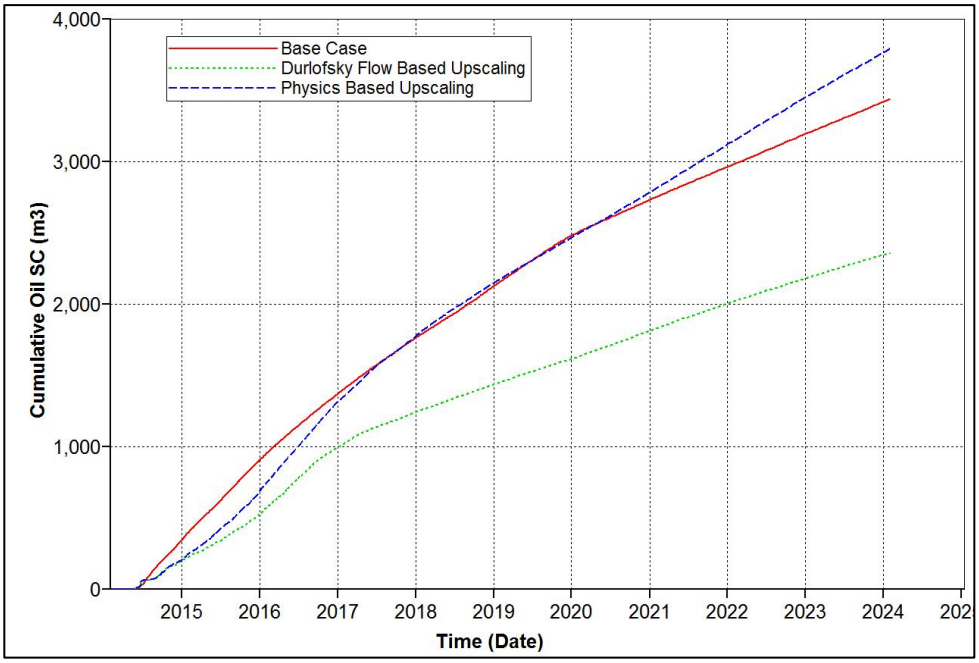

Figure 3.26: Model 5 (50% shale frequency) - Comparison of cumulative oil produced in fine scale model and models upscaled using traditional flow based upscaling and physics based upscaling.

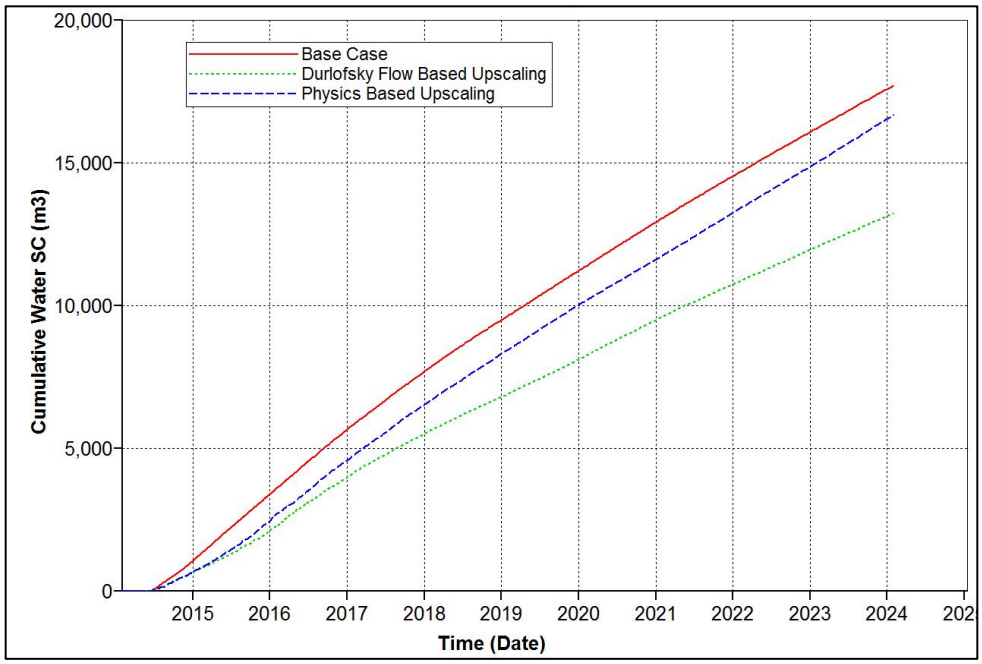

Figure 3.27: Model 5 (50% shale frequency) - Comparison of cumulative steam injected in fine scale model and models upscaled using traditional flow-based upscaling and physics based upscaling.

In Figure 3.28, we present the profile of the steam chamber for Model 4 in Case II. In this figure, we show the temperature distribution for the fine scale and upscaled models at the end of 10 years from the start of the simulation. Figure 3.28a shows the permeability distribution for the model. Figure 3.28b shows the temperature distribution for the base model. The temperature distributions from the upscaled models, traditional flow-based upscaling and physics-based upscaling, are presented in Figures 3.28c and 3.28d, respectively. It can be observed that the physics based upscaling does a fairly good job of reproducing the steam chamber growth observed in the base model compared to the traditional flow based upscaling technique.

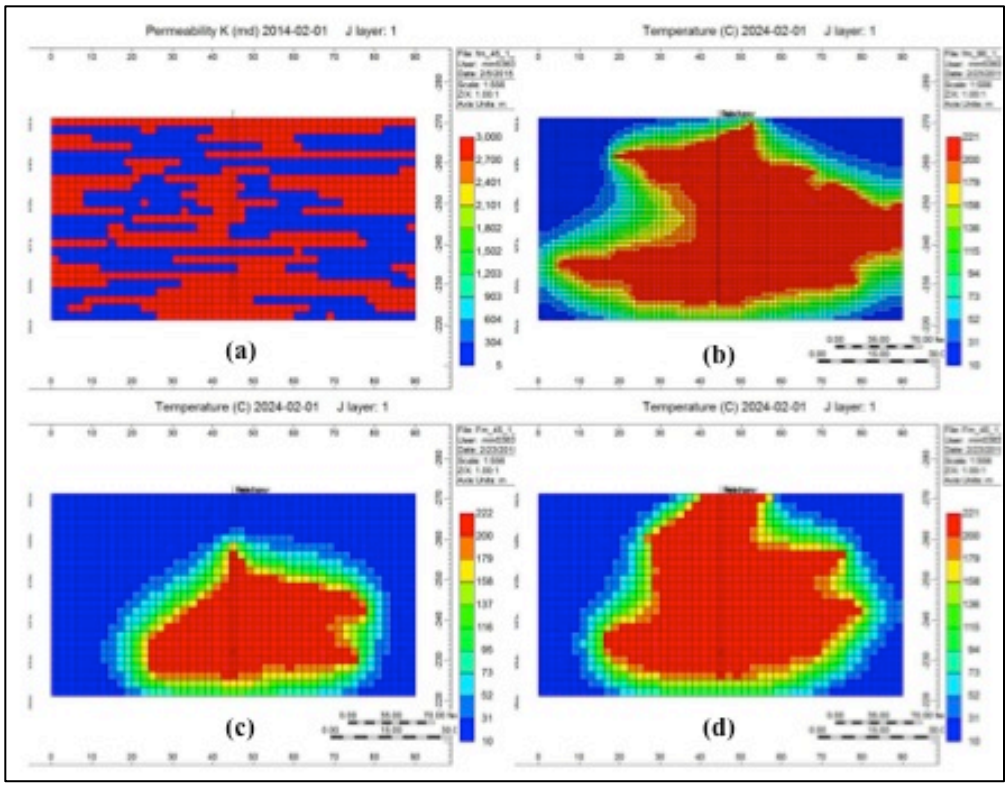

Figure 3.28: Steam chamber growth for Model 4 – (a) Permeability distribution in fine scale model (b) Steam chamber (in terms of temperature distribution) in fine scale model (c) Steam chamber in model upscaled using traditional flow-based technique (d) Steam chamber in model upscaled using physics-based technique

3.3 Chapter Summary

In this chapter, we compared two conventional upscaling techniques for permeability- based on geometric averaging and traditional flow-based upscaling, with fine scale numerical simulation. The results from the thermal simulations indicate that conventional upscaling techniques do not effectively capture the oil production and the propagation of the steam front in SAGD. A physics-based upscaling technique that simulates the convergent flow pattern observed during SAGD is proposed. This is formulated as a global upscaling technique that involves minimizing the difference

between the fine scale and upscaled model solutions. Several two dimensional stochastic shale models were generated and used to validate and illustrate the effectiveness of the method. The physics-based upscaling scheme exhibits improvement over the geometric averaging and the traditional flow based-upscaling techniques, reducing the error between the results using the fine scale and upscaled models.

In the next chapter, we discuss the development of a semi-analytical model to describe the SAGD rising phase for an isotropic and homogeneous reservoir. This model is extended in Chapter 5 for application in heterogeneous reservoirs with discontinuous shale barriers. The physics-based upscaling technique developed in this chapter will be applied to the steam rise model in heterogeneous reservoirs.

Chapter 4: Semi-Analytical Modeling of the Steam Assisted Gravity Drainage (SAGD) Rising Phase

Steam assisted gravity drainage (SAGD) consists primarily of the rising phase and the spreading phase. During the rising phase, the steam chamber grows rapidly in the vertical direction until it reaches the top of the formation. The spreading phase applies when the steam chamber has grown to the top of the formation and is expanding horizontally till it reaches the confines of the reservoir. Much of the research efforts on describing and analyzing the SAGD process have focused on the stable spreading phase, and there exist very few analytical/semi-analytical models of the unstable rising phase.

In this chapter, we present an approximate semi-analytical method based on the Myhill and Stegemeier (MS) frontal advance model, which was originally developed for application in steam drive processes, to quantitatively describe the SAGD rising phase. The chapter begins with a discussion of relevant theoretical background on the Myhill and Stegemeier frontal advance model. The Myhill and Stegemeier frontal advance model is then modified for application to the SAGD rising phase and the modified semi-analytical model is referred to as MS-SAGD. The MS-SAGD semi-analytical model tracks the growth of the steam chamber as a function of time.

Two different approaches to calculate the oil production rates are proposed and are used in conjunction with the MS-SAGD model to describe the SAGD rising phase. The proposed oil production rate models are compared with each other and with reservoir simulation results.

4.1 Theoretical Background on Myhill and Stegemeier Frontal Advance Model

Myhill and Stegemeier (1978) presented a model for steam drive correlation and prediction that combines the approach of Marx and Langenheim (1959) with the ideas of Mandl and Volek (1969). Marx and Langenheim (1959) developed theoretical relations to describe the growth of a steam zone that is limited by the loss of heat to the overburden and underburden and by the rate at which steam is introduced. Energy balance states that the total heat injected is the summation of the heat loss to the reservoir rock, heat loss to the fluids (in-situ oil and water), and heat losses to the overburden and underburden as expressed by Equation 4.1 (Green and Willhite, 1998).

$$\dot{m}_s H_s = M_R (T_s - T_r) \frac{\Delta V}{\Delta t} + 2 \int_0^{A_h} q \, dA_h \qquad [4.1]$$

In Equation 4.1, $\dot{m}_s$ is the steam injection rate, H_s is the energy content of the injected steam relative to the reservoir temperature in Btu/lb_m, M_R is the volumetric heat capacity of the heated region, and A_h is the heated area. The parameter "q" in Equation 4.1 is the instantaneous rate of conduction to overburden or underburden and is a function of $(t - \lambda)$ where t is the total time since start of injection and λ is the time of arrival of heated zone at a specific location (i.e. out to a specific area). The term on the left hand side (LHS) of Equation 4.1 represents the heat injection rate. The first term on the right hand side (RHS) of Equation 4.1 represents the heat required to raise the temperature of the reservoir rock from reservoir temperature, T_r, to steam temperature, T_s when the steam zone expands by an increment of bulk volume, ΔV. The second term on the RHS of

Equation 4.1 represents the heat loss rate from the heated zone to the overlying and underlying formations (Green and Willhite, 1998). The concept presented by the expression in Equation 4.1 is schematically shown in Figure 4.1.

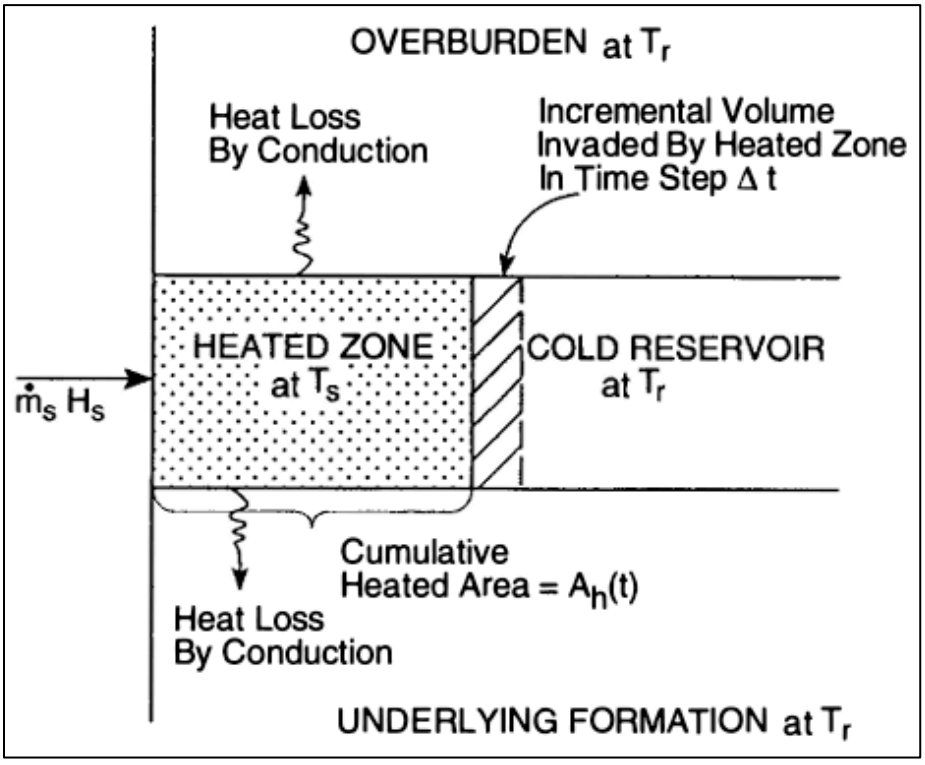

Figure 4.1: Marx and Langenheim Reservoir Heating Model (Ref: Green and Willhite, 1998).

In the development of their theoretical model, Marx and Langenheim (1959) assumed that steam is introduced at a constant rate and that no heat is transferred ahead of the steam front. A steam zone can be maintained throughout the heated region that is predicted by Marx and Langenheim's (1959) model as long as there is sufficient latent heat to keep the steam zone at a constant temperature i.e. when there is still latent heat arriving at the heat front (Green and Willhite, 1998). However, as the heated zone

expands, a time is reached when the injected steam is no longer sufficient to supply all the losses. At this time, called the critical time, t_c, the heated region separates into a steam zone and a hot water zone (Green and Willhite, 1998). A schematic of the steam drive process before the critical time is shown in Figure 4.2a. The heated region consists only of the steam zone. A schematic of the steam drive process after the critical time is shown in Figure 4.2b. The heated region now consists of a steam zone and a hot water zone.

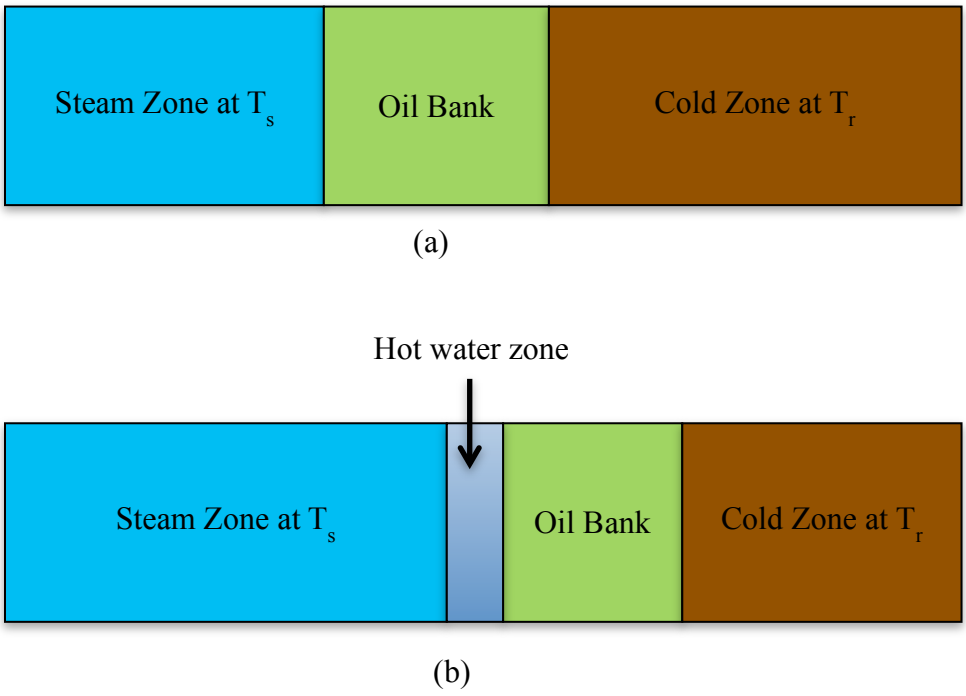

Figure 4.2: Schematic Representation of Steam Drive (a) Before critical time (b) After critical time

The critical time, t_c, when formation of a distinct hot water zone occurs was determined by Mandl and Volek (1969) from an energy balance at the condensation front. The critical time, t_c, marks an important change in the heat flow across the condensation front and depends on the reservoir thickness, temperature, and quality of the steam

(Mandl and Volek, 1969). At time, t, before the critical time ($0 < t < t_c$), the heat flow across the condensation front is purely conductive (Mandl and Volek, 1969). At time equal to the critical time ($t= t_c$), the heat flow across the condensation front becomes predominantly convective (Mandl and Volek, 1969). Thus, the equations which govern the expansion of the steam zone change at $t = t_c$ (Mandl and Volek, 1969). Though the concept of critical time is relevant to steam drive processes, it is not of importance to the SAGD rising phase as the process remains at $t < t_c$ for the entire duration of the process.

The basic assumptions in the development of the Myhill and Stegemeier frontal advance model are given below (Myhill and Stegemeier, 1978):

1. The reservoir is horizontal, isotropic and homogeneous with constant thickness, H.
2. Thermal properties, including initial formation temperature, heat capacity of reservoir rock, and heat capacity and conductivity of cap and base rock are assumed constant throughout the zone.
3. Steam is injected at a constant pressure, quality, and rate per injector.
4. Vertical temperature gradients in the reservoir are zero.
5. Temperature of the heated zone is uniform and equal to the injected fluid temperature, while the regions outside the heated zone are at the initial reservoir temperature.
6. The temperature front is sharp and vertical and defines the boundary at which the temperature falls from injection temperature to formation temperature.

7. Heat losses from the steam zone are by conduction only and occur normal to the reservoir into the cap and base rock.
8. Heat is transferred in the reservoir by convection only, and heat passes through the condensation front only after Mandl and Volek's critical time.

The volume of the steam zone predicted by the Myhill and Stegemeier model before critical time, t_c, is given by Equation 4.2 (Green and Willhite, 1998) and is a function of the heat injected, the volumetric heat capacity of the heated region, and the thermal efficiency of the process.

$$V_s = \frac{\dot{m}_s H_s t}{M_R(T_s - T_r)} E_h(t_D) \qquad [4.2]$$

Where V_s is the volume of the steam zone, E_h is the thermal efficiency, t is time, and t_D is the dimensionless time for heat transfer. The enthalpy of the steam entering the formation, H_s, is given by Equation 4.3 (Green and Willhite, 1998).

$$H_s = H_{wt} + f_{sd} L_{vdh} - H_{wr} \qquad [4.3]$$

Where H_{wt} is the enthalpy of saturated water at steam temperature, H_{wr} is the enthalpy of water at reservoir temperature, f_{sd} is the steam quality at the injection well, and L_{vdh} is the latent heat of vaporization at sandface. The thermal efficiency, E_h, is given by Equation 4.4 and is a function of the dimensionless time, t_D, given by Equation 4.6 (Green and Willhite, 1998).

$$E_h = \frac{G(t_D)}{t_D} \qquad [4.4]$$

The parameter G (t_D) in Equation 4.4 is given by Equation 4.5 (Green and Willhite, 1998).

$$G(t_D) = \left(e^{tD} erfc\left(\sqrt{t_D}\right) + 2\sqrt{\frac{t_D}{\pi}} - 1 \right) \quad [4.5]$$

$$t_D = \frac{4(M_s)^2 \alpha t}{(M_R)^2 H^2} \quad [4.6]$$

In Equation 4.6, M_s is the volumetric heat capacity of the over burden and under burden, α is the thermal diffusivity of the over burden and under burden, M_R is the volumetric heat capacity of the heated region and H is the reservoir thickness. The dimensionless time is defined in terms of the relative heat loss to the over/underburden as compared to the heated reservoir interval.

The critical dimensionless time, t_{cD}, is a function of the steam temperature and quality only and is given by Equation 4.7 (Green and Willhite, 1998).

$$e^{t_{cD}} erfc\sqrt{t_{cD}} = 1 - f_{hv} \quad [4.7]$$

In Equation 4.7, f_{hv} is the fraction of injected energy in the form of latent heat and is given by Equation 4.8 (Green and Willhite, 1998).

$$f_{hv} = \frac{f_{sd} L_{vdh}}{H_s} \quad [4.8]$$

The critical time, t_c, is calculated given the critical dimensionless time, t_{cD}, using Equation 4.9 (Green and Willhite, 1998). If the thickness of the formation changes, the critical time changes.

$$t_{cD} = \frac{4(M_s)^2 \alpha t_c}{(M_r)^2 H^2} \quad [4.9]$$

As indicated earlier, the critical time is not reached in SAGD and $t < t_c$ at all times during the rising phase.

In the next section, we discuss the modification of the Myhill and Stegemeier frontal advance model to apply it to the SAGD rising phase.

4.2 Application of Myhill and Stegemeier Frontal Advance Model to Steam Assisted Gravity Drainage (SAGD) Rising Phase

In the previous section, we reviewed the Myhill and Stegemeier frontal advance model and presented the assumptions that apply in the development and application of the model. For steam drive processes, the model assumes a piston like displacement with a constant reservoir thickness, H. During the SAGD rising phase, the steam chamber grows very rapidly in the vertical direction. The process during this stage is thermally efficient as all of the latent heat released by the condensation of the steam is directed to heating the heavy oil/bitumen at the edges of the steam chamber (Chakrabarty et al., 2006). This results in an expansion of the steam zone horizontally and vertically as the steam chamber grows. The width of the steam zone/chamber in SAGD is thus not a constant value but increases with time as the steam chamber grows and will need to be modified accordingly in the Myhill and Stegemeier theoretical model to apply the model to the SAGD rising phase. A simple schematic to illustrate the differences between the steam drive process and the SAGD rising phase is given in Figure 4.3. The horizontal steam drive process shown in Figure 4.2a is rotated and made vertical as shown in Figure 4.3a. In comparison, a simple schematic of the SAGD process is presented in Figure 4.3b.

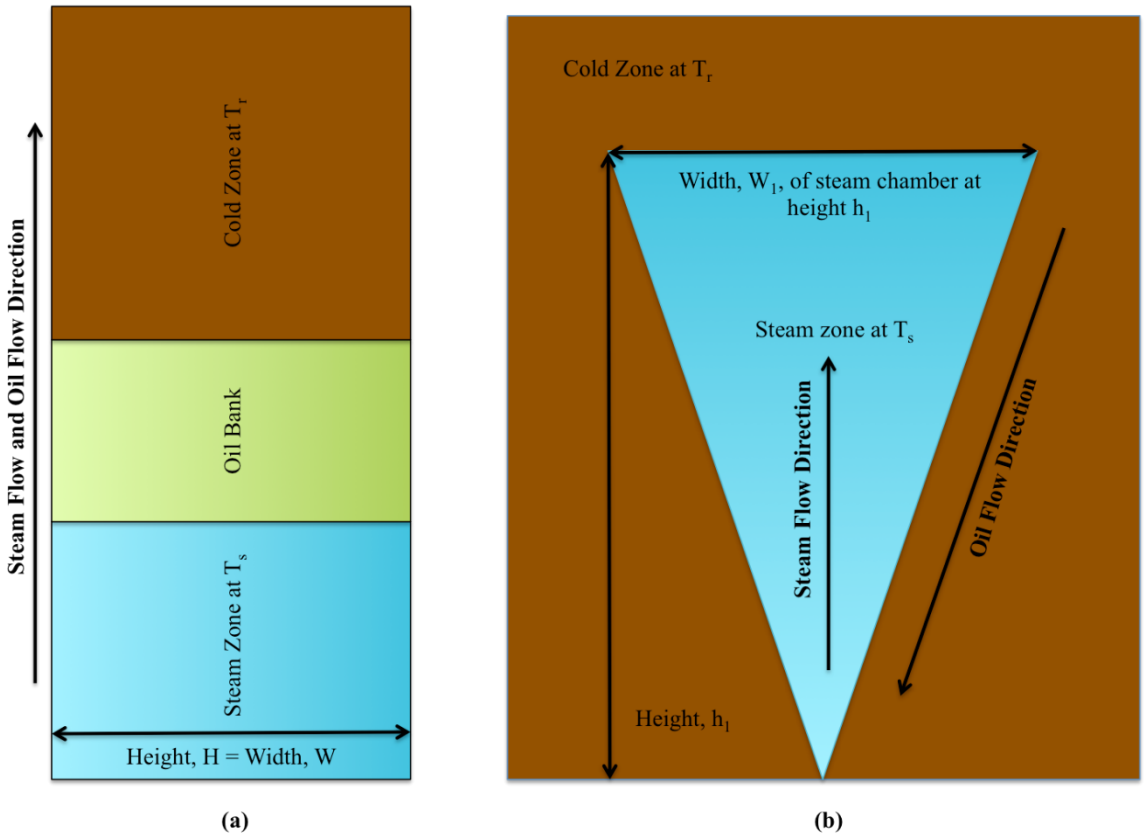

Figure 4.3: Schematic of (a) Steam Drive and (b) SAGD

The modified Myhill and Stegemeier model for SAGD application will be referred to as MS-SAGD. The primary difference between the original Myhill and Stegemeier frontal advance model and the MS-SAGD semi-analytical model is the width, W, input in the model. A constant reservoir thickness (H), is used in the original Myhill and Stegemeier frontal advance model whereas a variable width that is a function of time, W(t), as shown in Figure 4.4, is used in the MS-SAGD semi-analytical model. Figure 4.4 shows the growth of the steam zone/chamber assuming a piston like displacement. The area of cross section over which the piston advances is no longer a constant but expands

with time as the width, W, of the steam zone/chamber increases with time (as shown in Figure 4.4).

The MS-SAGD semi-analytical model is based on an energy balance and does not capture the impact of gravity on the rise of the injected steam although the impact of gravity on the heated oil flow is accounted for in the oil production models (that will be discussed in the subsequent sections). It should be noted that the reservoir thickness, H, used in the Myhill and Stegemeier theoretical relation is equivalent to the width, W, of the steam chamber in SAGD. In the next subsection, we discuss in detail the development of the MS-SAGD semi-analytical model.

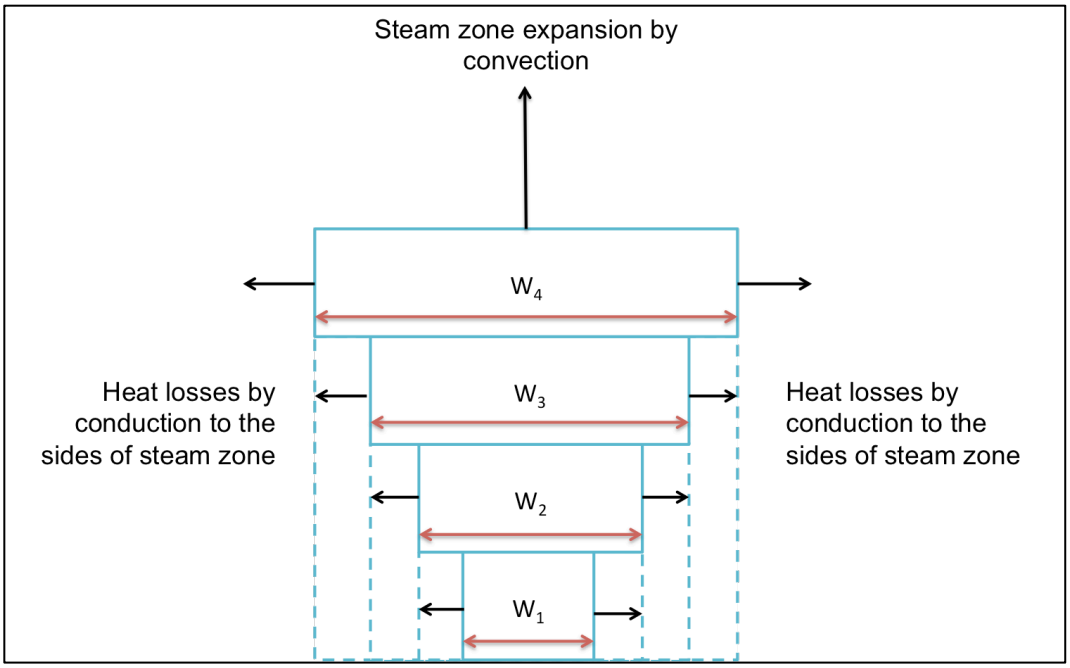

Figure 4.4: Modeling SAGD rising phase using Myhill and Stegemeier model with variable width input.

4.2.1 MS-SAGD Semi-Analytical Model

Similar to the original assumption of the Myhill and Stegemeier frontal advance model, the MS-SAGD semi-analytical model assumes a piston like displacement; however, the area of cross section over which the piston advances is no longer a constant but expands with time. Since the width, W, of the steam chamber is an unknown and changes with time along with the height of the steam chamber, an iterative approach is taken to solve for the heated volume and determine the width and height of the steam chamber as a function of time. In the development of his model for the SAGD rising phase, Butler (1991) assumed that the shape of the steam chamber is approximately a sector of a circle inclined at an angle of 64° from the horizontal. This assumption is relaxed in the MS-SAGD semi-analytical model and the shape of the steam chamber is not fixed but obtained through a simple energy balance that is given by Equation 4.10 which states that the heat loss to the sides of the steam chamber, Q_{loss}, is simply the heat injected, Q_{inj}, minus the heat required to raise the temperature of the reservoir rock from reservoir temperature, T_r, to steam temperature, T_s when the steam zone expands by an increment of bulk volume, Q_{rise}.

$$Q_{loss} = Q_{inj} - Q_{rise} \quad [4.10]$$

Equation 4.11 gives the expression for Q_{rise}.

$$Q_{rise} = M_R(T_s - T_r)\Delta V \quad [4.11]$$

The rate of growth of the heated zone, given by Equation 4.12 (Green and Willhite, 1998), is modified to obtain the expression for the incremental bulk volume ΔV (given in Equation 4.13) needed to solve Equation 4.11.

$$\frac{dA_h}{dt} = \frac{\dot{m}_s H_s}{M_R(T_s - T_r)h} e^{t_D} erfc\sqrt{t_D} \quad [4.12]$$

$$\Delta V = \frac{\dot{m}_s H_s}{M_R(T_s - T_r)} e^{t_D} erfc(\sqrt{t_D})\Delta t \quad [4.13]$$

The dimensionless time, t_D, in equation 4.13 is given by Equation 4.6 and is a function of the width, W, of the steam zone.

The heat required to raise the temperature of the reservoir rock from reservoir temperature to steam temperature when the steam zone expands by an increment of bulk volume, Q_{rise}, is a function of the width, W_{new}, that is needed to determine the dimensionless time, t_D, in Equation 4.13. However, W_{new} given by Equation 4.14 is obtained by adding the incremental width, W_{inc}, arising from heat losses to the sides of the steam chamber to the width of the steam chamber from the previous time step, W_{prev}.

$$W_{new} = W_{prev} + W_{inc} \quad [4.14]$$

The incremental width, W_{inc}, is a function of Q_{loss} and is given by Equation 4.15.

$$W_{inc} = \frac{Q_{loss}}{M_R(T_s - T_r)L_{well}h} \quad [4.15]$$

It is thus an iterative process such that the width used in the calculation of Q_{rise} is equal to that obtained from Equation 4.14. An illustration of the iterative concept presented in Equation 4.10 is presented in Figure 4.5. Figure 4.5a shows the various heat transfer terms in Equation 4.10. The iterative changes to the steam chamber shape are shown in Figure 4.5b.

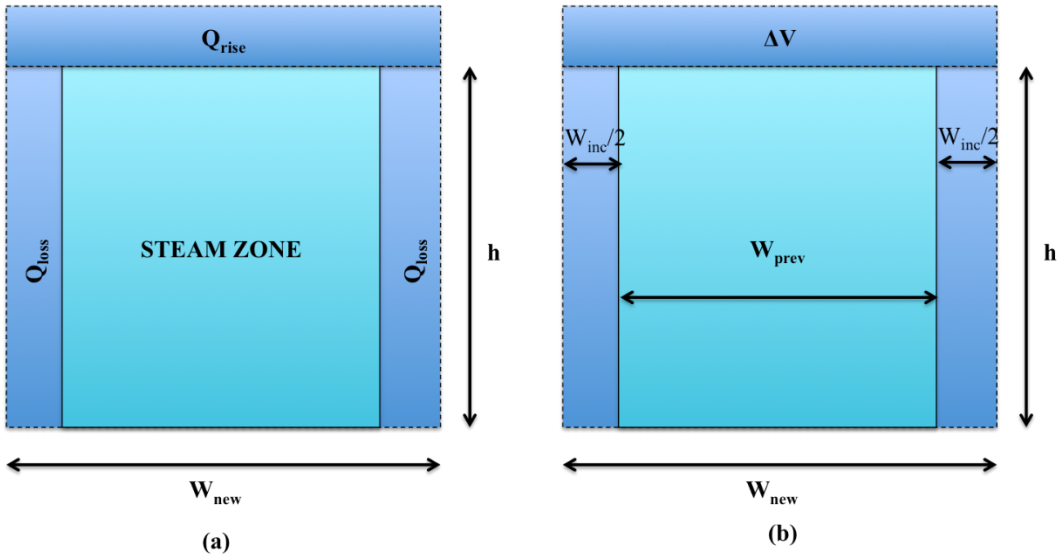

Figure 4.5: Modeling Steam Chamber Expansion in the MS-SAGD Semi-Analytical Model (a) Distribution of injected heat (b) Expansion of steam chamber

The MS-SAGD model algorithm can be divided into two primary steps. The algorithm for Step 1 is given in Figure 4.5. The algorithm begins with an initial guess for the width, W_{rise}, which is used to calculate the dimensionless time, t_D, and obtain the incremental bulk volume ΔV and Q_{rise}. We then solve for the heat losses, Q_{loss} and the incremental width arising because of steam expansion, W_{inc}. W_{new} is calculated using Equation 4.14 and checked against the initial guess, W_{rise}. The iteration continues until

the square of the difference between the W_{rise} and W_{new} is below a specified error tolerance.

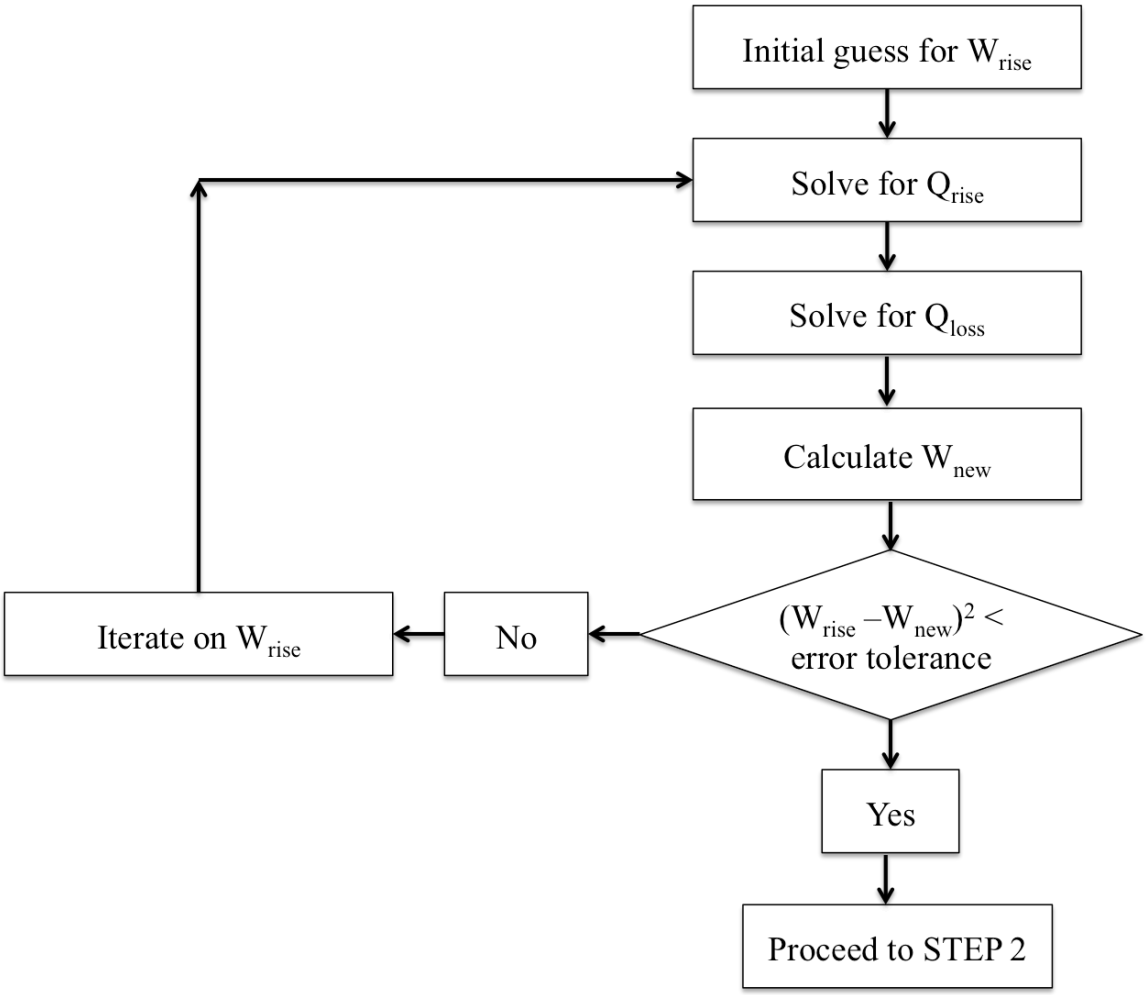

Figure 4.6: Algorithm for Step 1 of MS-SAGD Model

The algorithm for Step 2 is given below:

I. Solve for the height of steam chamber.

II. Solve for the oil production rate (will be discussed in Section 4.2.2).

III. Proceed to next time step.

The MS-SAGD semi-analytical model tracks the growth of the steam chamber as a succession of rectangular rings of increasing width. The outputs from the model, the steam chamber height and width, are used in the models given in the next section to estimate the oil production rates during the SAGD rising phase.

4.2.2 Oil Production Rate Models Used in Conjunction with MS-SAGD

The MS-SAGD semi-analytical model described in the previous section tracks the steam chamber growth as a function of time. The outputs from the model, the height and/or width of the steam chamber as a function of time, are used as inputs in two oil production rate models that are proposed for the SAGD rising phase. The two models are discussed in the subsections below.

4.2.2.1 Model 1: Oil Production Rate Based on Darcy's Law

The first model proposed for the oil production rate is based on Darcy's law and is similar to Butler's (1987) approach to model the oil production rate in his rising steam finger theory. The oil flow is assumed to be parallel to the steam chamber interface as shown in Figure 4.6. The interface is inclined to the horizontal at an angle, θ, which is a function of time and is obtained from the MS-SAGD semi-analytical model using the height and width of the steam chamber.

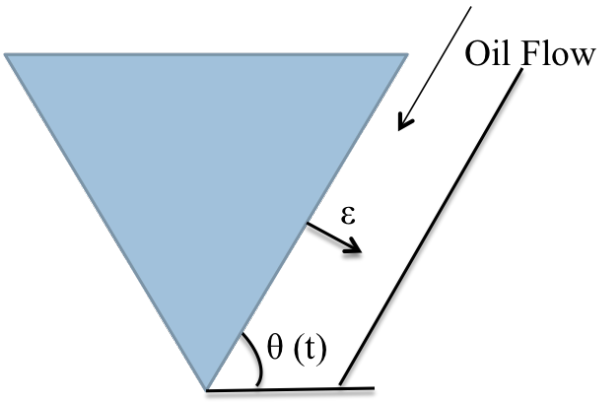

Figure 4.7: Model for SAGD Rising Phase

According to Darcy's law, the flow rate through an incremental area, dA, normal to the direction of flow (shown in Figure 4.7), is given by Equation 4.16.

$$dq_o = -\frac{kk_{ro}}{\mu_o}\left(\partial P/_{\partial y} - \rho_o g\right) sin\theta d\varepsilon \qquad [4.16]$$

Equation 4.16 can be written as given in Equation 4.17.

$$dq_o = -\frac{kk_{ro}\rho_o}{\mu_o}\left(\frac{1}{\rho_o}\partial P/_{\partial y} - g\right) sin\theta d\varepsilon \qquad [4.17]$$

Rearranging equation 4.17 and integrating results in Equation 4.18 for the oil production rate (Butler, 1987).

$$q_o = kk_{ro}(g - \frac{1}{\rho_o}\frac{\partial P}{\partial y}) \sin\theta \int_0^{\varepsilon_1} \frac{d\varepsilon}{\nu_o} \qquad [4.18]$$

Where k is the absolute permeability, k_{ro} is the relative permeability to the flow of oil, ν_o is the kinematic viscosity of oil, ρ_o is the oil density, ε is the distance measured along the normal from the steam chamber interface, and $\frac{\partial P}{\partial y}$ is the pressure gradient in the steam phase and is given by Equation 4.19 similar to the expression by Butler (1987). In his

model, Butler assumes $\frac{\partial P}{\partial y}$ to be a function of the steam finger width and to be a constant value. In Equation 4.19, we use the width of the steam chamber instead of the steam finger width. Also, since the width of the steam chamber is no longer a constant, $\frac{\partial P}{\partial y}$ changes with time as the width changes.

$$\frac{\partial P}{\partial y} = \frac{m_s \mu_g}{k k_{rg} w(t)} + \rho_g g \qquad [4.19]$$

Where k_{rg} is the relative permeability for steam flow. The integral in Equation 4.18 can be evaluated knowing the temperature gradient and the dependence of viscosity on temperature and is given by Equation 4.20 (Butler, 1987). In the derivation of Equation 4.20, it is assumed that the temperature varies linearly with distance (Butler, 1987).

$$\int_0^{\varepsilon_1} \frac{d\varepsilon}{\nu_o} = \frac{\sqrt{\pi \alpha t}}{(m+1)\nu_{oS}} \qquad [4.20]$$

4.2.2.2 Model 2: Oil Production Rate Based on Modification of Butler's Semi-Analytical Model for the Spreading Phase

In the derivation of his model for the SAGD rising phase, Butler (1991) differentiated the equation for the cumulative oil production during the SAGD rising phase (given by Equation 2.3) to obtain an expression for the production rate during the rising phase that is a function of the height and differential change in height with time. He equated this rate expression to his analytical model for the spreading phase to obtain an expression for the height, h, of the steam chamber as a function of time.

The second model proposed for the estimation of the oil production rate is based on this approach of Butler's (1991) and is obtained by modifying Butler's model for the spreading phase by making the height a function of time instead of a constant value. In his original theoretical relationship for the spreading phase, the height of the steam chamber is kept constant. For the rising phase, the height is no longer constant but a function of the rise time that is obtained from the MS-SAGD semi-analytical model. Equation 4.19 gives the proposed model for the oil production rate that includes the modification to the height variable. In Equation 4.21, the effective permeability of oil is used to estimate the oil production rate instead of the absolute permeability.

$$q_o = 2\sqrt{\frac{1.5\phi\Delta S_o k k_{ro} g \alpha h(t)}{m v_{os}}} \qquad [4.21]$$

4.3 Validation of MS-SAGD and Proposed Oil Production Rate Models

Thus far, we have discussed the development of the MS-SAGD semi-analytical model and proposed two oil production rate models to describe the SAGD rising phase. It is however necessary to verify that the process physics is represented well by these models. We thus compare the output from the proposed models to results obtained from reservoir simulation using CMG-STARS^{TM}. The steam chamber rise time (i.e. the time it takes for the steam chamber to rise to the top of the formation) estimated using the MS-SAGD semi-analytical method is also compared to the output from Butler's (1987) model, given by Equation 2.6, and Murtaza and Dehghanpour's (2012) "Corrected Butler" model, given by Equation 2.10, that estimate the steam chamber velocity. The

results from the proposed oil production rate Models 1 and 2 are also compared with the output from Butler's (1991) oil production rate model given by Equation 2.5. These model verification cases and results are discussed in the sections below.

4.3.1 Model Setup and Input Parameters

To validate the proposed models, two-dimensional, isotropic and homogeneous reservoir simulation models containing 150 by 1 by 100 grid blocks with grid sizes of 0.5m by 1m by 0.5m in the x, y, and z directions, respectively, were created in CMG-STARS^{TM}. Three validation cases are presented in Table 4.1 along with the model permeability and average cold water equivalent (CWE) steam injection rate. In the reservoir simulator, the injection wells were specified to be on a pressure constraint, thereby keeping the steam injection temperature and pressure constant and allowing the injection rates be a function of the reservoir permeability. This allows us to implicitly model the impact of permeability on the predictions using the MS-SAGD semi-analytical model. The steam injection rates used in the validation of the MS-SAGD model were obtained by linearly averaging the daily steam injection rates from the simulator over the period of the rising phase estimated by the simulator.

Table 4.1: Validation Cases for MS-SAGD and Oil Production Rate Models

Case	Permeability (mD)	Avg. Steam Injection Rate (CWE m^3/day)
Case 1	1500	0.65
Case 2	2000	0.85
Case 3	2500	1.05

Relevant input parameters for the reservoir simulation models are given in Table 4.2.

Table 4.2: CMG-STARS™ Input Parameters for Validation Cases 1 - 3

Description	Value	Units
Reservoir thickness (h)	50	M
Porosity (φ)	30	%
Thermal conductivity of rock (K_{rock})	2.74E5	J/(m-day-°C)
Thermal conductivity of water (K_{water})	56160	J/(m-day-°C)
Thermal conductivity of oil (K_{oil})	13400	J/(m-day-°C)
Volumetric heat capacity of reservoir (M_S)	2.35E6	J/(m^3-°C)
Initial reservoir temperature (T_r)	10	°C
Maximum injection BHP	2400	kPa
Steam injection quality	0.8	-
Steam temperature (T_s)	220	°C
Minimum production well BHP	1500	kPa

Relevant input parameters for the analytical and semi-analytical models mentioned earlier and used in the validation are given in Table 4.3.

Table 4.3: Input Parameters for Analytical and Semi-Analytical Models

Parameter	Value	Units
Movable oil saturation (Δs_o)	0.50	
Thermal diffusivity (α)	5.08E-7	m^2/sec
Volumetric heat capacity of heated region (M_r)	2.14E6	J/(m^3-°C)
Volumetric heat capacity of surrounding region (M_s)	2.35E6	J/(m^3-°C)
Kinematic viscosity of flowing oil (v_{os})	9.37E-6	m^2/sec
Flowing oil density (ρ_o)	855.8	Kg/m^3
Relative permeability of oil (K_{ro})	0.58	
Relative permeability of steam (K_{rg})	0.2	
Viscosity exponent (m)	3.8097	

The volumetric heat capacity of the heated region, M_R, was calculated using Equation 4.22 (Green and Willhite, 1998).

$$M_R = (1-\varphi)\rho_r C_r + \varphi S_o \rho_o C_o + \phi S_w \rho_w C_w + \phi S_g \rho_s C_s \quad [4.22]$$

Where C_r, C_o, C_w, and C_s are the heat capacities at constant pressure for the rock, oil, water, and steam, respectively, and ρ_r, ρ_o, ρ_w, and ρ_s are the densities of the rock, oil, water, and steam, respectively. A nonlinear mixing rule, given by Equation 4.23, is used to obtain the overall thermal conductivity from phase values in CMG-STARS™ reservoir simulator (CMG, 2014). The nonlinear option accounts for the complicated distribution of different phases in the reservoir, such as water wetting the rock (CMG, 2014). The same non-linear rule was used to calculate the thermal conductivity of the composite rock for estimation of the thermal diffusivity..

$$k_{composite} = KL * a^b \quad [4.23]$$

Where KL is given by Equation 4.24, Equation 4.25 gives the parameter "a", and the parameter "b" is given by Equation 4.26 (CMG, 2014).

$$KL = \frac{(S_o K_{oil} + S_w K_{water})}{S_o + S_w} \quad [4.24]$$

$$a = \frac{K_{rock}}{KL} \quad [4.25]$$

$$b = 0.28 - 0.757 \log(\varphi) - 0.057 \log(a) \quad [4.26]$$

The heat capacities of the hydrocarbon oil, water, and steam are calculated using Equations 4.27 (Butler, 1991), 4.28 (Green and Willhite, 1998), and 4.29 (Green and Willhite, 1998), respectively

$$C_o = 1.605 + 0.004361T - 4.046\times10^{-6}T^2 \quad [4.27]$$

$$C_w = \frac{H_{wT} - H_{wr}}{T_s - T_r} \quad [4.28]$$

Where H_{wT} is the enthalpy of saturated water at steam temperature, T_s, and H_{wr} is the enthalpy of water at initial reservoir temperature, T_r.

$$C_s = C_w + \frac{L_v}{T_s - T_r} \quad [4.29]$$

4.3.2 Results and Discussion

The time it takes for the steam chamber to rise to the top of the formation for the three validation cases are shown in Figure 4.7. Given in the figure are the outputs from CMG-STARS™ simulator, MS-SAGD semi-analytical model, Butler's (1987) analytical model, and Murtaza and Dehghanpour's (2012) "Corrected Butler" model. The solutions from Butler's (1987) and Murtaza and Dehghanpour's (2012) models underestimate the steam chamber rise velocity, resulting in longer steam chamber rise times as shown in Figure 4.7. These results are in agreement with the findings of Murtaza and Dehghanpour (2012). The results from the MS-SAGD semi-analytical model are in good agreement with the output from the simulator.

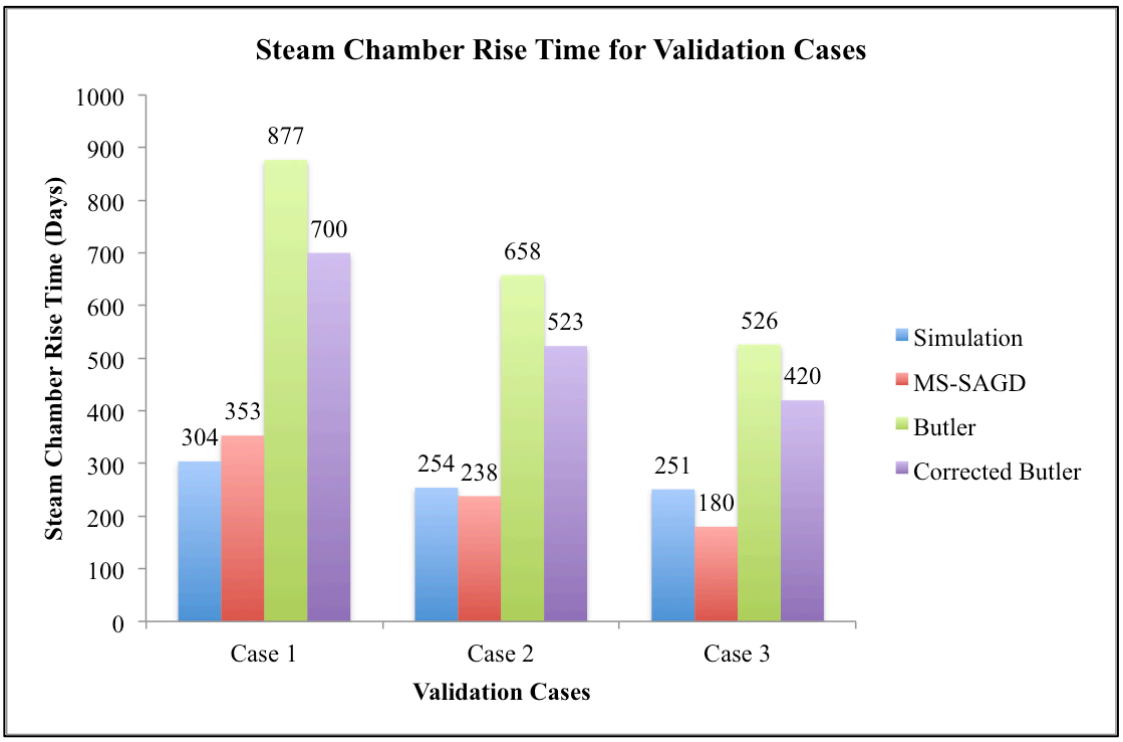

Figure 4.8: Steam Chamber Rise Times for Validation Cases 1 – 3

A comparison of the outputs, cumulative oil production and oil production rates, from the proposed oil production rate Models 1 and 2, Butler's (1991) model, and CMG-STARS^{TM} simulation are given in Figures 4.8 – 4.13. The stopping time for the calculation of the oil production are determined by the steam chamber rise times that are shown in Figure 4.7. As a result of this, the curves do not all end at the same time but rather at the time the steam chamber is predicted to reach the top of the formation using the particular model. The following observations can be made from the comparison plots:

- The proposed oil production rate Models 1 and 2 perform comparatively better than Butler's (1987) oil production rate model.
- The output from the proposed oil production rate Models 1 and 2 compare well with the results from CMG-STARS^{TM} simulation.
- Proposed Models 1 and 2 give similar results for the cumulative oil production, but Model 2 performs better in describing the behavior of the oil production rates observed in CMG-STARS^{TM} simulation.
- Oil rate prediction using Model 1 basically presumes that the steam rise is an unstable process resulting in steam fingers. This is somewhat incompatible with the frontal displacement model assumed in MS-SAGD. The formulation for oil rate in Model 2 on the other hand is completely compatible with the assumptions of the MS-SAGD model. In both these models, however, the model for temperature rise is dissociated from the model for oil drainage and this decomposition may be the reason for the departure from the CMG results.

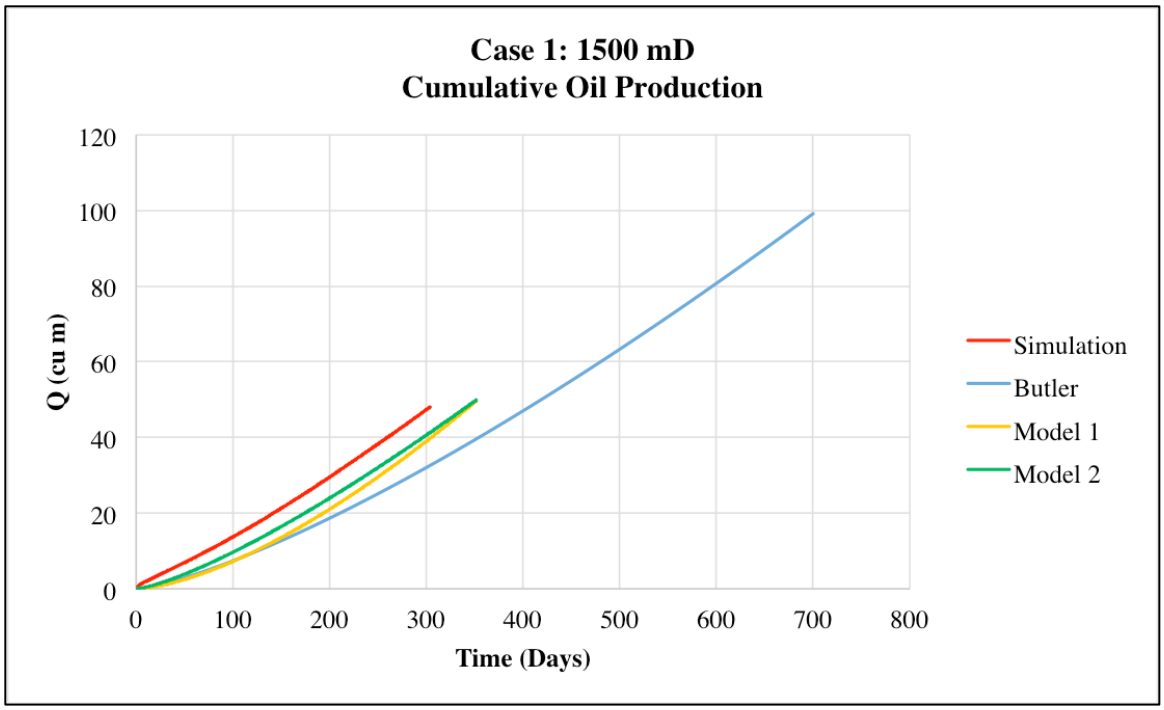

Figure 4.9: Case 1: Comparison of cumulative oil production output from CMG-STARS™ simulation, Butler's model, and proposed Models 1 and 2.

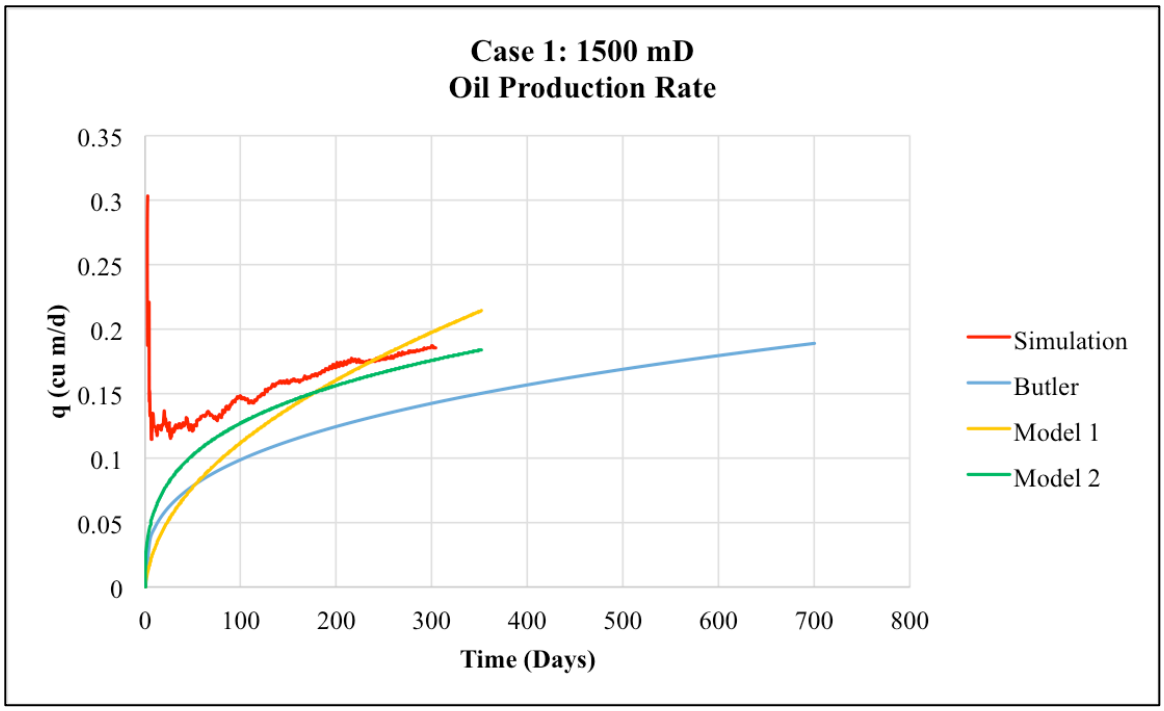

Figure 4.10: Case 1: Comparison of oil production rates output from CMG-STARS™ simulation, Butler's model, and proposed Models 1 and 2.

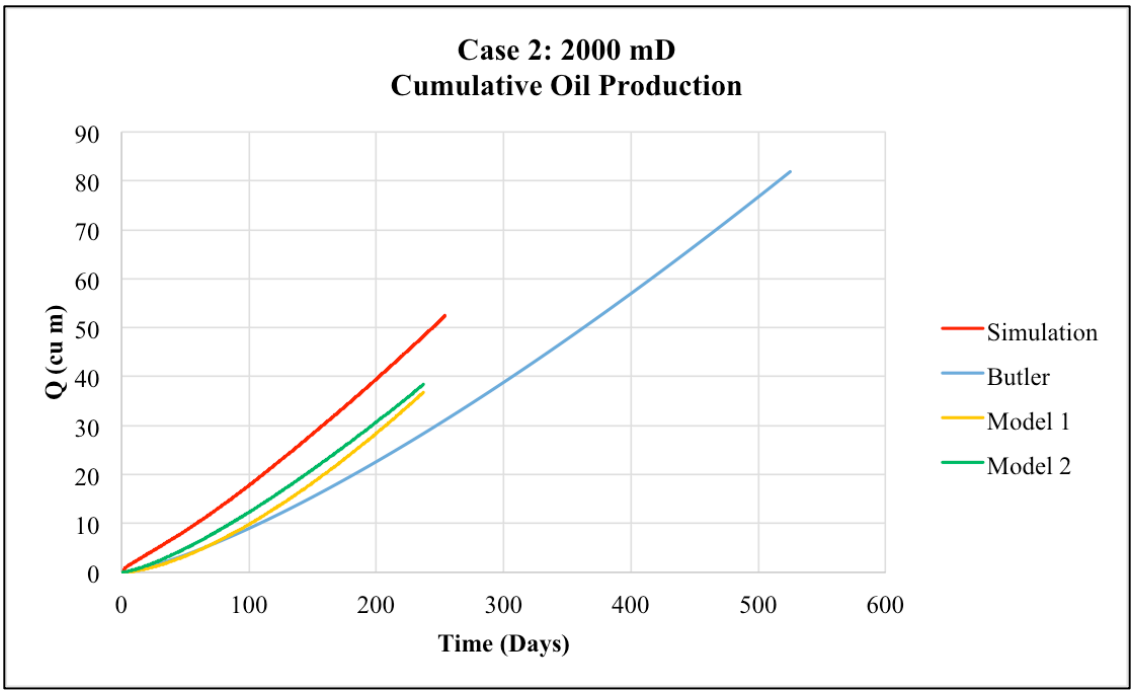

Figure 4.11: Case 2: Comparison of cumulative oil production output from CMG-STARS™ simulation, Butler's model, and proposed Models 1 and 2.

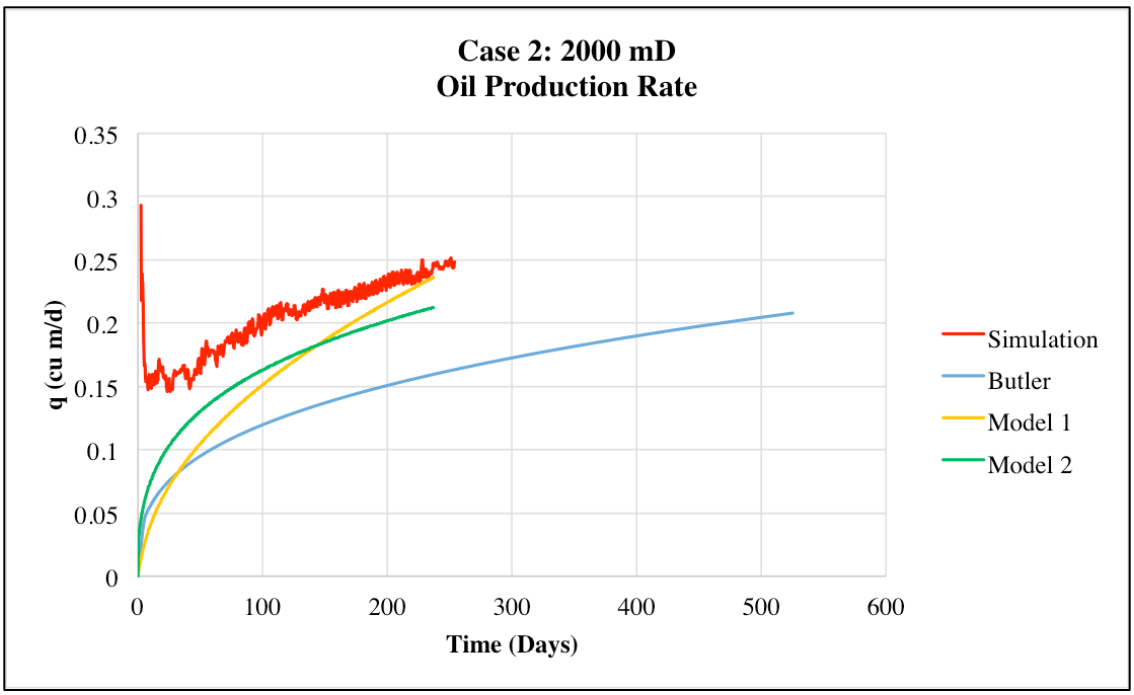

Figure 4.12: Case 2: Comparison of oil production rates output from CMG-STARS™ simulation, Butler's model, and proposed Models 1 and 2.

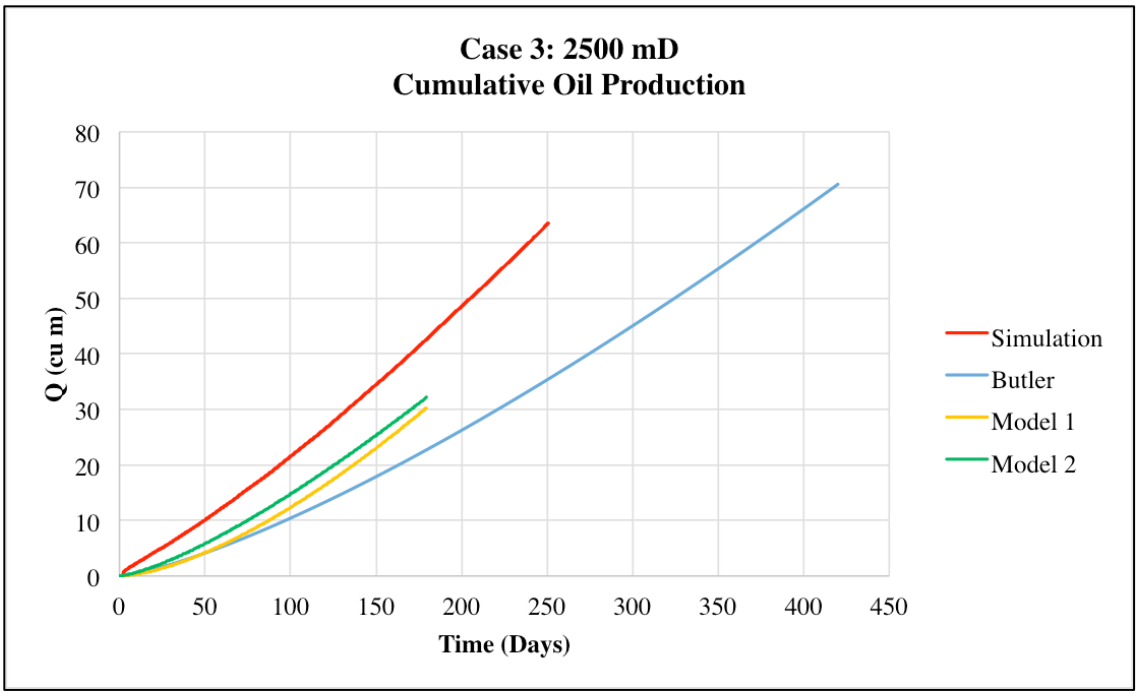

Figure 4.13: Case 3: Comparison of cumulative oil production output from CMG-STARS™ simulation, Butler's model, and proposed Models 1 and 2.

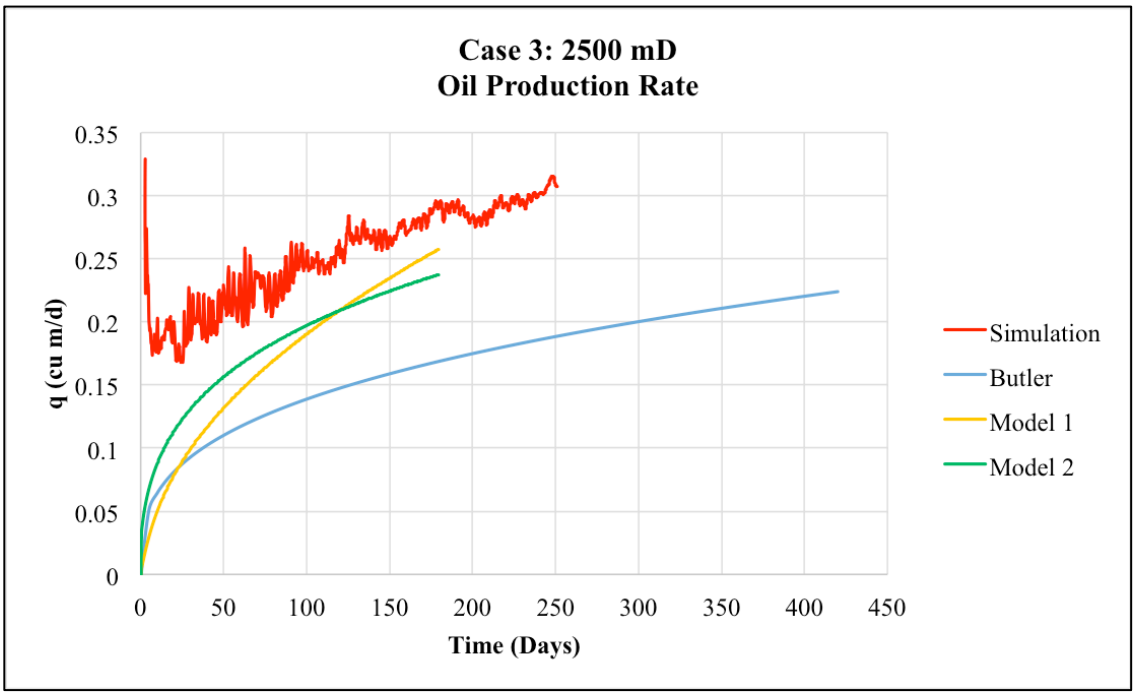

Figure 4.14: Case 3: Comparison of oil production rates output from CMG-STARS™ simulation, Butler's model, and proposed Models 1 and 2.

4.4 Transition from the Rising Phase to the Spreading Phase

So far we have discussed the development of a semi-analytical method to model the SAGD rising phase. In this section, we look at the transition from the rising phase model discussed in the previous sections to the spreading phase model developed by Butler and Stephens (1981) to describe the oil production during SAGD. We have modeled the transition from the rising phase of SAGD to the spreading phase as a step change in the oil production rate from the rising phase to the spreading phase. This is illustrated using a test case described below.

Outputs from both the rising phase and spreading phase models for Case 1 (presented in Section 4.3) are shown in Figures 4.15 and 4.16. The oil production rates are shown in Figure 4.15. The cumulative oil production is shown in Figure 4.16. Also plotted on the same graphs are the reservoir simulation results obtained using CMG STARS^{TM}. It can be observed that the outputs from both semi-analytical models (rising and spreading) compare very well with the reservoir simulation results. At the end of the rising phase, a jump in the oil production rate is observed in the output from the reservoir simulation that eventually declines and stabilizes at a fairly constant value. This happens over a period of time usually referred to as the transition period. In the semi-analytical model, we have modeled the jump observed in the reservoir simulation during the transition period as a step change in the oil production rate from the end of the rising phase to the start of the spreading phase. Our findings indicate that modeling the transition as a step change from the oil production rate at the end of the rising phase to

the beginning of the spreading phase adequately models the oil production observed during SAGD as shown in Figures 4.15 and 4.16.

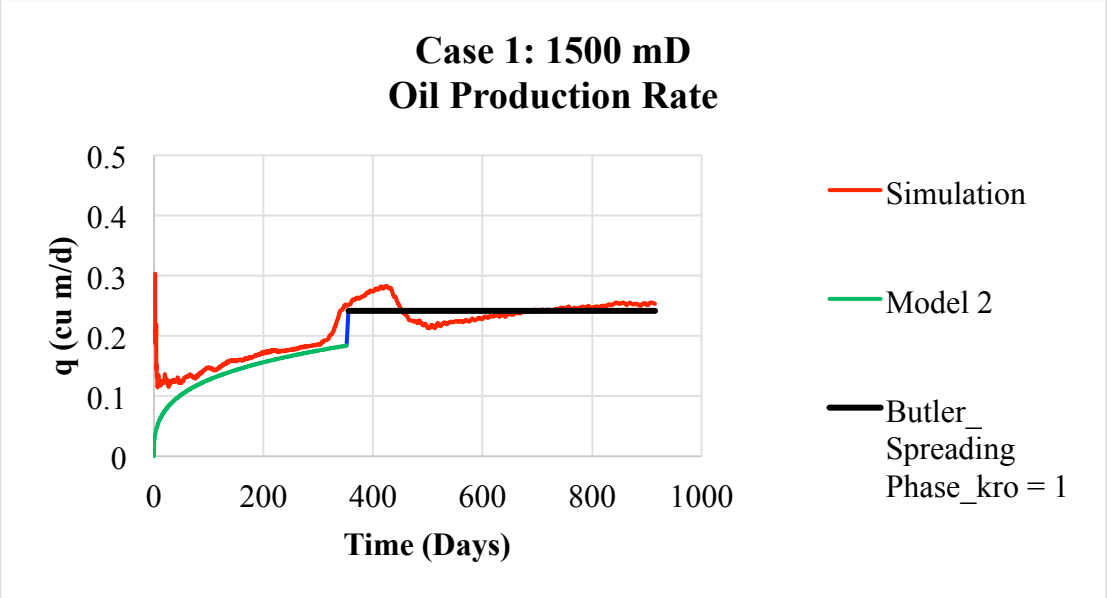

Figure 4.15: Oil Production Rate for SAGD including both the rising and spreading phases.

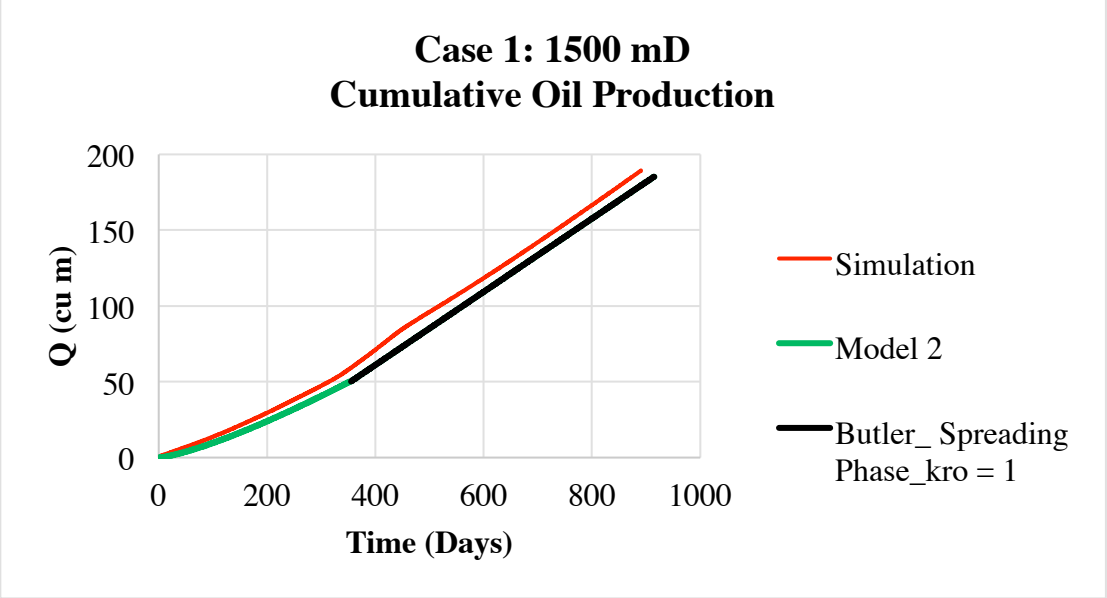

Figure 4.16: Cumulative Oil Production for the SAGD including both the rising and spreading phases.

4.5 Chapter Summary

In this chapter, we presented a semi-analytical method, MS-SAGD, based on the Myhill and Stegemeier frontal advance method, to model the SAGD rising phase. The MS-SAGD model tracks the growth of the steam chamber as a function of time. Two oil production rate models are proposed to be used in conjunction with the MS-SAGD model. Both models use the outputs of the MS-SAGD model, height and/or width of the steam chamber as a function of time, to estimate the oil production rates during the SAGD rising phase. The models were validated by comparing the outputs from the models to the outputs from CMG-STARS^{TM} reservoir simulation and existing analytical models developed by Butler (1987, 1991) and Murtaza and Dehghanpour (2012). The proposed models outperform the existing models for the SAGD rising phase and compare well with the results from CMG-STARS^{TM} reservoir simulation. Oil production rate Model 2 performs better than Model 1 in describing the behavior of the oil production observed in the reservoir simulation and is thus a better model for the SAGD rising phase. We modeled the transition from the rising phase to the spreading phase of SAGD as a step change in the oil production rate from the end of the rising phase to the beginning of the spreading phase. This models the oil production observed in the reservoir simulation for SAGD reasonably well. In the next chapter, we discuss the extension of the MS-SAGD model and oil production rate Model 2 for application in heterogeneous reservoirs with discontinuous shale barriers.

Chapter 5: Extension of MS-SAGD Model for Application in Heterogeneous Reservoirs

In the previous chapter, we discussed the development of the MS-SAGD semi-analytical method, based on the Myhill and Stegemeier (MS) frontal advance model, to quantitatively analyze and describe the SAGD rising phase for homogeneous reservoirs. In Chapter 2, we reviewed the impact of permeability heterogeneity on SAGD performance reported by several researchers and highlighted the important impact of shale barriers on SAGD process performance. In Chapter 3, we used upscaled simulation models to model the performance of SAGD in heterogeneous reservoirs containing discontinuous shale barriers. A quicker alternative to numerical simulation is the use of semi-analytical methods to study the impact of heterogeneity on SAGD. In this chapter, we extend the application of the MS-SAGD semi-analytical method and the oil production rate Model 2 from Chapter 4 to study the effect of permeability heterogeneity on the vertical steam rise phase of SAGD.

5.1 Extension of MS-SAGD Semi-Analytical Model

For the validation cases in Chapter 4, the impact of reservoir permeability on steam chamber growth was implicitly accounted for by adjusting the steam injection rates that are used in the MS-SAGD flow rate equations. By specifying pressure constraint at the injection wells, thereby keeping the steam injection temperature and pressure constant in the simulator, the injection rates are a function of the reservoir permeability. The average

injection rate reflecting the average permeability of the model was then used for the validation of the MS-SAGD model in Chapter 4. In strongly heterogeneous reservoirs with discontinuous shale barriers (similar to those shown in Figures 3.3 – 3.5 in Chapter 3), the shale barriers can impede and re-route the steam and oil flow, although conductive heat transfer can continue through the shale barriers. As a result of this, the steam chamber growth in the vertical direction is severely limited and this is accompanied by an increased lateral growth because of the diversion of the steam by the shale barriers. It is not possible to capture the impact of the permeability heterogeneity on SAGD simply by adjusting the injection rates and there is a need for alternative means to account for it in the MS-SAGD semi-analytical method.

The MS-SAGD model assumes a piston-like displacement and does not explicitly model the convective flow path of the steam in the reservoir. To model the impact of the shale barriers on the steam chamber rise time, the heated volume calculated using the original MS-SAGD model is treated as an effective heated volume, V_{eff}. Within this effective volume, there is a proportion of shales that has similar thermal conductivity to the sand but has much lower permeability and hence low convective heat flux. Thus, to distribute the heat over an equivalent heated volume, thermal heat transfer would occur over a larger volume of the sand. This would mimic the lateral spread of the heat into a larger extent of the sand when there are extensive shale barriers in the vicinity of the well. We elaborate further on this concept using an example whose schematic is given below in Figure 5.1. The example is given for a single time step calculation.

Figure 5.1a shows the heated volume (for a reservoir of unit thickness) estimated using the original MS-SAGD model (same procedure as Chapter 4). The heated volume is given by $W_1\Delta h$ in Figure 5.1a. Assuming similar thermal properties for the sand and shale, the heated volume can be distributed between the facies based on the volume fraction of sand and shale. Given that the ratio of sand to shale is 80:20 in this example, 80% of the heated volume consists of sand and the remaining 20% consists of shale. Thus far, no changes have been made to the MS-SAGD model and the calculation is similar to that of Chapter 4. We shall refer to this model as the "original MS-SAGD" model for the remainder of this discussion.

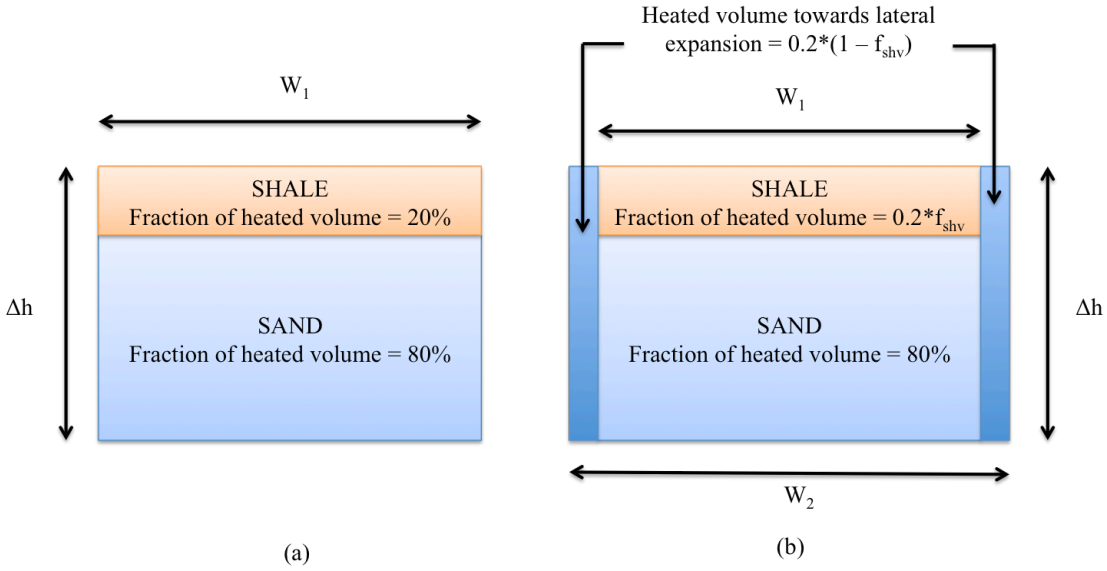

Figure 5.1: Distribution of Heated Volume (a) Weighted distribution based on fraction of shale and sand (b) Using the concept of Effective heated volume

In Figure 5.1b, the sand to shale ratio is the same as in Figure 5.1a i.e. 80:20. The heated volume by the original MS-SAGD model is given by $W_1\Delta h$ (same as in Figure 5.1a). Based on the volume fraction of sand, 80% of the heated volume consists of sand

i.e. 80% of the energy used in expansion of the steam zone vertically is used to heat the sand. However, to model the diversion of the steam flow by the extensive shale barriers resulting in greater lateral growth of the steam chamber, we assume that only a fraction of the remaining injected energy, Q_{rem}, heats the shale and the rest goes towards lateral expansion of the steam chamber. The shale volume, 20% for the example given in Figure 5.1 (equivalent to the fraction of energy remaining after heating the sand, Q_{rem}), is multiplied by a heat allocation factor, f_{shv}, that determines how to distribute Q_{rem}. This is illustrated in Figure 5.1b. When doing this, we keep the height of the steam chamber remain the same as that given by the original MS-SAGD model, but allow the width to expand, thereby capturing the effect of heterogeneity on the steam chamber rise time observed in reservoir simulations.

The heat allocation factor, f_{shv}, given by Equation 5.1, is simply the ratio of the effective permeability of the heated volume determined by the original MS-SAGD model to the absolute permeability of the sand and ranges between 0 and 1. Low values of f_{shv} indicate higher shale content whereas higher values closer to 1 indicate lower shale content.

$$f_{shv} = \frac{k_{eff_{\,heated\ volume}}}{k_{sand}} \qquad [5.1]$$

The heat allocation factor captures the effect of different convective heat fluxes in the sand and shale. Equation 5.2 gives the expression for the spread volume used in determining the lateral expansion of the steam chamber.

$$V_{spread} = (1 - f_{shv})V_{shale} \qquad [5.2]$$

Where V_{shale} is the volume of shale present in the heated volume given by the original MS-SAGD model. V_{spread} simulates the diversion of the steam flow because of the shale barriers. When the shale proportion in the heated volume is high, f_{sh} will be low and so the spread volume will be high. When the shale proportion in the heated volume is low, f_{sh} will be high and the spread volume will be low. The algorithm for the extended MS-SAGD semi-analytical model is given in Figure 5.2.

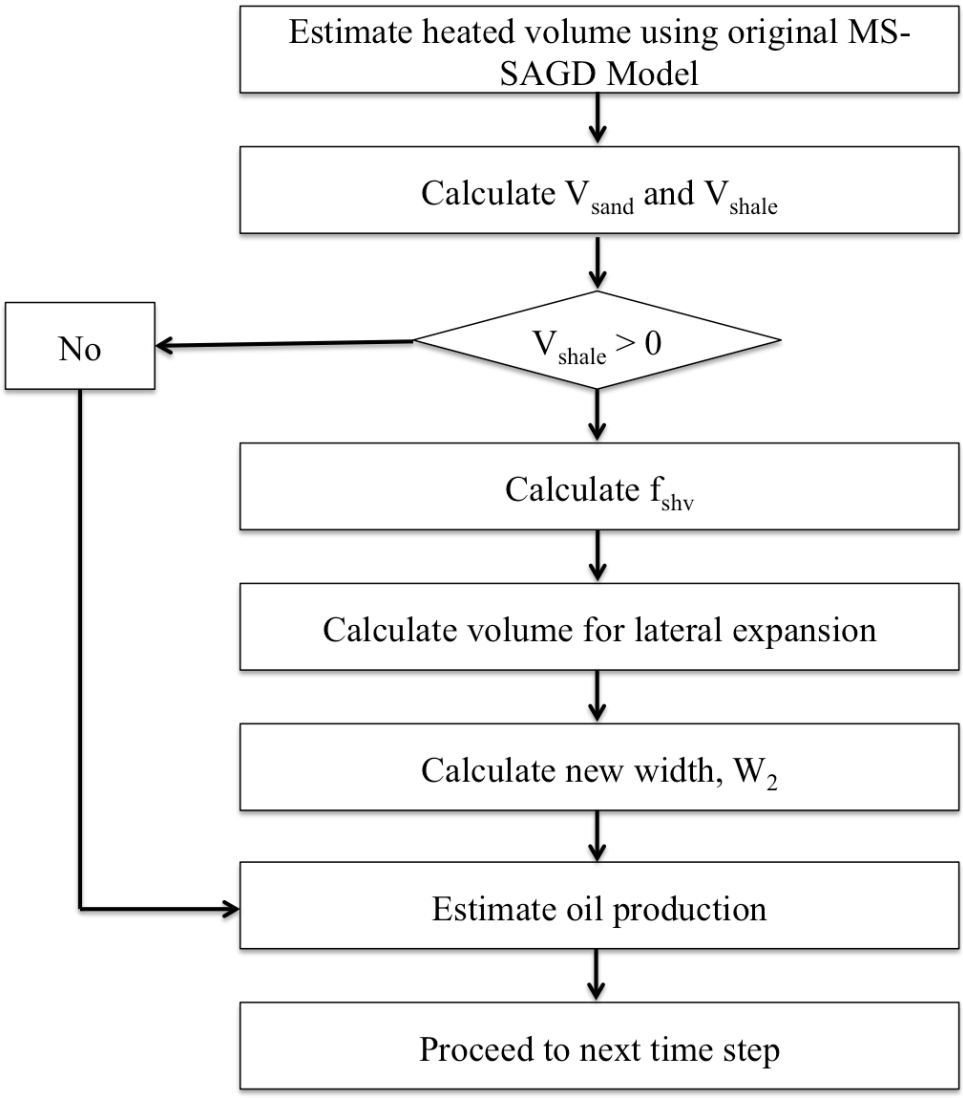

Figure 5.2: Algorithm for Extended MS-SAGD Semi-Analytical Model

5.2 Modification to Oil Production Rate Model

Chapter 4 concluded that the oil production rate Model 2 performed comparatively better than Model 1 in describing the oil production observed in the simulation results for the SAGD rising phase. In this chapter, we shall proceed with the modification of Model 2 to account for heterogeneity. This is achieved by replacing the homogeneous permeability, k, in the oil production rate model with an effective permeability, k_{eff}, that is a function of time as given in Equation 5.3.

$$q_o = 2\sqrt{\frac{1.5\phi\Delta S_o k_{eff}(t) k_{ro} g\alpha h(t)}{m v_{os}}} \qquad [5.3]$$

The fine scale permeability distribution within the heated volume from the extended MS-SAGD semi-analytical model is upscaled at each time step to obtain an effective permeability that is a function of time, $k_{eff}(t)$. We illustrate this using the example given in Figure 5.3. The propagation of the steam chamber as well as the volume heated by thermal losses to the sides of the steam chamber for four consecutive time steps are shown on the left hand side of Figure 5.3. The growth of the total heated volume in time, which includes the steam chamber and the volume heated by thermal losses, is shown on the right hand side of Figure 5.3. At each time step, the fine scale permeability distribution in the total heated volume is upscaled using the physics-based upscaling to obtain an effective permeability that is a function of time, $k_{eff}(t)$. Later we present effective permeability values that are invariant in time, k_{eff}, obtained by upscaling the fine scale permeability model using geometric averaging and the physics-based upscaling. In

the next section, we shall discuss the validation of the extended MS-SAGD model and the modified oil production rate model (Equation 5.3).

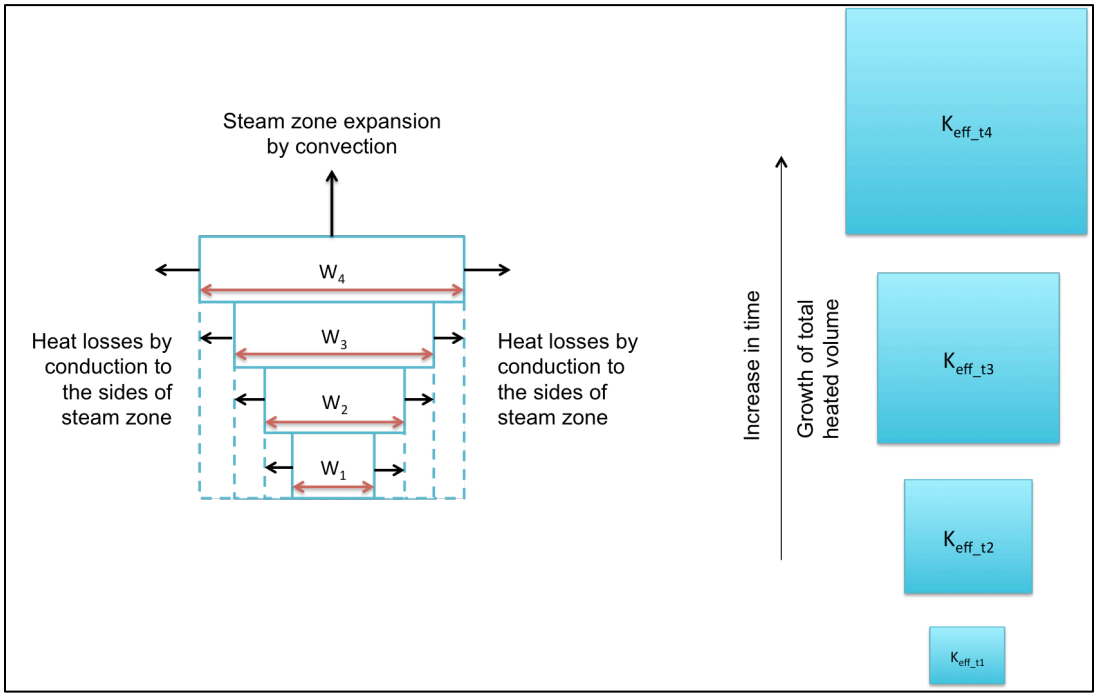

Figure 5.3: Calculation of Effective Permeability as a Function of Time

5.3 Validation of Extended MS-SAGD Model Accounting for Heterogeneous Permeability Field

To validate the extended MS-SAGD semi-analytical model and the modified oil production rate model, two dimensional stochastic shale models, shown in Figures 5.4 and 5.5, were generated in SGeMS (Remy et al., 2009) for the two cases given in Table 5.1. Both cases have a shale correlation length of 25m.

Table 5.1: Validation Cases for Extended MS-SAGD and Modified Oil Production Rate Model

Case	Shale Frequency	Avg. Steam Injection Rate (CWE m^3/day)
Case 1	30%	0.72
Case 2	50%	0.55

Also given in Table 5.1 are the shale frequencies and the average cold water equivalent (CWE) steam injection rates for the two cases. The specifications and input parameters for the semi-analytical models and CMG-STARS™ reservoir simulator are the same as that given in Chapter 4 except for the permeability model and average steam injection rate.

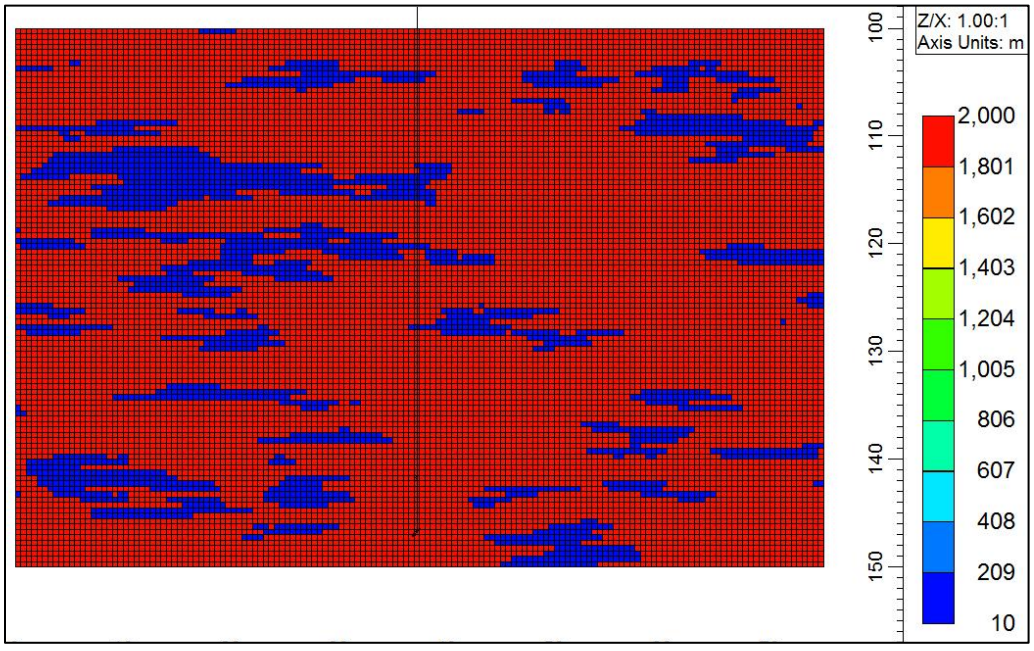

Figure 5.4: Permeability Distribution for Case 1 with 30% Shale Frequency

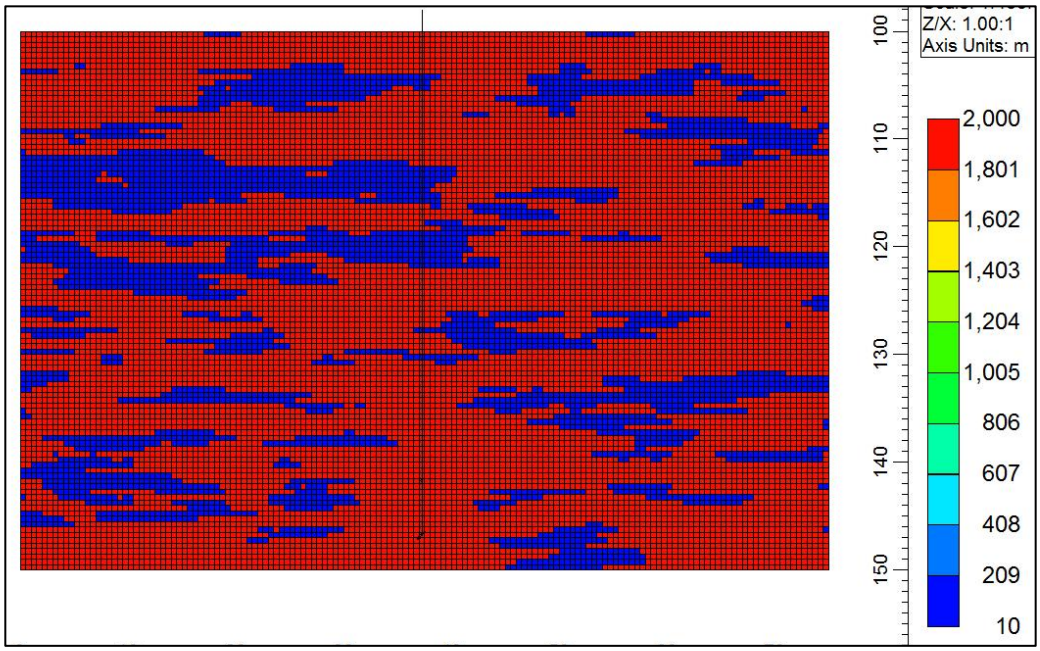

Figure 5.5: Permeability Distribution for Case 2 with 50% Shale Frequency

The outputs from the modified models are compared with the results from reservoir simulation using CMG-STARS^{TM}. The time it takes for the steam chamber to rise to the top of the formation for the two validation cases are shown in Figure 5.6. Given in the figure are the outputs from CMG-STARS^{TM} simulator and the extended MS-SAGD semi-analytical model. The results from the extended MS-SAGD model are in good agreement with the output from the simulator.

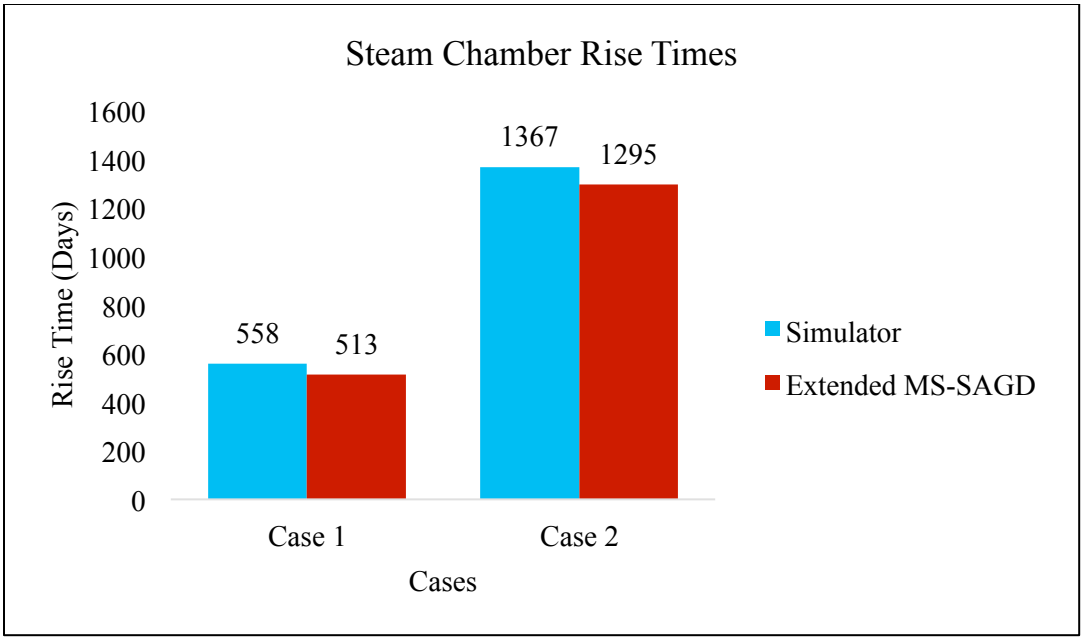

Figure 5.6: Steam Chamber Rise Times for Validation of Extended MS-SAGD

As indicated in Section 5.2, the permeability of the heated volume from the extended MS-SAGD model is upscaled at each time step to obtain an effective permeability that is a function of time, $k_{eff}(t)$. We also upscaled the permeability models using the geometric averaging and the physics-based upscaling technique presented in Chapter 3 to obtain the effective permeabilities given in Table 5.2. Note that these upscaled values are invariant in time. Output from the oil production rate model using these effective permeabilities in its formulation is compared with the results from the model that uses effective permeability as a function of time.

Table 5.2: Effective permeabilities obtained using geometric averaging and the improved physics-based upscaling techniques

Case	k_{eff}_geometric averaging (mD)	k_{eff}_improved upscaling technique (mD)
Case 1	800	1265
Case 2	507	1130

Figures 5.7 – 5.10 present a comparison of the outputs from the oil production rate models using different upscaled permeability values to the results from reservoir simulation in heterogeneous reservoirs.

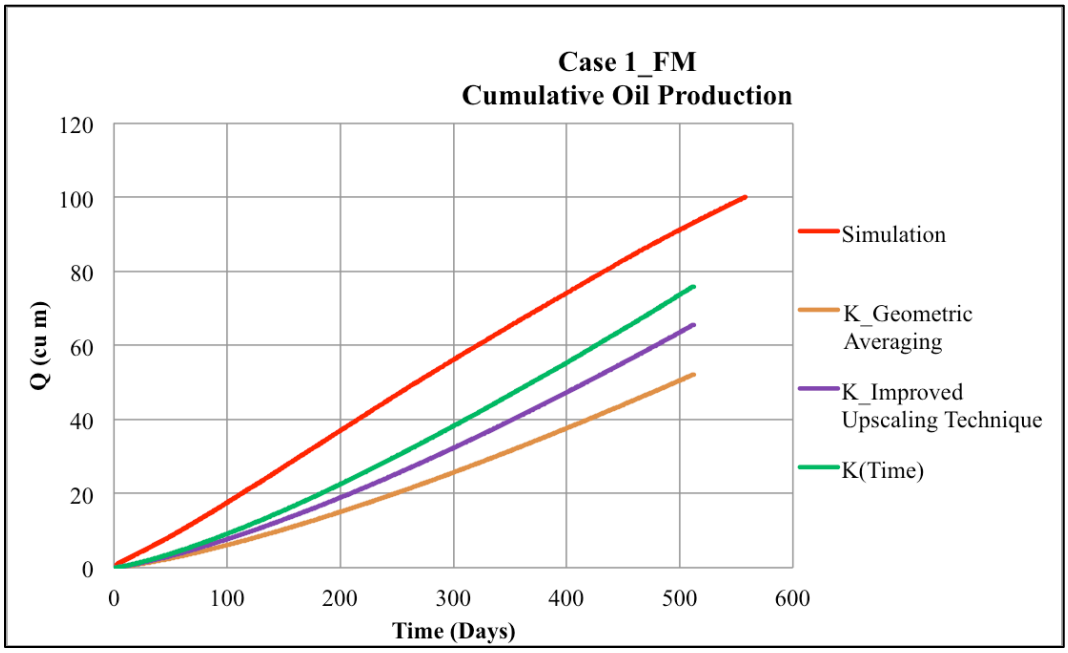

Figure 5.7: Case 1: Comparison between cumulative oil production obtained from simulation and proposed models. These results are corresponding to the case with low shale proportion.

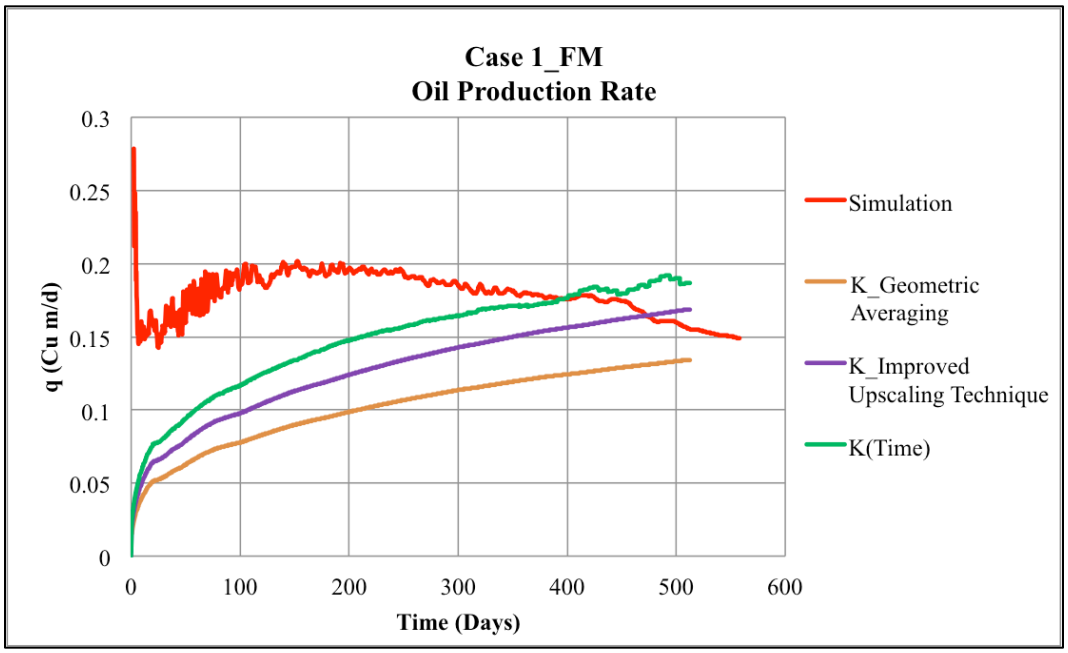

Figure 5.8: Case 1: Comparison between oil production rates results obtained from simulation and proposed models. These results are for the case with high shale proportion.

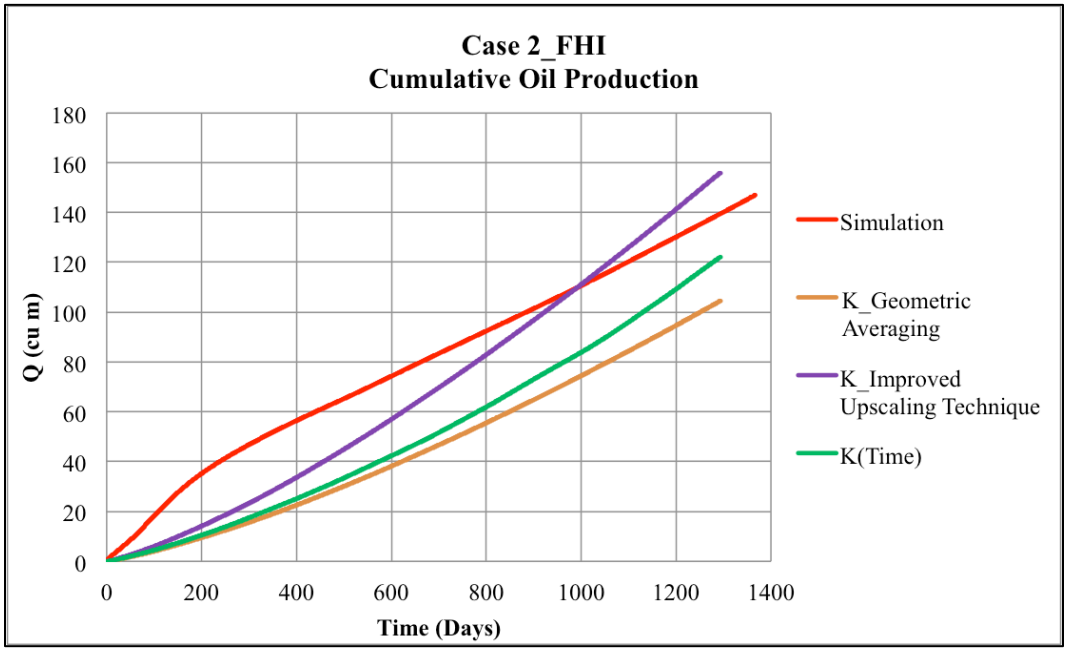

Figure 5.9: Case 2: Comparison between cumulative oil production obtained from simulation and proposed models. These results are for the case with high shale proportion.

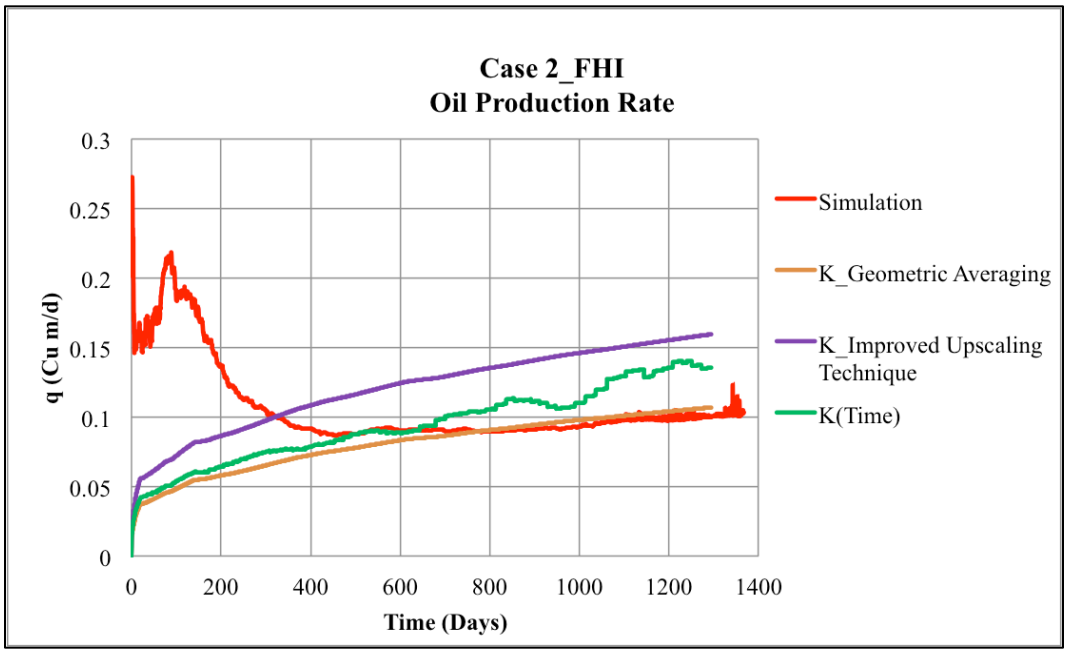

Figure 5.10: Case 2: Comparison between oil production rates results obtained from simulation and proposed models. This is for the case with high shale proportion.

It can be observed from the comparison plots that for both validation cases, the oil production rate model that is a function of $k_{eff}(t)$ performs better than the models that used a single effective permeability. The cumulative oil production output from the oil production rate model that is a function of $k_{eff}(t)$ compares well with the results from CMG-STARS^{TM} reservoir simulation. The matches between the oil production rates from the semi-analytical method and the reservoir simulation are reasonable though not as great as the matches between the cumulative oil productions and the steam chamber rise times. In Figure 5.10, we observe a significant mismatch of the oil production rates at early times. In analyzing the results, we find that at early times, the shale layers near the vicinity of the well (shown in Figure 5.5) are not extensive in the direct pathway of the steam flow i.e. although they slightly divert the steam flow, they do not significantly

thwart the vertical rise of the steam chamber as observed during the middle and later times. The extended MS-SAGD model assumes that the shale layers are extensive which impedes and reroutes the steam flow, resulting in an increased lateral spread of the steam chamber and decreased steam chamber rise velocity when the steam flow encounters these shale barriers. As a result of this, the extended MS-SAGD model predicts a steam chamber rise velocity that is lower than that observed in the simulation during the early times and hence the mismatch observed in the oil production rates.

Furthermore, although we used the concept of the effective heated volume to model the impact of the permeability heterogeneity on the steam chamber rise time, the distortion to the steam chamber shape that occurs because of the presence of the shale barriers in not fully captured in these models. The naturally occurring low permeability barriers result in a steam chamber shape that is quite different from that assumed for the development of the oil production rate model (triangular steam chamber). It is conceivable that the rate matches could be improved significantly by explicitly modeling the convective flow path of the steam and this is recommended for future work.

5.4 Chapter Summary

In this chapter, we extended the application of the MS-SAGD semi-analytical model to heterogeneous reservoirs by treating the heated volume estimated by the original MS-SAGD model as an effective heated volume. This allows distribution of a fraction of the injected energy towards lateral expansion of the steam chamber based on the shale content in the original heated volume. Oil production rate Model 2 from Chapter 4 was

modified to account for heterogeneity by replacing the homogeneous permeability in the model with an upscaled effective permeability that is a function of time. Two dimensional stochastic shale models were chosen to validate and illustrate the efficiency of the proposed models. The results obtained compare well with reservoir simulation results. The oil production rate matches could be improved by explicitly modeling the convective flow path of the steam.

Chapter 6: Conclusions and Future Work

Full physics numerical simulation models can be time consuming and computationally expensive. Semi-analytical methods developed by employing simplifying assumptions provide an attractive alternative to study SAGD while retaining a balance between the computational time and accuracy of the results. However the performance of the semi-analytical techniques to predict the performance of SAGD in heterogeneous reservoirs has been shown to be inadequate by previous researchers (Kumar et al., 2013). This thesis presents an improved upscaling technique that takes into account the unique flow geometry observed during SAGD to compute the effective permeability corresponding to a heterogeneous permeability field. This improved permeability upscaling technique is demonstrated to predict SAGD performance more accurately in heterogeneous reservoirs. The thesis also presents a semi-analytical method, MS-SAGD, to model the SAGD rising phase and subsequently extends this method to predict steam-rise in a heterogeneous reservoir.

6.1 Summary and Conclusions

The key summary and conclusions from this study are given as follows:

- The impact of permeability heterogeneity on SAGD can be modeled using analytical/semi-analytical methods or coarser simulation models that require less computational resources compared to full physics reservoir simulation. The performance of both these approaches in the presence of reservoir heterogeneity is dependent on specification of an effective upscaled permeability value. We

investigated the applicability of conventional upscaling techniques and discovered that these conventional techniques do not accurately predict the oil and steam injection rates during the SAGD.

- An improved upscaling technique that simulates the convergent flow behavior observed during SAGD and minimizes the difference between the fine scale and upscaled model solutions was proposed. An advantage of this approach is that it does not require any assumption regarding the local boundary conditions. Several two dimensional stochastic shale models were chosen to validate and illustrate the efficiency of the method. The improved upscaling scheme improves the performance prediction using both semi-analytical as well as coarse scale simulations, successfully reducing the error between the fine scale and upscaled model solutions.
- Our literature review revealed that very few models exist for predicting the unstable steam rising phase. Furthermore, we found that the existing models underestimate the steam chamber rise velocity during the SAGD rising phase. We consequently presented a semi-analytical method, MS-SAGD, based on the Myhill and Stegemeier frontal advance method. We adapted this theory to model the SAGD steam rise phase. The MS-SAGD model tracks the growth of the steam chamber as a function of time. We also proposed two different oil production rate models to be used in conjunction with the MS-SAGD model. Model 1 is based on Darcy's law and is similar to Butler's (1987) approach to model the oil production rate in his rising steam finger theory. Model 2 is obtained by modifying Butler's

model (1991) for the spreading phase and applying it to the rising phase by making the height in the semi-analytical model a function of time and using an effective permeability for the oil flow. Both models use the outputs of the MS-SAGD model, height and/or width of the steam chamber as a function of time, to estimate the oil production rates during the SAGD rising phase. The proposed models outperform the existing methods and compare well with reservoir simulation results. The steam chamber rise times estimated by the proposed MS-SAGD are close to the values obtained from CMG-STARS™ reservoir simulation. Both oil production rate models give similar results in terms of cumulative oil production but Model 2 performs better than Model 1 in describing the behavior of the oil production observed in the reservoir simulation and is thus a better model for the SAGD rising phase.

- We modeled the transition from the rising phase of SAGD to the spreading phase in a homogeneous reservoir as a step change in the oil production rate from the end of the rising phase to the beginning of the spreading phase. This was validated by comparing the outputs from the rising phase semi-analytical model proposed in this work and the spreading phase semi-analytical model developed by Butler and Stephens (1981)) to the results from CMG STARS™ reservoir simulator. The results indicate that modeling the transition period in homogeneous reservoirs as a step change performs adequately well in quantitatively describing the oil production observed in the reservoir simulation.

- We extended the application of the MS-SAGD semi-analytical model to heterogeneous reservoirs by treating the heated volume estimated by the original MS-SAGD model as an effective heated volume and by replacing the homogeneous permeability in the oil production rate model with an effective permeability that is a function of time. Treating the heated volume from the original MS-SAGD model allows distribution of a fraction of the injected energy towards lateral expansion of the steam chamber that simulates the spreading of the steam chamber when a shale barrier is encountered in its path. Two dimensional stochastic shale models were chosen to validate and illustrate the efficiency of the proposed models. The extended MS-SAGD model gave rise times that are close to the values obtained from the reservoir simulation. The cumulative oil production output compares well with reservoir simulation results. The rate matches are also consistent with the simulation results. It is conceived that the matches can be improved by explicitly modeling the convective flow path of the steam and is recommended for future work.

6.2 Recommendations for Future Work

1. In the development and application of the extended MS-SAGD model for heterogeneous reservoirs, we have assumed that the shale barriers are extensive, which impede and reroute the steam flow. As a result of this, the steam chamber vertical rise velocity is reduced and there is an increased lateral spread of the steam chamber compared to that observed in a homogeneous reservoir. This is not

always the case as was observed during the early times for Case 2 in Figure 5.10. During the early times for this case, though the steam flow was diverted, the reduction in the steam chamber rise velocity was not as significant as the extended MS-SAGD model predicted. Furthermore, the distortion of the steam chamber shape that occurs because of the presence of the discontinuous shale barriers is not fully captured by the extended MS-SAGD model and the modified oil production rate model. Incorporating a way to explicitly model the steam flow path in these models would relax the assumptions made in the development and application of the extended MS-SAGD model and also lead to improved results and is recommended for future studies.

2. The transition from the rising phase of SAGD to the spreading phase in homogeneous reservoir was modeled as a step change in the oil production rate from the rising phase to the spreading phase. Studies to model the transition from the rising phase to the spreading phase in heterogeneous reservoirs are recommended for future work.

Appendix

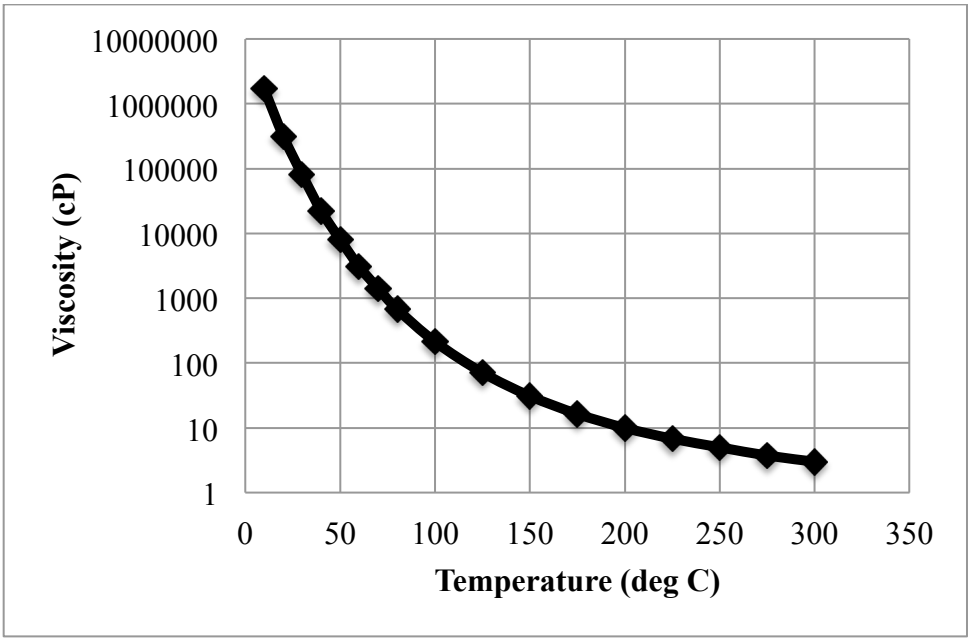

Figure A.1: Viscosity Change with Temperature (Ref: Chen, 2009)

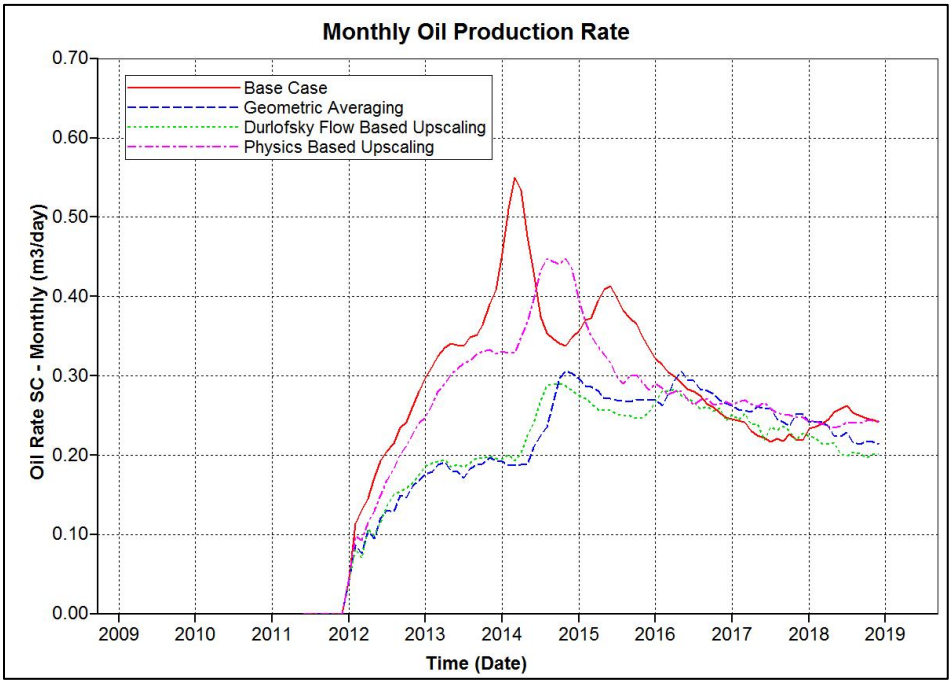

Figure A.2: Model 1 (10% shale frequency) - Comparison of oil production rates between fine scale model and models upscaled using conventional techniques and physics based technique.

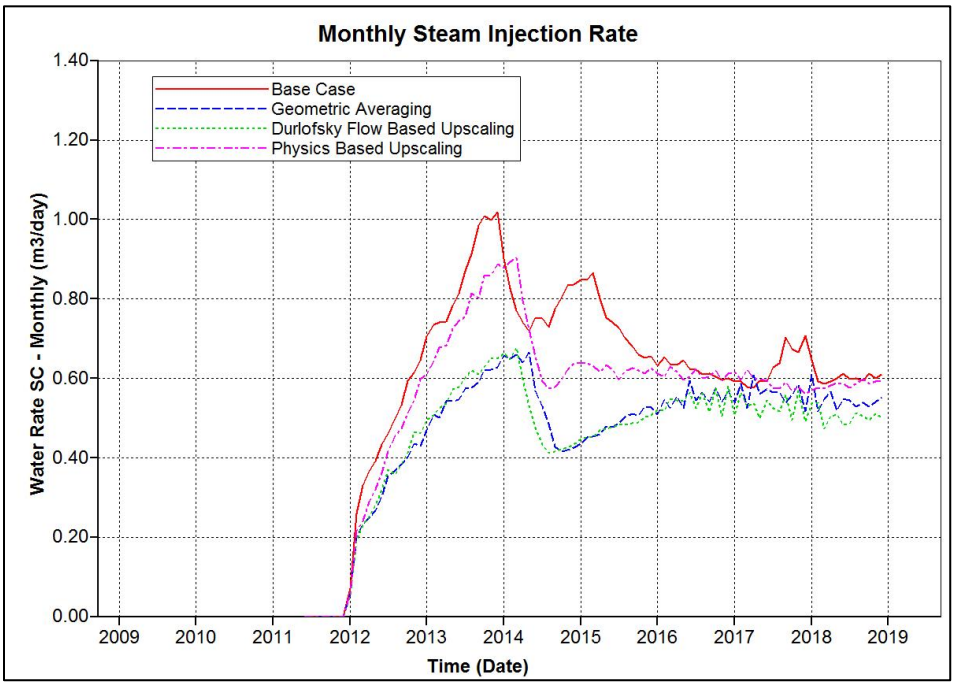

Figure A.3: Model 1 (10% shale frequency) - Comparison of steam injection rates in fine scale model and models upscaled using conventional upscaling and physics-based upscaling.

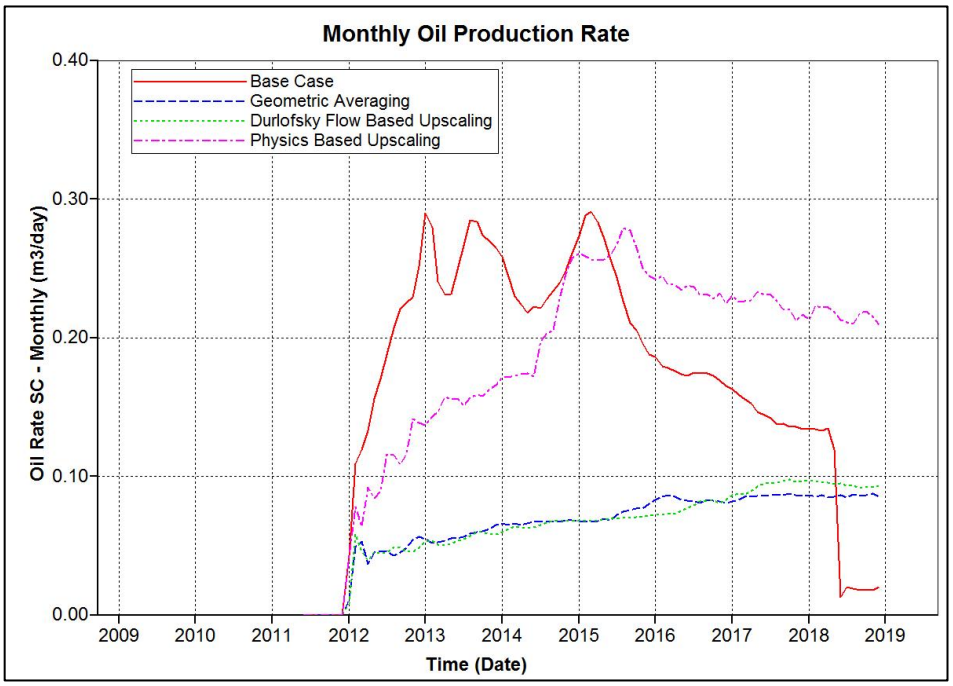

Figure A.4: Model 2 (30% shale frequency) - Comparison of oil production rates in fine scale model and models upscaled using conventional upscaling and physics-based upscaling.

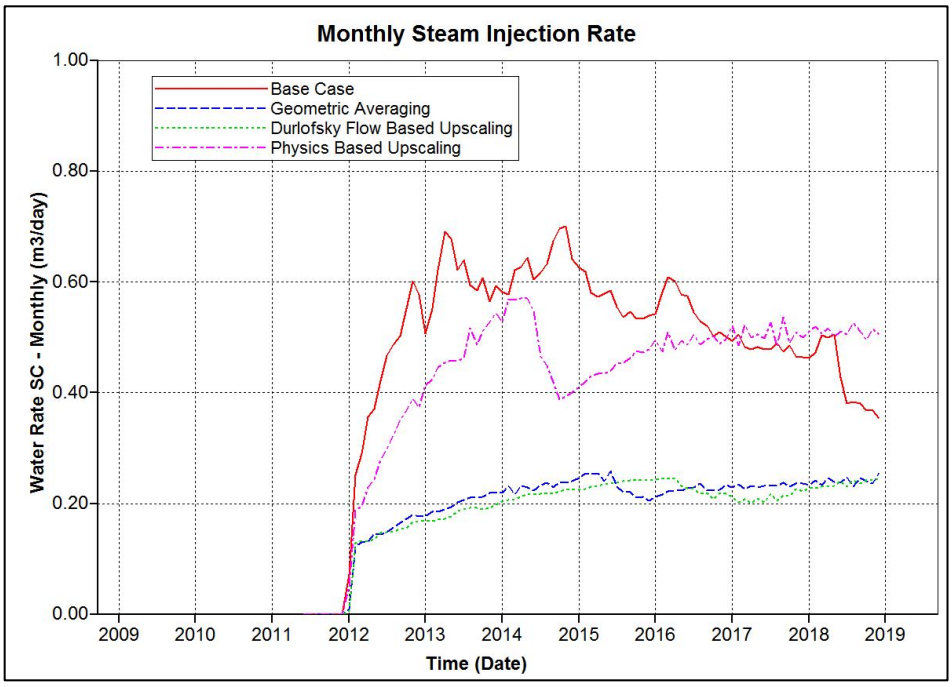

Figure A.5: Model 2 (30% shale frequency) - Comparison of steam injection rates in fine scale model and models upscaled using conventional upscaling and physics-based upscaling.

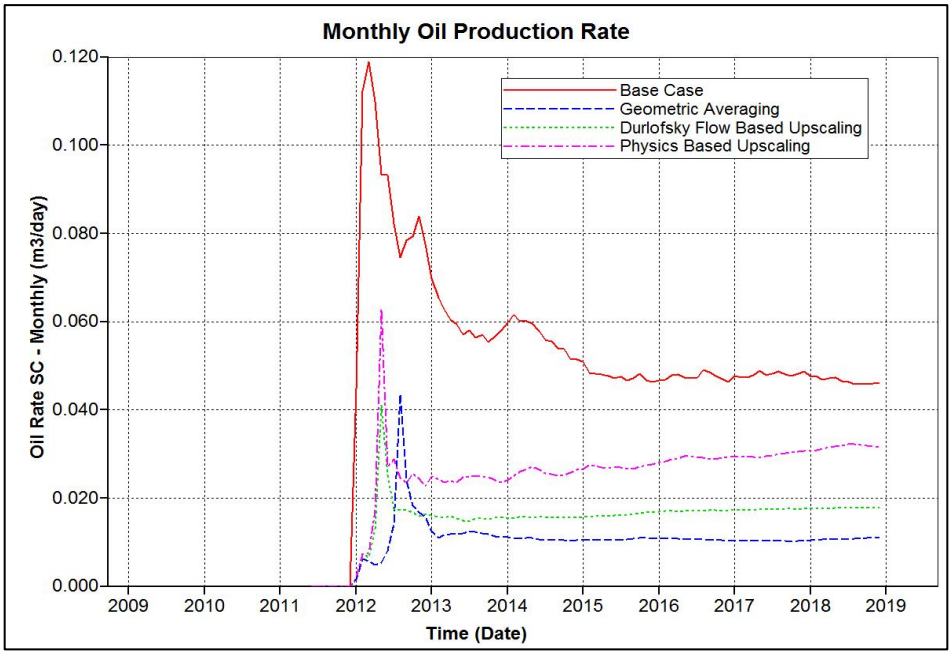

Figure A.6: Model 3 (50% shale frequency) - Comparison of oil production rates in fine scale model and models upscaled using conventional upscaling and physics-based upscaling.

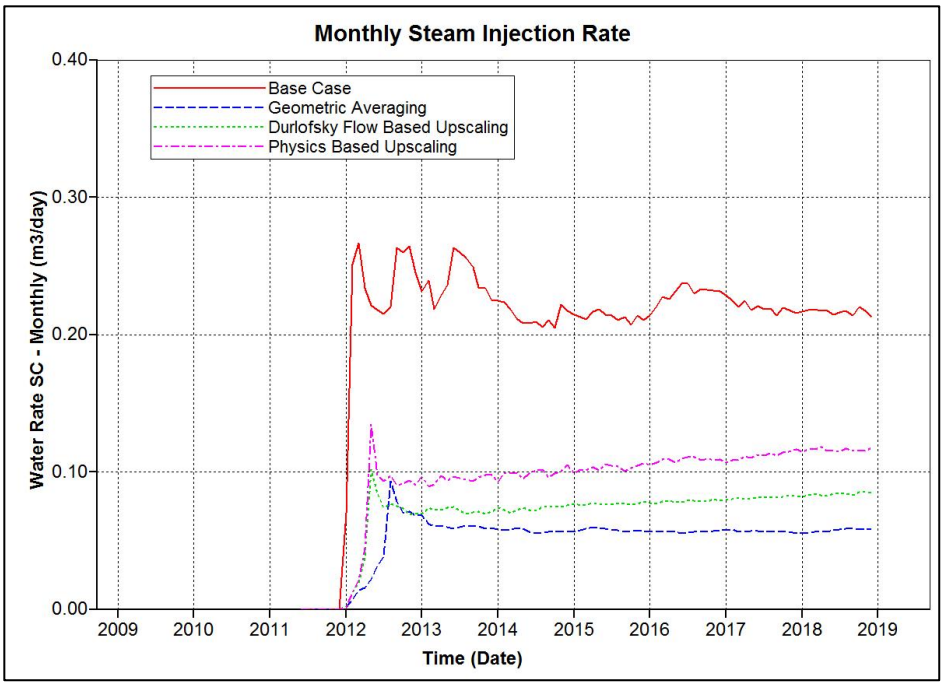

Figure A.7: Model 3 (50% shale frequency) - Comparison of steam injection rates in fine scale model and models upscaled using conventional upscaling and physics-based upscaling.

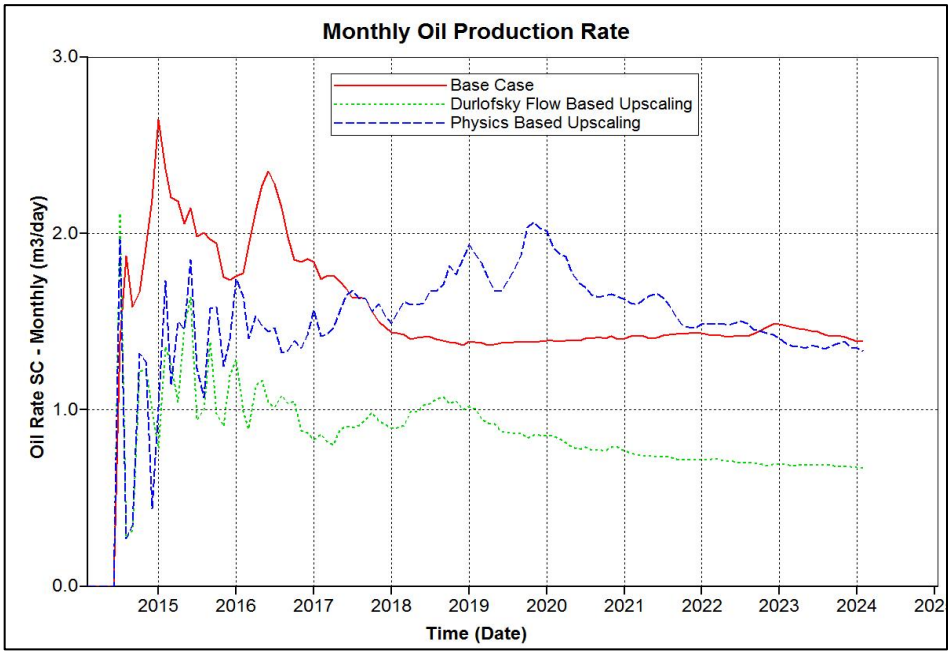

Figure A.8: Model 4 (30% shale frequency) - Comparison of oil production rates in fine scale model and models upscaled using traditional flow-based upscaling and physics-based upscaling.

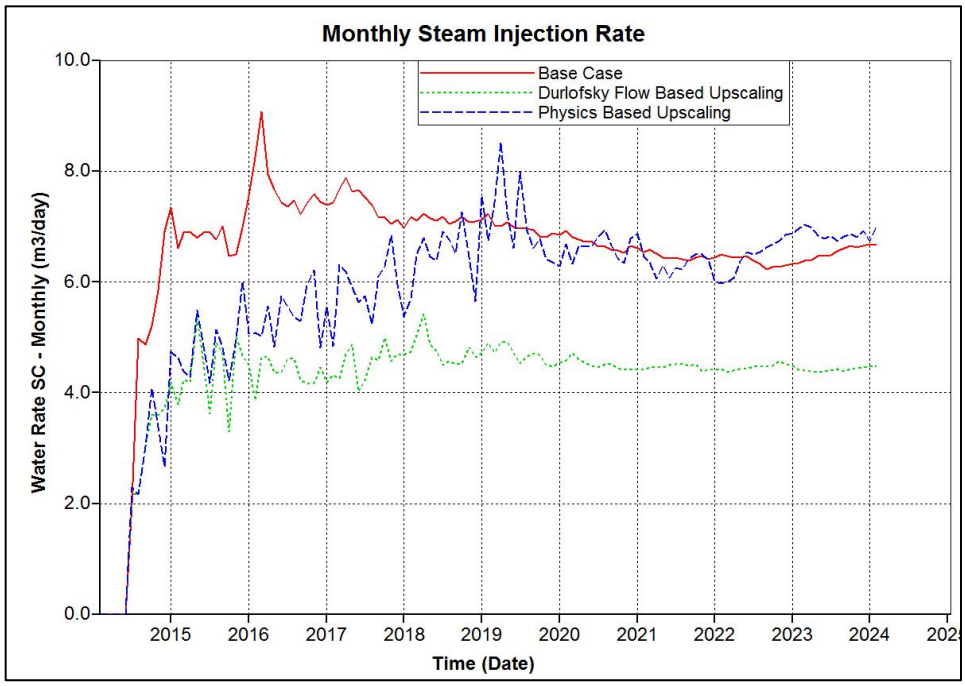

Figure A.9: Model 4 (30% shale frequency) - Comparison of steam injection rates in fine scale model and models upscaled using traditional flow-based upscaling and physics-based upscaling.

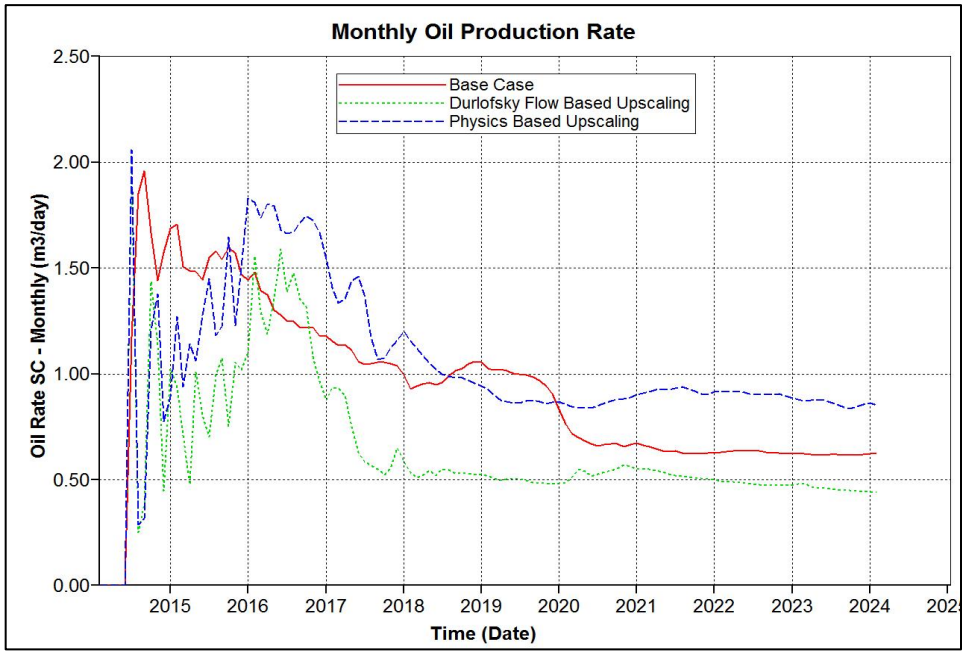

Figure A.10: Model 5 (50% shale frequency) - Comparison of oil production rates in fine scale model and models upscaled using traditional flow-based upscaling and physics-based upscaling.

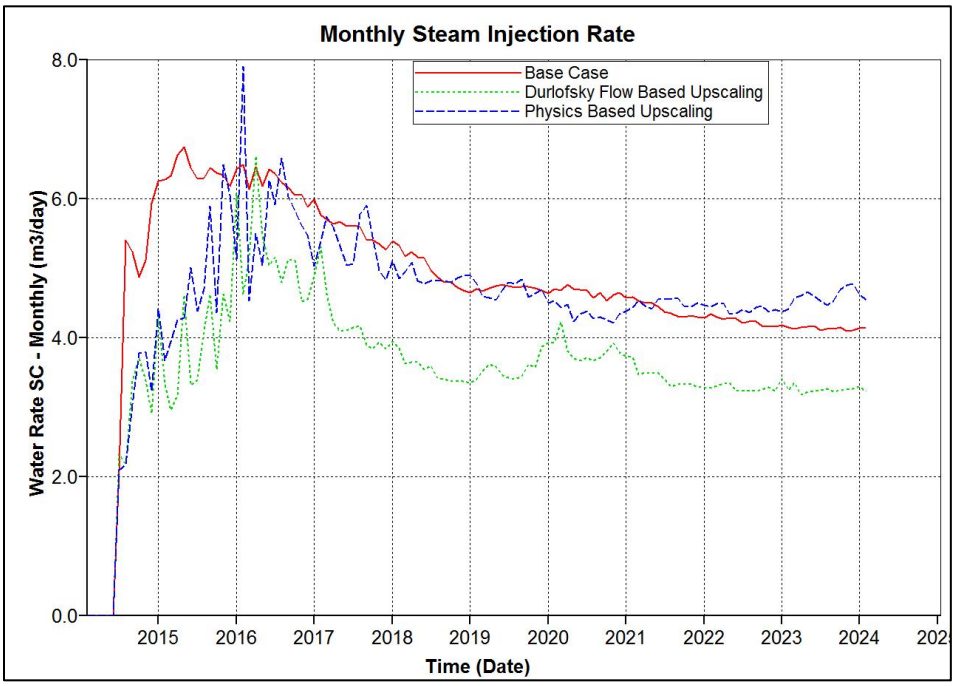

Figure A.11: Model 5 (50% shale frequency) - Comparison of steam injection rates in fine scale model and models upscaled using traditional flow-based upscaling and physics-based upscaling.

References

Akin, S.: Mathematical Modeling of Steam Assisted Gravity Drainage. SPE Reservoir Evaluation and Engineering, 8 (5), October 2005.

Alali, N., Pishvaie, M.R., and Jabbari, H.: A New Semi-Analytical Modeling of Steam Assisted Gravity Drainage in Heavy Oil Reservoirs. Journal of Petroleum Science and Engineering 69, 261 – 270, 2009.

Azad, A. and Chalaturnyk, R.: A Mathematical Improvement to SAGD Using Geomechanical Modeling. Journal of Canadian Petroleum Technology, 49 (10), October 2010.

Azom, P.N.: Improved Modeling of The Steam-Assisted Gravity Drainage (SAGD) Process. Dissertation, The University of Texas, Austin, 2012.

Azom, P.N. and Srinivasan, S.: Modeling the Effect of Permeability Anisotropy on the Steam-Assisted Gravity Drainage (SAGD) Process. Canadian Unconventional Resources Conference, Calgary, Alberta, 15-17 November, 2011.

Bakr, A. A., Gelhar, L. W., Gutjahr, A. L., and MacMillan, J. R.: Stochastic Analysis of Spatial Variability in Subsurface Flows: 1. Comparison of One- and Three-Dimensional Flows. Water Resour. Res., 14(2), 263-271, 1978.

Butler, R. M.: Thermal Recovery of Oil and Bitumen. Prentice Hall, 1991.

Butler, R.M.: Rise of Interfering Steam Chambers. The Journal of Canadian Petroleum Technology, 70 – 75, May-June, 1987.

Butler, R.M., McNab, G.S., Lo, H.Y.: Theoretical Studies on the Gravity Drainage of Heavy Oil During In-situ Steam Heating. The Canadian Journal of Chemical Engineering 59, 455–460, 1981.

Butler, R. M., and Stephens, D. J.: The Gravity Drainage of Steam-heated Heavy Oil to Parallel Horizontal Wells. Journal of Canadian Petroleum Technology, 90-96, (April-June), 1981.

CABS: Center for Applied Basin Studies. University of Calgary, http://www.ucalgary.ca/cabs/Students.

Carlson, M.: Practical Reservoir Simulation: Using, Assessing, and Developing Results. Tulsa, OK, PennWell Corporation, 2006.

Chakrabarty, N., and Gates, I.D.: Automated Global Optimization of Commercial SAGD Operations. Canadian International Petroleum Conference, Alberta, Canada, 13-15, June 2006.

Chen, Q.: Assessing and Improving Steam-Assisted Gravity Drainage: Reservoir Heterogeneities, Hydraulic Fractures, and Mobility Control Foams. Dissertation, Stanford University, May 2009.

Chen, Q., Gerritsen, M.G., and Kovscek, A.R.: Effects of Reservoir Heterogeneities on the Steam-Assisted Gravity Drainge Process. SPE Annual Technical Conference and Exhibition, Anaheim, California, 11-14, November 2007.

Cheung, K.: SAGD Well Pair Spacing Evaluation with Consideration of Central Processing Facility Constraints. SPE Heavy Oil Conference, Calgary, Canada, 11-13 June, 2013.

Christie, M.A.: Upscaling for Reservoir Simulation. Journal of Petroleum Technology, November 1996.

CMG: CMG-STARS User Manual. Computer Modeling Group. 2014.

Dagan, G.: Models of Groundwater Flow in Statistically Homogeneous Porous Formations: Water Resour. Res., v. 15, 47-63, 1979.

Dagan, G.: Analysis of Flow Through Heterogeneous Random Aquifers by the Method of Embedding Matrix 1. Steady Flow: Water Resour. Res., v. 17, 107-121, 1981.

Dang, C.T.Q., Chen, Z.J., Nguyen, N.T.B., Bae, W.: Fast-SAGD vs. SAGD: A Comparative Numerical Simulation in Three Major Formations of Alberta's Oil Sands. SPE Heavy Oil Conference, Calgary, Canada, 12-14, June 2012.

Deutsch, C.: Estimation of Vertical Permeability in the McMurray Formation. Journal of Canadian Petroleum Technology 49, 2010.

Durlofsky, L. J.: Numerical Calculation of Equivalent Grid Block Permeability Tensors for Heterogeneous Porous Media. Water Resources Research 27, 699–708, 1991.

Durlofsky, L. J.: Upscaling and Gridding of Fine Scale Geological Models for Flow Simulation. Proceedings of the 8th International Forum on Reservoir Simulation, Iles Borromees, Stresa, Italy, 2005.

Farmer, C. L.: Upscaling: A Review. International Journal for Numerical Methods in Fluids 40, 63–78, 2002.

Gotawala, D.R., and Gates, I.D.: Flow and Energy Dynamics at the Edges of Steam-Assisted Gravity Drainage Chambers. Canadian International Petroleum Conference/SPE Gas Technology Symposium 2008 Joint Conference, Calgary, Canada, 17-19 June, 2008.

Green, D. W. and Willhite. G. P.: Enhanced Oil Recovery. Henry L. Doherty Memorial Fund of AIME, Society of Petroleum Engineers, 1998.

Holden, L., and Nielsen, B.F.: Global Upscaling of Permeability in Heterogeneous Reservoirs: The Output Least Squares (OLS) Method. Transport Porous Media, 40: 115 – 43, 2000.

Ipek, G., Frauenfeld, T., and Yuan, J.Y.: Numerical Study of Shale Issues in SAGD. Canadian International Petroleum Conference/SPE Gas Technology Symposium 2008 Joint Conference, Calgary, Alberta, 17-19 June, 2008.

Ito, Y., and Ipek, G.: Steam-Fingering Phenomenon During SAGD Process. SPE International Thermal Operations and Heavy Oil Symposium, Calgary, Alberta, 1-3 November, 2005.

JAPEX: www.japex.co.jp/english/business/oversea/sa

Kasap, E., and Lake, L.W.: Calculating the Effective Permeability Tensor of a Grid block. SPE Formation Evaluation, 5:192-200, 1990.

King, M. J., MacDonald, D. G., Todd, S. P. and Leung, H.: Application of Novel Upscaling Approaches to the Magnus and Andrew Reservoirs. SPE European Petroleum Conference, The Hague, The Netherlands, 1998.

King, M. J. and Mansfield, M.: Flow Simulation of Geological Models. SPE Reservoir Evaluation and Engineering 2(4), 351–36, 1999.

King, P.R.: The Use of Renormalization for Calculating Effective Permeability. Transport in Porous Media, 4:37-58, 1989.

Kumar, D.: Modeling Steam Assisted Gravity Drainage in Heterogeneous Reservoirs Using Different Upscaling Techniques. Thesis, The University of Texas, Austin, 2014.

Kumar. D., Hampton. T., Azom. P., and Srinivasan. S.: Analysis of Impact of Thermal and Permeability Heterogeneity on SAGD Performance Using a Semi-Analytical Approach. *SPE Heavy Oil Conference*, Calgary, Alberta, 11-13 June, 2013.

Le Ravalec, M., Morlot, C., Marmier, R., and Foulon, D.: Heterogeneity Impact on SAGD Process Performance in Mobile Heavy Oil Reservoirs. Oil and Gas Science and Technology - Rev. IFP 64 (4), 469-476, 2009.

Llaguno, P., Moreno, F., Garcia, R., Mendez, Z., Escobar, E.: A Reservoir Screening Methodology for SAGD Applications. Society of Petroleum Engineers, 2002.

Mandl, G. and Volek, C. W.: Heat and Mass Transport in Steam-Drive Processes, Soc. Pet. Eng. J., Trans., AIME, 246, 59-79, March 1969.

Marx, J.W. and Langenheim, R.H.: Reservoir Heating by Hot-Fluid Injection, Trans., AIME, 216, 312-315, 1959.

Matheron, G.: Elements Pour une Theorie des Milieux Poreux, Masson et Cie, Paris, 166 p, 1967

McLennan, J., Deutsch, C., Garner, D., Mus, E., Wheeler, T., Richy, J.F.: Permeability Modeling for the SAGD Process Using Minimodels. Society of Petroleum Engineers, 2006.

Murtaza, M., and Dehghanpour, H.: Three-Phase Flow During Steam Chamber Rise. SPE Improved Oil Recovery Symposium, Tulsa, Oklahoma, 14-18 April, 2012.

Myhill, N. A. and Stegemeier, G. L.: Steam-drive Correlation and Prediction. Journal of Petroleum Technology 30.2: 173-182, 1978.

Nukhaev, M., Pimenov, V., Shandrygin, A., Tertychnyi, V.: A New Analytical Model for the SAGD Production Phase. Society of Petroleum Engineers, SPE 102084-MS, 2006.

O'Rourke, J.C., Begley, A.G., Boyle, H.A., Yee, C.T., Chambers, J.I., and Luhning, R.W.: UTF Project Status Update May 1997. 48th Annual Technical Meeting of the Petroleum Society in Calgary, Alberta, Canada, 8-11 June, 1997.

Reis, J.: A Steam Assisted Gravity Drainage Model for Tar Sands: Linear Geometry. Journal of Canadian Petroleum Technology 31 (10) October 1992.

Reis, J.: A Steam Assisted Gravity Drainage Model for Tar Sands: Radial Geometry. Journal of Canadian Petroleum Technology 32 (8) August 1993.

Remy, N., Boucher, A., and Wu, J.: Applied Geostatistics with SGeMS: A User's Guide. Cambridge University Press, 2009.

Renard, P. and de Marsily, G.: Calculating Equivalent Permeability: A Review. Advances in Water Resources 20, 253–278, 1997.

Salazar, M.O., and Villa, J.R.: Permeability Upscaling Techniques for Reservoir Simulation. SPE Latin American and Caribbean Petroleum Engineering Conference, Buenos Aires, Argentina, 15-18 April, 2007.

Sheng, J.: Enhanced Oil Recovery Field Case Studies. Gulf Professional Publishing, 2013.

Shin, H. and Choe, J.: Shale Barrier Effects on the SAGD Performance. SPE/EAGE Reservoir Characterization and Simulation Conference, Abu Dhabi, UAE, 19-21 October, 2009.

Su, Y., Wang, J. Y., and Gates, I. D.: SAGD Well Placement in Ultra-Defined Point Bar Deposit. *SPE Heavy Oil Conference*, Calgary, Alberta, 12-14 June, 2012.

Vanegas, J.W., Deutsch, C.V., and Cunha, L.B.: Uncertainty Assessment of SAGD Performance Using a Proxy Model Based on Butler's Theory. SPE Annual Technical Conference and Exhibition, Denver, Colorado, 21-24 September, 2008.